Function of the transcription factor *Osr1* in the connective tissue-mediated control of muscle formation

Inaugural-Dissertation to obtain the academic degree
Doctor rerum naturalium (Dr. rer. nat.)

Doctoral thesis in agreement with the cotutelle contract between:

Freie Universität Berlin

and

Université Pierre et Marie Curie

PEDRO VALLECILLO GARCÍA

Doctoral thesis in agreement with the cotutelle contract between:

Freie Universität Berlin

Departament of Biology, Chemistry and Pharmacy

Laboratory: Max Planck Institut for Molecular Genetics

and

Université Pierre et Marie Curie

Doctoral School: Ecole Doctorale Complexité du Vivant

Laboratoire de Biologie du Développement-Institut de Biologie Paris Seine

This thesis was carried out during the period of January 2011 and June 2015 under the supervision of:

Prof. Dr. Sigmar Stricker and Dr. Delphine Duprez.

Publically presented and defended on the 30^{th} of September 2015

Members of the dissertation committee:

Prof. Dr. Sigmar Stricker

Dr. Delphine Duprez

Prof. MD. Simone Spuler

Prof. Dr. Ketan Patel

Prof. Dr. Manuel Koch

Dr. Fabien Le Grand

Dr. Doreen Janke

I hereby declare that this thesis entitled "*Osr1* in the connective tissue-mediated control of muscle formation" and the work presented in it are my own, done independently and with no others sources or aids than cited. I confirm that any part of this thesis has previously been submitted for a degree or any other qualification at this University or any other institution.

Berlin, den 11.08.2015

Acknowledgements

I would like to thank the people that in different ways has been part of my PhD and has helped me during this fascinating period.

First, I would like to thank Prof. Sigmar Stricker. First, I would like to thank him for entrusting me this interesting project and his continuous support during this period. He has given me the time and place to develop my own ideas, which he has welcomed and considered. He was always there, whenever I had a problem independently how stupid it was. I also want to thank him for constructive scientific discussion and instructive writing correction.

To my co-supervisor in Paris Dr. Delphine Duprez I would like to thank firstly for the warm welcome to her lab and instructive discussion during my period in Paris. She was always there when it came to scientific discussion and has been a great help during the writing period.

I would like to express my gratitude to Prof. Ketan Patel and Prof. Manuel Koch for accepting to be reviewers of my thesis and for their availability. I thank them also their comments and suggestions.

I would like to thank Prof. Simone Spuler. First, I would like to thank her for thinking I could be part of the project 8 of MyoGrad, what it turned out it was a good idea. Second, I thank her for accepting to be part of my disputation committee. Third, I would like to thank her for guiding the first international PhD program in the field of myology and put so much effort to maintain and promote this international cooperation from which so many people benefit.

I would like to thank Susanne Wissler for essential support in the complicated (I probably did not make easier) administrative work that imply an international program between two different universities.

I would like to thank all the MyoGrad community for these fantastic years sharing summer schools, retreats and other meetings. I hope to see you somewhere.

I thank Prof. Stefan Mundlos for accepting me in his lab and for constructive comments during our Monday seminar.

I would like to thank the animal caretaker Katja Zill at the MPI-MG for her great work from what I have benefited during these years.

I would like to thank all my colleagues in the AG Mundlos who I had the pleasure to accompany during this last years. Hendrijke, Daniel, Martin, Ivana, Till, Saniye, Anja, Sinje, Julia, Malte, Dario, Fany, Guillaume, Katharina, Cristina, Björt, Norbert, Asita, Nicole, Moni and so on and so on. You have welcomed me, we had fun working together and outside work, it was a pleasure. You are a great group and I hope I can enjoy you for some more months.

Now I would like to thank the members of the Stricker group. We are not many but I could thank you for many things. Firstly, I would like to thank Verena Kappert, her work has been partially included in this thesis. Verena, your work has been of great help and I have enjoyed teaching you the few things I could.

Aru and Sophie I would like to thank you for the nice time in the lab as well as outside the lab.

"Mi Mi Migüel" I want to thank you for several things. First, I thank you for the nice time in the lab, what included among others important conversation in Spanish or French.

Second, I thank you for your bioinformatics work, which has turned out a very important part of my thesis and very constructive. Lastly, I would like to thank you for all the great time outside the lab.

Now it comes to "El Jürgen-o". I really want to thank you for thousands of scientific discussion about your project or my project. I have really enjoyed coming every day to lab knowing that you will be there. It was a lot of fun to have you there and this time without you would be only half so great. I also want to thank you for the great time outside the lab, where in contrast to the lab scientific discussion and stupid jokes were mixed with some ethanol-based beverage.

Lastly, I want to thank "you". Thank you for holding me during this period, for being part of my project and a soft base. I hope I will have enough time to thank you properly, Kerstin.

Contents

1 Abstract

The musculoskeletal system allows body motion. Despite the distinct mesodermal origins of its components, the development of muscle, connective tissue (CT) and bone is highly coordinated. Osr1 encodes a zinc-finger transcription factor expressed in muscle CT in limbs. The aim of the PhD thesis was to elucidate *Osr1* function in the non-cell autonomous regulation of mouse limb muscle formation.

Genetic lineage tracing revealed that Osr1+ cells are progenitors for several CTs, including muscle, dermal and lung CTs, but also for smooth muscle and brown adipocytes. Comprehensive phenotypic analysis of skeletal muscles in E13.5 *Osr1*$^{GCE/GCE}$ mouse embryos revealed impaired muscle formation. Transcriptomic analysis highlighted two major molecular characteristics caused by the lack of *Osr1* activity. First, *Osr1* actively repressed the expression of genes associated with cartilage and tendon development, suggesting that *Osr1* confers a muscle connective tissue identity. Second, *Osr1* positively regulated the expression of components of the extracellular matrix (ECM). In addition to the decrease of ECM components, numerous signaling molecules were significantly down-regulated in *Osr1*-deficient cells of mutant embryos.

This highlights the function of Osr1+ resident connective tissue cells in limb muscle formation. It also establishes that *Osr1* regulates the transcription of ECM components in limb muscle CT. Lastly, it suggests that Osr1 exerts its function via chemokines and secreted factors to ensure proper muscle development.

2 Zusammenfassung

Das muskuloskeletale System ist essentiell für die Fähigkeit zur Fortbewegung. Dieses aus mehreren Komponenten bestehende System erfordert eine koordinierte Morphogenese während der Entwicklung. Das *Osr1* (Odd skipped-related 1) Gen kodiert für einen Zink-Finger Transkriptionsfaktor der im Muskel-Bindegewebe der Extremität im Huhn, wie auch in der Maus exprimiert ist. Das Ziel dieser Arbeit war, die Funktion von *Osr1* in der nicht-Zell-autonomen Regulation der Muskelentwicklung in der Extremität der Maus zu analysieren.

Durchgeführte Analysen der Osr1 Zelllinie zeigten, dass Osr1 Zellen Vorläufer für verschiedene Arten von Bindegewebe sind, darunter das Muskelbindegewebe, das Bindegewebe der Dermis oder retikuläre Fibroblasten der Lunge. Außerdem wurde gefunden, dass Osr1 Zellen Vorläufer für glatte Muskelzellen darstellen und für braune Fettzellen. Eine komprehensive Analyse des Muskelphänotyps in Osr1-defizienten Mäusen (*Osr1*$^{GCE/GCE}$) zeigte klare Defekte in der lokalen Musterbildung. Durch eine Transkriptomanalyse konnte gezeigt werden, dass zwei Hauptaspekte durch das Fehlen von *Osr1* betroffen waren. Zum einen wird *Osr1* benötigt, um die Aktivität von Genen, die mit der Entwicklung von Knorpel- und Sehnenzellen assoziiert sind, zu reprimieren. Dies suggeriert, dass *Osr1* an der Festlegung einer zellulären "Bindegewebsidentitätïn den mesenchymalen Vorläufern der Extremität beteiligt ist. Zum anderen wird *Osr1* benötigt, um Gene der muskulären extrazellulären Matrix zu aktivieren. Zusätzlich zu einer Reduktion der Matrixkomponenten, zeigten zahlreiche Gene für Signalmoleküle eine Herunterregulation in Osr1+ Zellen aus *Osr1*$^{GCE/GCE}$ Embryos.

Zusammengefasst zeigen diese Daten eine funktionelle Rolle der Osr1 Bindegewebs-Zellpopulation im Prozess der Muskelentwicklung der Säugetier-Extremität. *Osr1* scheint in diesem Zusammenhang die Transkription von extrazellulären Matrixkomponenten positiv zu regulieren. Schließlich suggerieren die Daten, dass *Osr1* einen Teil seiner Funktion auch darüber bewerkstelligt, Chemokine und andere sekretierte Faktoren zu induzieren, welche die Musterbildung der Muskeln bestimmen.

3 Résumé

Le système musculo-squelettique permet la mobilité. Le développement des muscles, du tissu conjonctif (TC) et des os est coordonné de manière très précise. *Osr1* encode pour un facteur de transcription qui est exprimé au niveau du TC musculaire au cours du développement. Le but de cette thèse est d'élucider la fonction d'*Osr1* dans la régulation cellulaire non-autonome de la formation des muscles au niveau des membres dans le modèle murin.

Le traçage génétique a révélé que les cellules Osr1+ sont à l'origine de plusieurs TC, y compris musculaire, cutané et pulmonaire, mais aussi à l'origine du muscle lisse et des adipocytes bruns. L'analyse phénotypique des embryons de souris *Osr1*$^{GCE/GCE}$ à E13.5 a révélé des défauts dans l'organisation des muscles. L'analyse transcriptomique montre deux caractéristiques moléculaires causées par le manque d'activité d'*Osr1*. Tout d'abord, *Osr1* réprime l'expression de gènes associés au développement du cartilage et du tendon, ce qui suggère qu'*Osr1* confère une identité "tissu conjonctif musculaire". Ensuite, *Osr1* régule positivement l'expression des composants de la matrice extracellulaire (MEC). De plus, l'expression de nombreuses molécules de signalisation est diminuée dans les cellules déficientes pour *Osr1*.

Ces résultats montrent l'importance des cellules Osr1+ du TC dans la formation des muscles des membres. Ces résultats montrent également qu'*Osr1* régule la transcription des composants de la MEC au niveau du tissu conjonctif musculaire. Enfin, ils suggèrent qu'*Osr1* exerce sa fonction par l'intermédiaire de facteurs sécrétés pour assurer le bon développement musculaire.

4 Introduction

From rough and powerful actions to precise gesture, movements in the animal are achieved by the integration of tissues forming the musculoskeletal system. As a part of the musculoskeletal system, muscles provide the contraction force, which is transmitted to bones via tendons leading to a direct movement. Development of skeletal muscles requires continuous cellular and molecular interactions of different embryonic tissues.

4.1 Embryological origins of skeletal muscles

Skeletal muscles along the body share a common contractile function but evolutionary arose from different embryonic structures. Head muscles originate from cranial mesoderm, while body muscles derive from pairwise condensations of the paraxial mesoderm at both sides of the neural tube called somites (Dubrulle and Pourquié, 2004; Chevallier et al., 1977; Christ et al., 1977; Ordahl and Douarin, 1992). The genetic players involved in myogenic specification as well as the processes underlying muscle differentiation and patterning vary among the different anatomical regions of the body.

4.1.1 Genetic networks controlling myogenesis

4.1.2 Generic program

Activation of myogenesis in vertebrates depends on a family of basic helix-loop-helix (bHLH) transcriptions factors, known as myogenic regulatory factors (MRFs). Four transcription factors have been identified with some functional redundancy in myogenesis *Myf5*, *MyoD*, *Mrf4* and *myogenin*. MRFs drive transcription of specific myogenic genes. Each MRF can activate the expression of different muscle genes in vitro and present dynamic expression patterns during development (Buckingham, 1992). Targeted null mutations in mice as well as studies in the avian model allowed the elucidation of the genetic hierarchy within the principal transcription factors responsible for myogenesis. Single null mutations in *Myf5*, *MyoD* and *Mrf4* lead to normal muscle patterning, whilst mutation in myogenin results in a severe reduction of muscle differentiation. Only the combined abolishment of MyoD, Myf5 and Mrf4 leads to complete lack of myoblasts and myofibers in the body, proposing them as key regulators for myoblast commitment (Kassar-Duchossoy et al., 2004).

The genetic network controlling myogenesis activation involves interactions of different transcriptional effectors depending on the anatomical regions.

4.2 Genetic cascades underlying skeletal muscle specification differ depending on muscle position in the embryo

4.2.1 Head Muscles

In vertebrates, head muscles include extra-ocular muscles (EOMs), jaw and facial muscles, which are derived from the pharyngeal arches (PA). They all derive from the cranial mesoderm. Like the cranial mesoderm, the craniofacial muscles are specific for vertebrates and therefore were proposed as an evolutionary novel tissue. MRFs are the core of the myogenic network within craniofacial muscles but their role differs within EOMs and PA muscles. A remarkable difference with somitic muscles is the absence of the paired-homeodomain genes *Pax3* and *Pax7* (see below). However, the MRFs activation role relies on the genetic interaction of several transcription factors with differential roles within EOMs and PA muscles. Pituitary homeobox 2 (*Pitx2*) is a key regulator specifying craniofacial muscles. In contrast, T-box gene 1 (*Tbx1*) is critical specifying PA muscles but not EOMs. Both transcription factors exert a cross-regulation of each other. Furthermore, the bHLH transcription factors Msc (*MyoR*) and *Tcf21* (Capsulin) play an important function regulating PA muscle formation but are not expressed in EOM muscles (Sambasivan et al., 2011; Braun and Gautel, 2011).

4.2.2 Axial Muscles

Muscle progenitors in the dermomyotome of the somites are labelled by the expression of two paired box transcription factors, *Pax7* and *Pax3*, with similar structure (Buckingham, 2003). The expression pattern of both genes, despite their close relation, differs during development. *Pax3* is already expressed early in the presomitic mesoderm, later its expression becomes more restricted to the dermomyotomal lips. Later, *Pax3* expression is shut down in muscle progenitors at the stage E13.5, only being present in a small subpopulation of satellite cells in the adult (Relaix, 2006). *Pax7* is expressed later in the central dermomyotome. During myotome formation in the somite the bHLH transcription factor *paraxis* plays an important role in myogenic specification acting upstream of *Pax3* and controlling *MyoD* expression (Bismuth and Relaix, 2010). Similarly, the genes *sine oculis* homeobox 1 and 4 (*Six1/4*) can act upstream of *Pax3* or trigger *Myod* and *myogenin* expression (Spitz et al., 1998). On the next level of the genetic hierarchy, *Myf5* is the first MRF to be activated and regulates either *myogenin* or *MyoD* expression (Bismuth and Relaix, 2010).

4.2.3 Limb muscles

Myogenesis in the limb can be driven either by the direct binding of *Pax3* to the Myf5-promoter or by the activation of the MRFs by other upstream regulators. *Pax3* expression has been shown to be modulated by the closely related homeobox gene *Meox2*. Inactivation of *Meox2* in the mouse reported down-regulation of *Pax3* and *Myf5* and not *MyoD* (Mankoo et al., 1999), suggesting that *Pax3* and *Myf5* act in the limb at a different hierarchical levels than *MyoD*. In mammals, inactivation of the co-expressed genes *Six1/4* highlighted their requirement for *Pax3* and MRF expression during myogenesis (Grifone et al., 2005). *Six1* and *Six4* are expressed in muscle progenitors cells acting upstream of *Pax3*. *Six1/4* as well as *Pax3* modulate expression of the transcription factor ladybird homeobox 1 (*Lbx1*).

In the limb, *Pax3* is expressed in muscle progenitors from their arrival at the limb bud until stage E13.5, when its expression is downregulated. In contrast *Pax7* has been seen as soon as the stage E11.5 in the proximal muscle mass of the limb bud and its expression is maintained during fetal myogenesis as well as in the adult in muscle satellite cells. These differences in expression pattern have suggested a distinct role for *Pax3* and *Pax7* in muscle formation. Further characterization of muscle precursor cells expressing *Pax7* or *Pax3* has reported differences in gene expression (Biressi et al., 2007). Moreover, ablation experiments of either Pax3-population or Pax7-population demonstrated that Pax7+ cells are dispensable for early embryonic myogenesis (Hutcheson et al., 2009). Thus, two populations of myogenic cells can be defined depending on the requirement of *Pax7* to further activate myogenesis. The first wave of myogenesis is Pax7-independent and Pax3+ cells give rise to the embryonic muscles. The second population, although derived from Pax3+ cells, does not express *Pax3*, but instead *Pax7* and drives fetal myogenesis (Hutcheson et al., 2009) (Figure 1). Additionally, the discovery of the transcription factor nuclear factor one X (*Nfix1*), which is activated by *Pax7* only during fetal myogenesis, activates genes responsible for fetal myogenic characteristics, has reinforced the idea of a transcriptional switch between embryonic and fetal myogenesis (Messina et al., 2010).

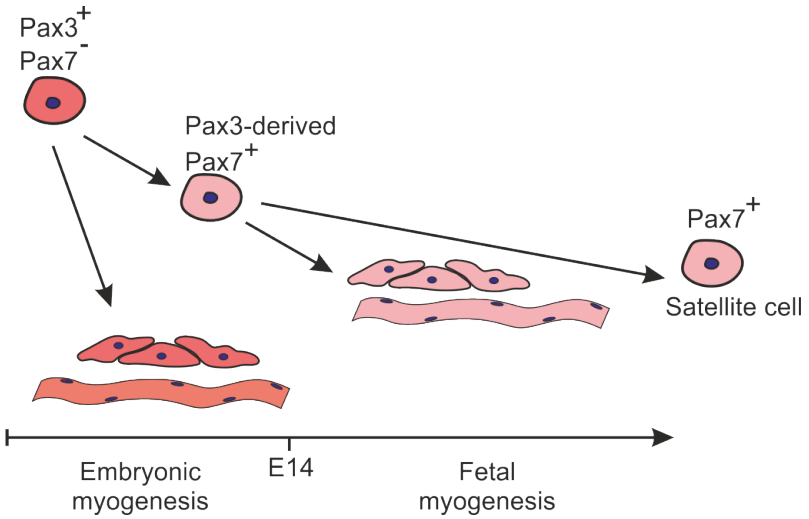

Figure 1: **Muscle fibers with differential characteristics and origins are formed during development**. A population of Pax3+ Pax7- progenitors gives rise to the pattern of embryonic muscles. Precursor cells derived from this population express and require *Pax7* to form muscle fibers at fetal stages. Embryonic and fetal muscle fibers differ in size, shape and protein content. Satellite cells in the adulthood are characterized by the expression of *Pax7*.

4.3 Extrinsic signals regulating axial muscle formation

Formation of the somites (somitogenesis) occurs via sequential induction of pairwise condensations of the presomitic mesoderm. According to their head-to-tail fashion of appearance (i.e. anterior somites are generated first), somites further differentiate in the same order of appearance (Christ and Ordahl, 1995). The mechanism proposed for somite initiation involves a combinatory gradient of signals inducing condensations of the paraxial mesoderm in a clockwise manner along the rostro-caudal axis of the embryo (Dubrulle and Pourquié, 2004; Aulehla and Pourquié, 2010). These signals include members of the Wnt and fibroblast growth factor (FGF) signaling pathways in the caudal part of the embryo, whereby cells are maintained in an undifferentiated state. Concomitantly, retinoic acid signaling pathways in the rostral part forms an opposing gradient of differentiation (Dubrulle and Pourquié, 2004). Periodical oscillations in the expression of target genes of the Notch and Wnt signaling pathway have been proposed to be determinant for the presomitic mesoderm clock-wise segmentation (Palmeirim et al., 1998). Immediately after segmentation, the somitic mesoderm becomes epithelialized. Among other signals, sonic hedgehog (Shh) produced by the neural tube and notochord has been shown to be involved in further differentiation of the somite, leading to a dorso-ventral compartmentalization. Epithelial-mesenchymal transition events result in the formation of the sclerotome in the ventral part of the somite, later forming the axial skeleton. The dorsal part of the somite maintains its epithelial morphology and gives rise to the dermomyotome, the source of

the majority muscles of the trunk (Figure 2A).

The dermomyotome can be further subdivided depending on the muscles formed from its compartments. First, the most dorsal part of the dermomyotome, the dorsomedial lip (DML), will form the epaxial dermomyotome and gives rise to deep muscles of the back. On the other side the ventral part of the dermomytome, the ventral lateral lip (VLL) gives rise to the hypaxial dermomyotome. Muscle progenitors in this region are divided into a non-migrating subpopulation that gives rise to muscle of the lateral trunk and into a population that acquires migratory capacities forming muscles distant from the somites. At the tips of the dorsal and ventral lips, muscle progenitors undergo terminal differentiation after transient Notch-signaling activation from migrating neural crest cells (Rios et al., 2011) and form the myotome beneath the dermomyotome (Parker et al., 2006; Buckingham, 1992) (Figure 2A and B).

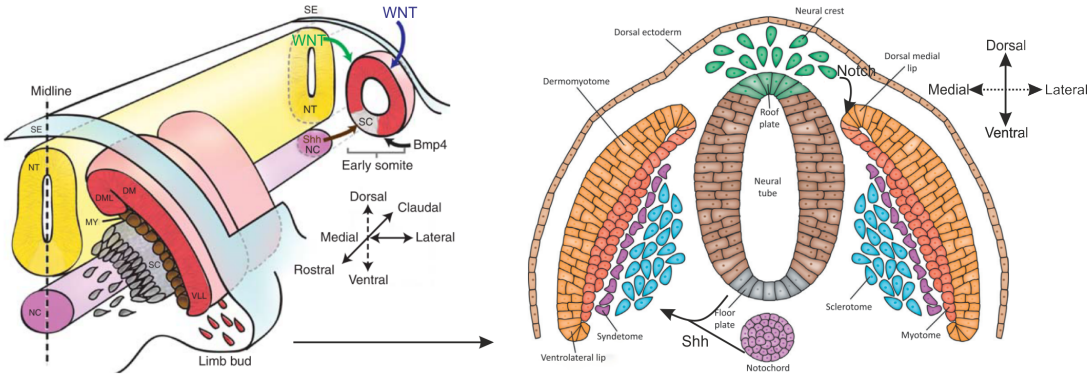

Figure 2: **Formation of the somites and signaling pathways driving to somite compartmentalization**. (A) Schematic representation through the early embryo showing different somitogenesis stages. In the caudal part of the embryo the freshly segmented somites are influenced by neighboring tissues that secrete signals of the Wnt, Shh, and BMP signaling pathways driving further compartmentalization. In the rostral part a more advanced somite already subdivided into the epithelial dermomyotome (red) and the mesenchymal sclerotome (grey). (B) Transverse section of the rostral region shows tissue conformation during somite maturation. The mesenchymal sclerotome (blue) is induced by Shh signal from the notochord and floor plate. The sclerotome contains the syndetome subcompartment (purple). The myotome (red) has already differentiated from the ends of the epithelial dermomyotome (orange) after previous activation of Notch signaling by migrating neural crest cells (green). Sc, Sclerotome; NC, notochord; DM, dermomyotome; NT, neural tube; MY, myotome; DML, dorsomedial lip; VLL, ventrolateral lip. Adapted from Bentzinger et al. (2012) and von Maltzahn et al. (2012).

4.4 Limb muscle patterning

At the level of limb somites, muscle progenitors at the ventral part of the dermomayotome delaminate and migrate following the distal elongation of the limb forming two premuscle masses before they start myogenic commitment.

? Myoblast commitment and myofiber formation are processes that have been in the focus of intensive research and to some extend are well characterized at the cellular and molecular level. This contrasts with our limited understanding of limb muscle patterning, probably due to the complexity of the signals involved in this process.

From the arrival of muscle progenitors in the limb mesenchyme, muscle progenitors proliferate and differentiate in a finely balanced fashion. They activate genes of the myogenic program and undergo further fusion in a very organized manner to form myofibers of the forty limb muscles. At the stage E14.5 in the mouse, muscle progenitors have already found their definitive positions and the final pattern of muscles is defined, with the exception of the forelimb superficialis muscles that relocate from the paw to the forelimb at later stages (Huang et al., 2013). Linage tracing experiments in the chick elegantly demonstrated that muscle progenitors that clonally divide in the somite and gives rise to muscle fibers in the limb are not autonomously committed to any specific region of the limb (Kardon et al., 2002). Formation of specific muscle masses or single muscle in the limb rather relies on extrinsic signals from the close environment (Jacob et al., 1979; Chevallier et al., 1977).

4.4.1 Migration

In contrast to the trunk musculature, limb muscles, diaphragm and tongue are formed by a distinct and evolutionary younger mechanism, which requires higher migratory capacity of muscle precursor cells from the hypaxial dermomyotome. Muscle progenitors from the VLL subsequently proliferate, delaminate and migrate to their target sites before they undergo differentiation and form muscle fibers (Birchmeier and Brohmann, 2000). Loss-of-function studies in mice have reported valuable information about the molecular mechanism necessary at these different stages of limb muscle formation. Proliferation of muscle progenitors at the VLL prior acquisition of migratory capacities, entering in an epithelial to mesenchymal transition, is required to ensure formation of limb muscles. Studies of mice carrying spontaneous mutation in *Pax3* (Splotch mutation) reported the importance of this gene in the establishment of the pool of muscle progenitors at the VLL. This pool is reduced in Splotch mutants due to increased apoptosis. In addition, they do not delaminate from the dermomyotome leading to the loss of muscles of the limb and diaphragm. The receptor tyrosine kinase *c-Met* and its ligand scatter factor/hepatocyte growth factor (*SH/HGF*) were involved in the formation of hypaxial muscles at the level of delamination of muscle progenitors from the dermomyotome. *SH/HGF* is expressed in the mesenchyme neighboring the somites allowing delamination of muscle progenitors, which express *c-Met*, and suggesting a role of this tissue in delamination of muscle progenitors

from the dermomytome (Brohmann et al., 2000).

Restricted expression of *Lbx1* to migrating hypaxial muscle progenitors proposed this transcription factor as a valuable marker for migrating cells (Jagla et al., 1995). Mutations in *Lbx1* allow muscle progenitors to delaminate but lead to impaired migration of muscle progenitors into the limb, accumulating in the mesoderm of the ventral body wall (Brohmann et al., 2000). Expression of *Pax3*, *c-Met/SH/HGF* and *Lbx1* remains active in muscle progenitors assuring pathfinding and proliferation of muscle progenitors previous activation of the myogenic program (A). Not all the muscles of the limb are formed under the same migratory process of proximal-distal invasion of muscle progenitors derived from the somites into the limb mesenchyme. It has been described that progenitors of the perineal muscles as well as of pectoral muscles migrate to the limb bud and differentiate to MYOD+ myoblasts, before they, via retrograde migration, translocate outside the limb in a process called "In-out" mechanism. (Valasek et al., 2005; Evans et al., 2006; Rehimi et al., 2010).

4.4.2 Establishment of the ventral and dorsal muscle masses

The first compartmentalization of muscle progenitors in the limb mesenchyme distributes them into dorsal and ventral muscle masses. Signaling molecules secreted by the limb mesenchyme were suggested to drive muscle progenitor migration to their corresponding domains in an attractive and repulsive manner (Wilkinson, 2001). In addition it was proposed that muscle progenitors were influenced by the locally secreted extracellular matrix (ECM) (Adams and Watt, 1993). *SH/HGF* and its receptor in *c-Met* expressed in muscle progenitors have been already introduced as important regulator of hypaxial muscle progenitors delamination (Jagla et al., 1995). Loss-of-function experiments in mice, after *c-Met/SH/HGF* disruption showed disturbed migration of muscle progenitors, in addition to an impaired delamination (Dietrich et al., 1999). Chick experiments highlighted the role of the mesenchymal expressed ligand ephrinA5 and its receptor Ephrina4 in muscle progenitor pathfinding (Swartz et al., 2001). Thus, they proposed that the ephrinA5/Epha4 axis acts in a repulsive manner maintaining muscle progenitors apart from regions highly expressing ephrinA5. Another example of mesenchymal guidance of muscle precursor migration is the axis *Cxcl12/CxcR4*. *Cxcl12* is expressed in the limb mesenchyme during and after muscle progenitor migration, while its receptor *CxcR4* is only transiently expressed by muscle progenitors during their migration into the limb (Vasyutina et al., 2005). Loss of function experiments revealed mislocated muscle progenitors that do not reach the distal parts of the limb in embryos lacking *CxcR4* (Vasyutina et al., 2005) (Figure 3A). Additionally to the pathfinding guidance signals, muscle progenitors reaching the limb bud

encounter a scenario with gradients of statics signals in the mesenchyme that pattern the limb bud and influence the dispersion of premuscle masses to a certain region of the limb. In this scenario bone morphogenetic proteins (BMPs) play a dual role promoting and inhibiting muscle growth in a concentration depending manner (Bonafede et al., 2006; Amthor et al., 1998). Expression patterns of *Bmp2* and *Bmp4* do not overlap with premuscle masses labelled by *Pax3* or *MyoD* but are in close association in the distal, dorsal and ventral parts of the limb. Surgical abolishment of the limb bud tissue where *Bmp2* and *Bmp4* are expressed results in muscle progenitor mislocation (Bonafede et al., 2006). In the distal-ventral part of the emerging limb bud, the so-called zone of polarizing activity (ZPA) has been described to be involved in limb anteroposterior and dorsoventral axis determination and represent a source of sonic hedgehog (SHH) signaling (Riddle et al., 1993). Alterations of SHH signaling using ectopic engraftments of SHH-expressing cells in the proximal part of the chicken limb lead to alterations in the patterning of muscle masses and later in muscle patterning (Duprez et al., 1999). Furthermore, the developing chondrogenic zone central to the two myogenic regions exhibit an improper extracellular matrix structure to support muscle progenitor migration (Schweizer et al., 2004). As a result, muscle progenitors are located below the ectoderm distantly from the high concentration signals of BMP in the distal part of the limb and close enough to enable the right balance of proliferation and differentiation as well as separated by the medial chondrogenic tissue in the central part of the limb bud (Figure 3B).

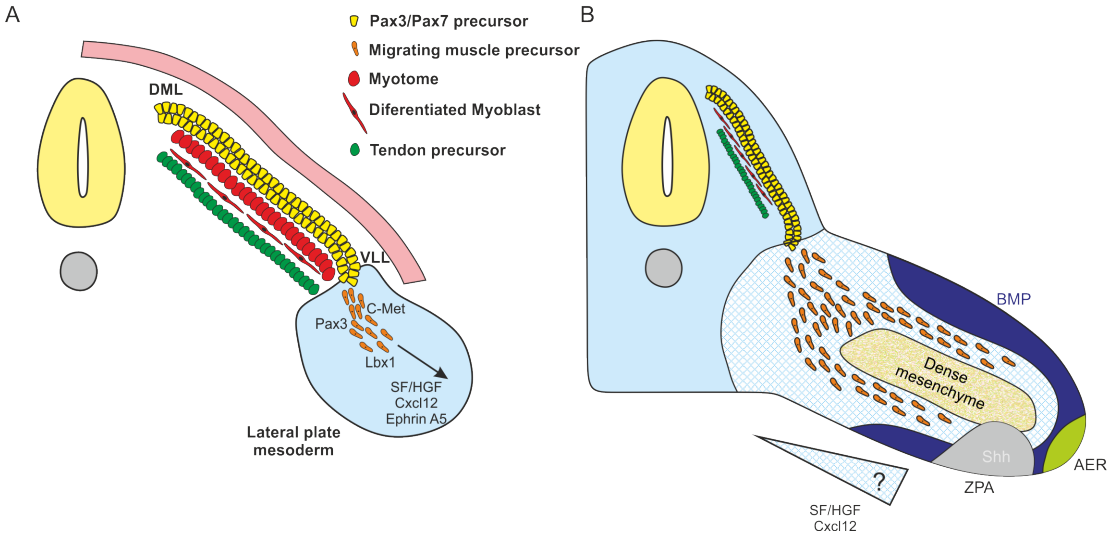

Figure 3: **Formation of muscle masses in the limb bud**. (A) Muscle progenitors (yellow) retain their epithelial conformation, at least for some time, dorsally located from the myotome (red). *SF/HGF* signaling from the surrounding mesenchyme activates muscle progenitors (orange) in the VLL, which delaminate and follow their guidance paths provided by *SF/HGF, Cxcl12* and EphrinA5 cues from the mesenchyme (arrow). Delaminated muscle progenitors continue to express *Pax3*, *c-Met* and *Lbx1*, which are crucial for their migration. (B) On the way into the limb mesenchyme, attracted muscle progenitors are confined in two dorsal and ventral domains delimited by signaling molecules and structures that influence their progression. The dense mesenchyme (beige) in the middle part of the limb bud makes this region inaccessible for muscle progenitors splitting them into two muscle masses. Located distantly from the intense AER and ZPA signaling centers , muscle progenitors are influenced by BMP signaling (blue) close to the ectoderm and migrate through the loose mesenchyme (striped blue) guided by its signals. ZPA, zone of polarizing activity, AER, apical ectodermal ridge.

4.4.3 Limb muscle splitting

When the dorsal and ventral muscle masses are correctly located, muscle progenitors continue to proliferate and differentiate in a balanced process. During this period muscle progenitors are arranged and oriented to form muscle fibers. Successive splitting and segregating events of the muscle masses give rise to the different shapes of muscle in the limb (Tozer et al., 2007). How muscle progenitors and subsequently muscle fibers are shaped and located in the right location for their insertion to tendons remains unknown.

Innervation and vascularization have been proposed to influence limb muscle splitting. However, studies showed that muscle pattern occurs independently of the neural tube in chick embryos (Rong et al., 1992; Edom-Vovard et al., 2002). However, the nervous system has an important role at later stages in myofiber contraction, hence in muscle fiber type determination and late muscle patterning (Huang et al., 2013). In the same line, the vasculature system has been reported to precede and delineate the future muscle splitting sites (Tozer et al., 2007), suggesting a role in muscle patterning. Additionally, disruption of vessel formation in chick limbs showed muscle cleavage impairments. Local angiogenesis induction following VEGF (vascular endothelial growth factor) resulted in ectopic cleavages

of muscle masses, while angiogenesis inhibition prevented muscle splitting (Tozer et al., 2007). However, the cues driving the specific pattern of blood vessels in the trunk are known to be located in non-endothelial cells (Bates et al., 2002; Weinstein, 2005).

4.5 Lateral plate mesoderm derived tissues and their roles in muscle patterning

The lateral plate mesoderm in the early embryo forms the mesodermal compartment located furthest away from the embryo midline. Chick-quail chimera experiments linked the origin of limb mesenchyme to the lateral plate mesoderm (Chevallier et al., 1977). Limb bud initiation has been recently shown to occur via an epithelial to mesenchymal transition process of the lateral plate mesoderm (Gros and Tabin, 2014). Cells of the lateral plate mesoderm have a diverse differentiation potential and give rise to a broad number of tissues, such as cartilage, bone and connective tissues (Chevallier et al., 1977; Kieny and Chevallier, 1979; Christ et al., 1977). The connective tissues (CT) can be broadly subdivided into proper CT and a heterogeneous group called specialized CT. In proper CT, the fibrous component is a predominant feature and comprises loose and dense CT. Characterization and influence of CT during development is still in its infancy. These lateral plate derived-tissues are in close spatial and temporal association with the developing muscles and therefore candidates to influence muscle patterning.

4.5.1 Cartilage and muscle interactions

The limb skeleton emerges from condensations of the limb mesenchyme after cartilage differentiation (Hall and Miyake, 2000). The autonomous formation of skeletal elements can be uncoupled of soft tissue development (Li et al., 2010), thus to some extent muscle patterning is independent of skeletal formation. However, in other instances communication between cartilage and muscle exists, e.g. via the secreted signaling molecule Indian hedgehog (Ihh) (Bren-Mattison et al., 2011).

4.5.2 Tendon and muscle interactions

As a part of the musculoskeletal system tendons transmit the force generated in muscle contraction to the skeletal elements. Tendons are formed of highly organized bundles of collagen fibers, which are embedded with sparse tendon cells, tenocytes. Tendons provide a robust and resilient connection between muscles and skeleton. Nonetheless, the molecular mechanisms involved in tendon formation and patterning remain poorly characterized.

A breakthrough unravelling the process of tendon formation was constituted by the discovery of the bHLH transcription factor scleraxis (*Scx*). *Scx* is specifically expressed in tendon cells from very early stages and has been suggested to be a marker for tendon progenitors (Schweitzer et al., 2001). Collagens the main structural and functional components of tendons are not specific of tendons and are expressed in many other CTs.

Tendon cells share similar functions throughout the vertebrate body but cellular and tissue developmental interactions differ according to anatomic locations of tendons. Axial tendons derive from a dorsally located subdomain of the sclerotome, the syndetome (Figure 4A). During development, the syndetome is thought to derive from a common tendo-chondro progenitor and syndetome formation is achieved by a mutual repression through the down-regulation of the transcription factors paired box 1 (*Pax1*) in the syndetome and *Scx* in the sclerotome (Brent et al., 2003). In the somites, the induction of myogenic factors is observed before *Scx* expression in the prospective syndetome suggesting a role of myotomes in syndetome formation. Indeed, removal of the myotome in chick embryos or the lack of the MRFs *Myod* and *Myf5* in mice resulted in an undetectable *Scx* expression in somites (Brent et al., 2005a). The loss of myotomal FGF signaling in somites in $Myf5^{-/-}$ and $Myod1^{-/-}$ mutant embryos together with the rescued *Scx*-expression in somites of mutant animals implanted with soaked FGF4 beads strongly suggested that the myotomal FGF acts as the inductive signal from somites necessary for *Scx* expression in the syndetome (Figure 4A, arrows).

In contrast to the scenario observed in somites, limb embryonic tissues are not segregated into discrete compartments. Tendon and muscle progenitors are mixed together in limbs. Lateral plate mesoderm-derived mesenchyme, which will give rise to cartilage and tendons, share spatial location with muscle progenitors derived from the ventral parts of somites. Different from the trunk, the initiation of Scx expression in limb buds is not dependent on muscles, since the expression of *Scx* is induced normally in limbs of muscleless mouse mutants and in chicken limbs after coleomics grafting (Schweitzer et al., 2001; Brent et al., 2005a; Kardon, 1998). The ectoderm has been described as one tissue required for the initiation of *Scx* expression in early limb buds (Schweitzer et al., 2001) (Figure 4B, arrows). However, muscles are essential for further tendon differentiation (Edom-Vovard et al., 2002; Kardon, 1998; Eloy-Trinquet et al., 2009; Bonnin et al., 2005). Proximal and distal tendons in limbs have a differential requirement for muscle interaction and *Scx* function during the tendon differentiation phase. In the proximal limb segments, tendon development is initiated in the absence of muscles but further development is disrupted (Edom-Vovard et al., 2002; Kardon, 1998; Bonnin et al., 2005). Digit tendons develop independently of muscle formation, but later degenerate without muscle (Kardon, 1998).

Similarly to the axial region of the body, the members of the FGF family *Fgf4* and *Fgf8* have been described to influence tendon development in limbs. *Fgf8* is expressed in tendons, while *Fgf4* is expressed in muscle cells, at muscle tips close to tendons (Figure 4C). In addition, application of ectopic FGF4 induces expression of *SCX* and *TNC* in chick embryos (Edom-Vovard et al., 2002; Eloy-Trinquet et al., 2009). Members of the TGF-β family have been also described to be necessary for normal tendon development. Although the initiation of limb tendon progenitors occurs normally in *Tgf*β2 *Tgf*β3 double mouse mutants, they are lost from E12.5, showing an essential role of TGF-β signaling in tendon maintenance and organization (Pryce et al., 2009). At the muscle side, tendons attach to muscles via the so-called myotendinous junction that connects the cord-like ECM of the tendons with the ECM secreted at the tips of the muscle fibers. Little is known about the molecular cues involved in the myotendinous junction assembly. However, removal of tendon primordia in chick embryos resulted in ectopic myofibers formation and suggested the role of tendon delimiting zones of muscle growth and differentiation (Kardon, 1998).

In summary, despite muscle and tendon initiate and pattern independently of the presence of each other, further tissue maintenance is comprised without the cross-regulatory presence of each tissue.

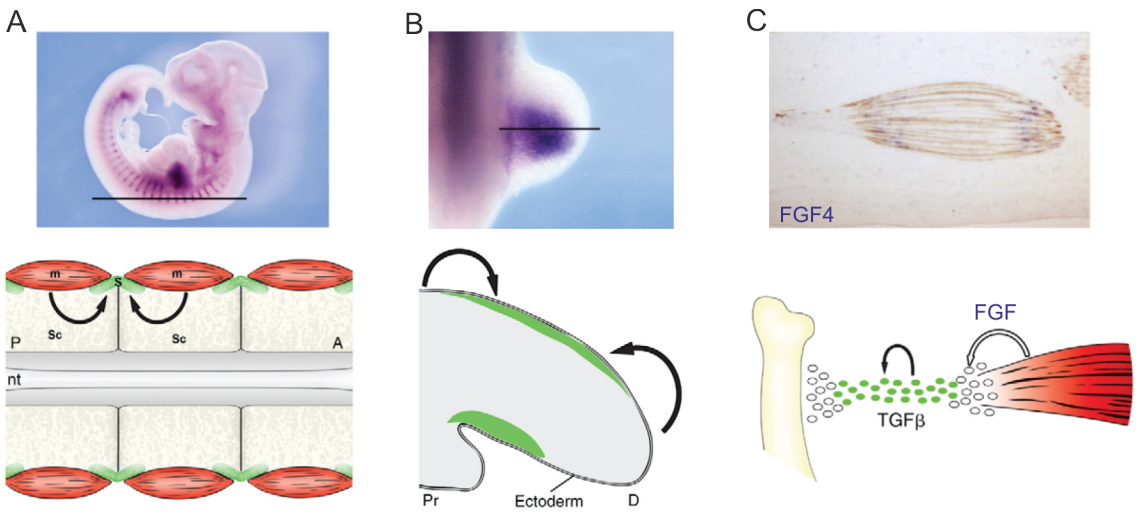

Figure 4: **Tissue interactions during axial and limb tendon formation**. (A) Whole-mount *in situ* hybridization in E10.5 mouse embryos shows expression of *Scx* in somites and limb buds. Black line represented the section illustrated below. The already differentiating myotome (m) provides a source of FGF signaling (arrows) able to induce *Scx* expression in the neighbor syndetome (S, green) located dorsally within the sclerotome (Sc, squares). (B) At the same stage in the limb, *Scx* expression is found in limb bud mesenchyme observed with whole mount *in situ* hybridization. Schematic representation of a sagittal section shows dorsal and ventral expression domains of *Scx*, influenced by ectoderm signaling (arrows). (C) Longitudinal section of a chick limb hybridized with a *FGF4* probe, revealed *FGF4* expression at the tips of muscle fibers (purple) immunolabelled with an anti-MF20 antibody (brown). Representation of tissue interaction and molecular signaling involved in the aggregation and maintenance of tendon progenitors. Similarly to somites, FGF signaling influences tendon differentiation activating *Scx* expression (white arrow). TGF-β signaling is crucial for the organization and maintenance of muscle progenitors (black arrow). Adapted from Schweitzer et al. (2010) and Edom-Vovard et al. (2002).

4.5.3 Muscle connective tissue and muscle interactions

Muscle connective tissue was commonly described as a solid structural interface holding, embedding and scaffolding muscles with relatively low cell density but high ECM content. This description resembles more to the tissue observed at late stages of development, rather than the structural loose mesenchymal tissue that accompanied muscle progenitors and muscle masses during early development. The close spatial and temporal association of muscle CT with muscle progenitors and differentiated myotubes during the time window of muscle patterning strongly suggested a role for muscle CT in this process. Its importance remained enigmatic for a long time due to the lack of any specific marker for muscle CT. Gabrielle Kardon and colleagues in an attempt to find genes specifically expressed in the mesenchymal tissue surrounding muscles and not in myogenic cells themselves identified the transcription factor TCF4, which is a downstream component of the Wnt/β-catenin signaling pathway, (Kardon et al., 2003). *Tcf4* expression was found in muscle mesodermal tissue associated with ventral and dorsal muscle masses at early stages and continuously expressed in muscle connective tissue until adulthood (Kardon et al.,

2003; Mathew et al., 2011) (Figure 4.4.3, above). However, the expression of *Tcf4* is not exclusive for muscle connective tissue; tendon cells, cartilage and, at very low level, myogenic cells also express *Tcf4*. Perturbation of the Tcf4-Wnt-β-catenin pathway using replication-defective vectors carrying activated or negative forms of TCF4 or β-catenin in chick embryos highlighted the role of this transcription factor and the Wnt pathway in the formation of limb muscle patterning (Kardon et al., 2003). In further experiments, it was demonstrated that *Tcf4* expression remains unchanged in the absence of muscles and delineates the muscle pattern even if muscles are not present (Kardon et al., 2003) (Figure 4.4.3, below). Thus, for the first time the role of connective tissue cells was addressed and showed that muscle CT forms a prepattern that delimited muscle growth and shape.

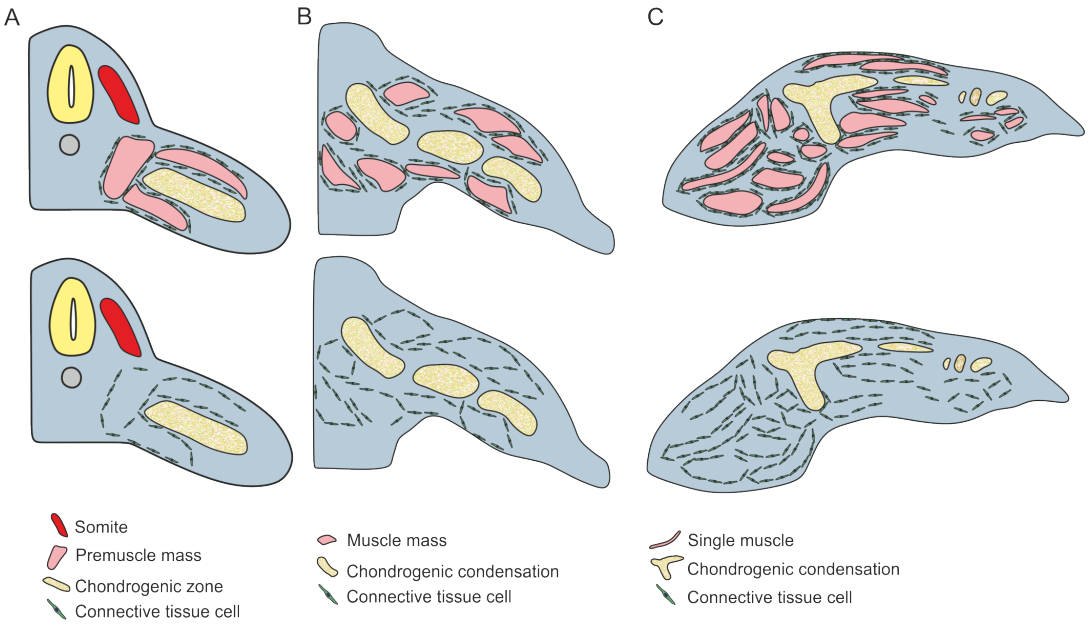

Figure 5: **Muscle connective tissue forms a prepattern for muscle segregation during embryonic development**. Schematic representation of muscles and (prospective) muscle connective tissue cells during muscle patterning (above) compared with muscleless limbs (down). (A) At E11.5 in mouse limbs, muscles masses are formed by groups of myogenic cells predominantly in the dorsal and ventral parts of the limb bud. Connective tissue cells share the same spatial region in the limb in close proximity. (B) One day later in development, muscle masses have split in subgroups that are orientated in future patterning planes. In the absence of muscles, connective tissue cells acquire a distribution delineating muscles masses. (C) At E14.5 muscle patterning is finished in mouse limbs and muscles have obtained their final shapes. Continuous splitting and re-arrangement processes of muscle progenitors led to a large variety of muscles shapes. During this process, connective tissue defines delimited areas, where muscle progenitors proliferate, differentiate and fusion to achieve muscle final forms. The *Tcf4* expression pattern illustrates muscle connective tissue.

How the transcription factor TCF4, controls muscle patterning remains poorly understood. *Tcf4* alone is not sufficient to drive myoblast differentiation (Hutcheson et al., 2009) and an indirect effect through downstream targets specific for muscle connective tissue has not been identified yet.

In addition to *Tcf4*, only two other transcription factors expressed in connective tissue have been involved in muscle patterning so far. Conditional ablation of *Tbx4* and *Tbx5* in hind and forelimb connective tissue respectively, revealed the crucial function of a correctly organized connective tissue in muscle and tendon patterning (Hasson et al., 2010). In addition, muscle connective tissue and the transcription factor *Tcf4* have a larger influence on muscle patterning than on muscle growth and differentiation. During fetal myogenesis, fiber specification is influenced by *Tcf4* and Tcf4+ connective tissue cells (Mathew et al., 2011). In addition it was shown that Tcf4+ cells are required for muscle regeneration in the adult (Murphy et al., 2011).

To date, only the transcription factors *Tbx4/5* and *Tcf4* have highlighted the importance of connective tissue cells in muscle formation. However, more genes have been described with similar expression pattern in muscle connective tissue. Elucidation of their importance, as in the present study, will help us to clarify the precise molecular mechanism underlying the influence of connective tissue on muscle development.

4.6 Odd-skipped related gene 1 (Osr1)

Odd-skipped (odd) was originally identified via its involvement in zygotic segmentation of Drosophila embryos, as mutations in this gene caused loss of even-numbered segments. *Odd* belongs to the pair-rule class of segmentation genes and is expressed in seven stripes during segmentation (Figure 6A) and acquires a dynamic expression during further Drosphila embryogenesis. *Odd* encodes a zinc-finger transcription factor that has been well characterized during this context. *Odd* can act as a transcriptional repressor recruiting proteins of the Groucho complex (Goldstein et al., 2005), as well as a transcriptional activator (Dréan et al., 1998a).

In vertebrates, two odd-skipped related genes exist homologous to *Drosophila odd*. *OSR1* and *OSR2* expression patterns have been well characterized during chick development and exhibit a dynamic expression showing mostly distinct expression domains with partial overlap (Stricker et al., 2006). In the developing chick embryo, *OSR1* is early expressed in the intermediate mesoderm and lateral plate mesoderm (Figure 6B, above),whilst *OSR2* is expressed in the endoderm (Figure 6B, below). Later in development, *OSR1* is predominantly found in limbs, branchial arches and in a variety of tissues such as developing heart, mesonephros, dermis of the trunk, gut and the developing eyes. In mouse limbs, *Osr1* expression has been found in limb mesenchyme associated to the early premuscle muscle masses and the forming muscles at E11.5 and E12.5 (Figure 6C, upper panel). *Osr2* expression in limbs has been found to partially overlap with *Osr1* expression in the middle part of the limb at E11.5 (Figure 6C, left) and appear mostly

exclusive more distally in the limb at E12.5 (Figure 6C, right). Additionally, *OSR1* was found to be expressed in the interdigital mesenchyme (Stricker et al., 2006) and limb joints (Gao et al., 2011). *OSR1* was proposed to be a general marker for irregular connective tissue (Stricker et al., 2012).

Functional analysis has been mainly performed using gene targeting approaches in mice. *Osr1* knock-out animals die intra-uterine before reaching late fetal stages and display severe defects in heart and intermediate mesoderm development (Wang et al., 2005). Compared with other tissues the role of *Osr1* in the formation of intermediate mesoderm-derived tissues has been better characterized. *Osr1* has been suggested as being the earliest marker for the nephrogenic mesenchyme. *Osr1* becomes restricted at later stages of kidney development to nephron progenitor cells (Mugford et al., 2008). Lack of *Osr1* interferes with the formation and establishment of the metanephric mesenchyme (James et al., 2006). In this process *Osr1* interacts with the transcription factor *sine oculis*-related homeobox 2 (*Six2*) to maintain kidney progenitor cells (Xu et al., 2014). In addition, lack of *Osr1* leads to agenesis of the urogenital track and adrenal gland, tissues also derived from the intermediate mesoderm (Wang et al., 2005). The genetic network associated to *Osr1* remains poorly characterized. Studies in *xenopus laevis* have revealed that *Osr1* and *Osr2* play a conjunctional function in lung formation, downstream of the retinoic acid and FGF signaling pathways regulating BMP4 expression (Rankin et al., 2012).

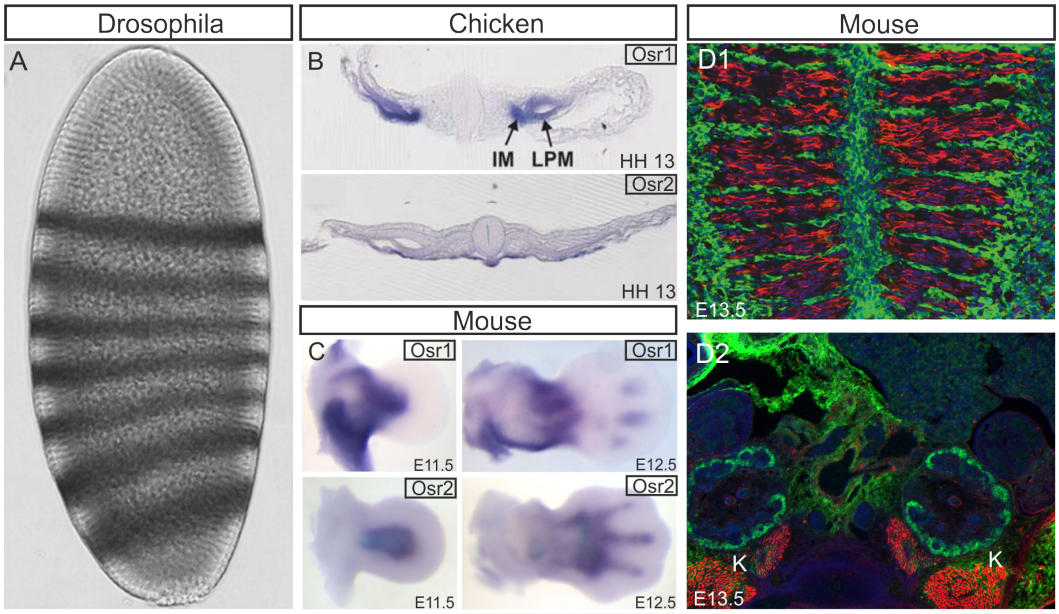

Figure 6: **Osr genes expression pattern during drosophila, chick and mouse development**. (A) Whole mount *in situ* hybridization reveals the seven stripes formed by the expression of pair-rule genes during *Drosophila* segmentation. (B) Whole mount *in situ* hybridization using *cOSR1* and *cOSR2* probes followed by vibratome sectioning highlighted early expression of *OSR1* in the intermediate mesoderm and lateral plate mesoderm in the chick embryo, whereas *OSR2* expression appeared in the endoderm. (C, left) In mouse forelimbs, whole mount *in situ* hybridization revealed *Osr1* and *Osr2* expression regions overlapping only in the medial part, while *Osr1* expression extends proximally in the limb bud. (C, right) At E12.5 *Osr1* and *Osr2* domains of expression are mostly exclusive, with *Osr2* expression confined more distally than *Osr1* expression, overlapping with digit condensations. (D) In the mouse *Osr1* is strongly expressed in the connective tissue of e.g. the tongue mesenchyme as well as in kidneys revealed by dual immnunohistochemical analysis using an anti-MyHC antibody to label muscle fibers and an anti-GFP antibody to assess *Osr1* reporter expression in Osr1$^{GCE/+}$ mice (Mugford et al., 2008). K, Kidneys. Adapted from Stricker et al. (2006) and Braid et al. (2010).

Furthermore, experiments using primary chicken cells demonstrated the role of OSR1 conferring connective tissue properties and concomitantly repressing chondrogenesis in chick primary limb mesenchyme cultures and osteogenesis in chick bone marrow stromal cell (BMSCs) cultures (Stricker et al., 2012). In vivo a similar effect was assigned to *Osr1* in the mouse tongue mesenchyme (Liu et al., 2013), where *Osr1* is highly expressed (Figure 6D1). In mouse limbs, *Osr1* function remains largely elusive.

4.7 Chemokines signaling molecules orchestrate tissue formation

Chemokines are small proteins classified in four groups depending on the two first cysteine residues, highly conserved in all chemokines. Chemokines are either secreted or membrane-bound proteins and exert their function through binding to G-protein-coupled seven-transmembrane receptors. Binding to their correspondent receptors, chemokines provide positional information to responsive cells that typically move towards a gradi-

ent of chemokine concentration (chemotaxis) or change cellular properties induced by signaling cascades downstream of their receptors (Raz and Mahabaleshwar, 2009).

Chemokines were commonly related to immune response trafficking and activation. They can be functionally classified in inflammatory chemokines depending on their abilities to recruit white blood cells in an inflammatory response (Luster et al., 1998) or in static chemokines, constitutively expressed by specific cell types. Static chemokines are also involved in several immune and also in non immune-related processes. In addition to their well-characterized roles in immune cell biology, static chemokines have been described to play crucial roles in a wide range of developmental processes among different species.

Immune cells are guided by static chemokines secreted from resident tissues to orchestrate the formation of lymphoid organs, as the initiation and maintenance of the secondary lymphoid organs during development or de novo formation of tertiary lymphoid tissues under acute inflammation conditions. The initiation of secondary lymph organs, such as spleen, lymph nodes or Peyert's patches, involves clustering of hematopoietic lymphoid-tissue inducer cells (LTi) with stromal organizer cells of mesodermal origin. This interaction triggers, via lymphotoxin-beta-receptor and lymphotoxin-$\alpha\beta$ ligands, the production of chemokines and attraction molecules in stromal organizer cells that retain and cluster LTi cells in the primordium of lymph nodes. The principal chemokines involved in this early step of lymphoid organ formation and posterior maintenance of secondary lymphoid organs are CXCL13, CCL19 and CCL21. Amongst the lymphoid chemokines, only CXCL13 was revealed to be crucial in the initiation step of lymph node formation and is induced by retinoic acid signal from the adjacent nervous system (van de Pavert et al., 2009). Although the three chemokines are involved in homing of LTi cells only the combined elimination of CXCL13, CCL19 and CCL21 or their corresponding receptors CXCR5 and CCR7 respectively results in the absence of most lymph nodes (Ohl et al., 2003).

Chemokines have been described to play manifold functions in the central nervous system. Previously described lymphoid chemokines are expressed in the CNS during homeostasis and also in disease (Lalor and Segal, 2010). Beyond the variety of chemokines involved in central nervous system (CNS) disease, recent studies highlighted the role of chemokines and chemokine receptors in physiological conditions during developmental processes. Among the different roles described for chemokines in the CNS, it is worth mentioning the modulatory capacities of CXC chemokines and their receptors such as *Cxcl2* and *CxcR2*, in neurotransmitter release (Ragozzino et al., 1998). Furthermore, other chemokines exert rather constitutive function in CNS as neuroprotective agents (Meucci et al., 2000).

The most widely characterized chemokine/receptor axis is the one formed by the

chemokine CXCL12 and its receptors CXCR4 and CXCR7. The CXCL12/CXCR4/7 axis is involved in many physiological processes during development and diseases and has been shown to direct cell migration and influence cell behavior in several tissues and organisms. Similar to the already mentioned lymphoid chemokines, CXCL12 exerts a crucial function in secondary lymph organ formation recruiting B-lymphocytes to the locations of lymph node formation (Okada et al., 2002). Additionally, the properties of this chemokine/receptor axis have been investigated in several processes of directional movement in neurons during CNS and peripheral nerve formation. During peripheral and CNS development binding of CXCL12 to CXCR4 or CXCR7 leads to the activation of receptor downstream targets that regulate cell proliferation, migration and survival processes (Li et al., 2008). One example is the role of *Cxcl12* and *Cxcr4* directing the projections formed by motor neurons of the peripheral nervous system (Lieberam et al., 2005).

The zebrafish model enables imaging of live cell processes during development and allows the use of genetics tools to accomplish their understanding. In zebrafish, the formation of the sensory organ lateral line has been shown to be driven by the interaction of CXCL12a and its receptor CXCR4b. The mass of cells in the posterior lateral line primordium moves collectively along the rostral-caudal axis of the animal in a process depending on the path defined by CXCL12a and CXCR4b (Haas and Gilmour, 2006). Interestingly, a variant of the implication of the chemokine Cxcl12 in cell movement is the instruction to maintain a stable position. During zebrafish gastrulation this signaling pathway coordinates the combined movement of endodermal and mesodermal cells, activating integrin-dependent endodermal cell adhesion (Raz and Mahabaleshwar, 2009).

A recent study has highlighted the role of this chemokine in the formation of coronary vessels in the zebrafish heart. In the juvenile zebrafish heart, endothelial cells derived from the endocardium sprout onto the ventricle to create a vascular network under the guidance of CXCL12a (Harrison et al., 2015). Apart from its developmental role in vascular formation, it is worth to mention the wide range of chemokines found either inhibiting angiogenesis or promoting the formation of vessels in physiological conditions as well as disease and cancer (Salcedo and Oppenheim, 2003).

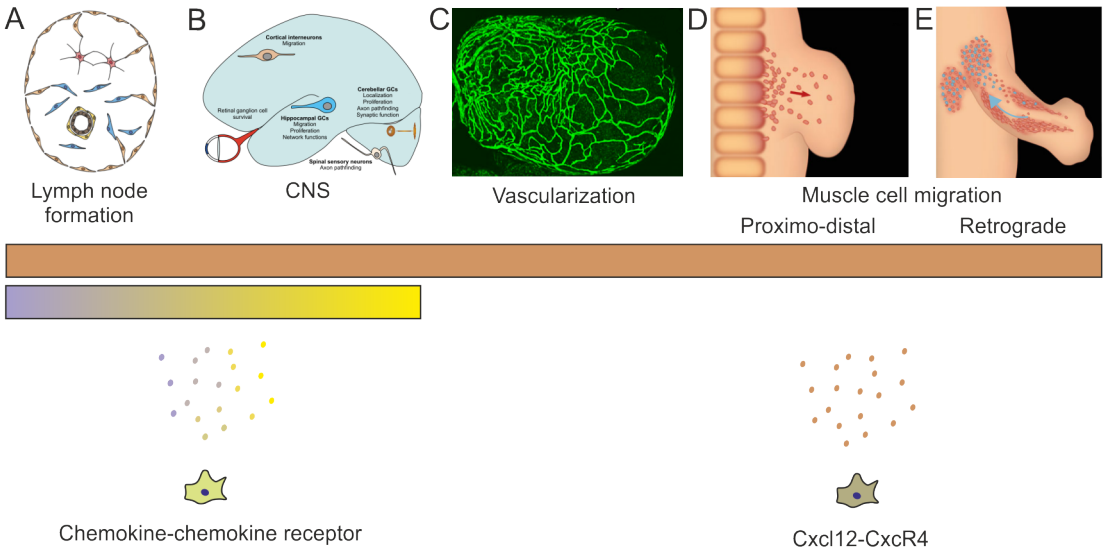

Figure 7: **Chemokines orchestrate tissue formation in several developmental processes.** (A) During lymph node formation, chemokines from mesenchymal precursors organize and structure the developing lymph node. (B) Many chemokines have been involved during CNS formation. (C) The CXCL12/CXCR4 axis in the developing zebrafish embryo guides coronary vessel formation. (D, E) *Cxcl12* influences the path of *Cxcr4*-expressing muscle precursor cells into the limb bud and during retrograde migration to form muscles outside the limb. Modified from Harrison et al. (2015), Klein and Rubin (2004), Aguzzi et al. (2014), Brand-Saberi (2015)

The interaction between the chemokine *Cxcl12* and its receptor *Cxcr4* has been also described to play an important role in limb skeletal muscle formation during development, tissue injury and regeneration. During embryonic development, muscle progenitors located in the hypaxial regions of the dermomyotome delaminate and migrate into their targeted places guided by signals provided by the limb mesenchyme. *Cxcl12* is expressed in limb mesenchyme and influences the CxcR4+ muscle progenitors in the pathfinding process into the limb. Lack of *Cxcr4* in *Cxcr4*$^{-/-}$ mouse mutant embryos led to mild impairment in muscle progenitor migration into the distal part of the forelimb (Vasyutina et al., 2005) and to perturbation of the limb musculature (Odemis et al., 2005). Lineage tracing experiments in chick reported that migration of CXCR4+ muscle progenitors not only occurs in the proximal/distal axis. Some myogenic cells exhibit a retrograde movement finding their target places soon after they have entered the limb. Formation of muscle of the cloacal region is another example. Perturbation of CXCL12/CXCR4 signaling in chick hindlimbs leads to a disturbed migration of myogenic cells towards the cloacal region (Rehimi et al., 2010). Similarly, muscles of the shoulder girdle are formed by myogenic cells that exhibit a retrograde migration, first entering the limb and after migrating back to the shoulder region. This "in-Out" mechanism of secondary trunk muscles was disturbed after manipulation of the CXCL12/CXCR4 signaling leading to defective limb girdle musculature (Masyuk et al., 2014).

The capacities of the CXCL12/CXCR4 axis to promote stem cell migration during embryogenesis have been intensively investigated in several organisms. Expression of *Cxcr4* is also found in muscle stem cells, satellite cells, and the role of this axis during skeletal muscle regeneration has started to be elucidated. Inhibition of the axis after muscle injury using siRNA or inhibitors directed to each of the components resulted in impaired muscle repair (Bobadilla et al., 2014). Although the role of chemokines during muscle regeneration must be further investigated, the intricate relations between immune cells and muscle resident cells to achieve proper regeneration suggest an important role of chemoattractant molecules in this process.

Additionally, cell culture experiments in the C2C12 muscle cell line indicated the differential expression of several chemokines and their respective receptors during the process of myogenic differentiation. During this period myoblasts exhibited a restriction of their migratory capacities and preferentially respond to changes in Cxc12/Cxcr4 axis rather than other migratory factors for myoblasts, such as SF/HGF or Ephrina5 (Griffin et al., 2010). Chemokines are usually secreted to the extracellular medium and in the case of Cxcl12, its interaction with proteoglycans of the extracellular matrix has been shown to play a role in tissue revascularization (Rueda et al., 2012). The way CXCL12 is presented to Cxcr4+ C2C12 cells, either soluble or bound to a matrix of proteins, influences the migratory capacities as well as their myogenic properties in culture (Dalonneau et al., 2014). Therefore, structural changes in ECM assembly would lead to chemokine indirect effects, being both necessary for correct cellular migration and consequently tissue organization.

4.8 Extracellular matrix involvement in myogenesis

Contrary to the simplistic view as a scaffold for cells, the last two decades of research have changed this view about the ECM. The ECM has in addition to its role as structural component a widespread functional importance in many cellular processes (Rozario and DeSimone, 2010). In the same time period, the accumulated knowledge about the molecular mechanisms involved in myogenesis has led to breakthroughs that have changed our view of this process. In contrast, our understanding about the influence of the ECM on the processes that govern muscle formation is more limited.

Components of the ECM can be classified into several families of glycosaminoglycans and proteoglycans depending of their structure. Large families of proteins such as collagens and laminins interact with other less diverse components such as elastin, fibulin, fibrillin, tenascin or small leucine-rich proteoglycans (SLRP) conferring the appropriated cellular environment. Far from being a static entity, the ECM is a highly dynamic structure that adapts to the necessity of each developmental process. During skeletal muscle

formation, myogenic cells proliferate, migrate, differentiate and fuse with each other to form multinucleated myotubes. All these processes need the right environment to develop, thus ECM is maintained in a continuous remodeling assuring the accomplishment of these processes.

ECM influence on myogenic cells is observed very early during development, already before they become committed to the myogenic lineage. Fibronectin is found surrounding the early dermomyotomes and was proposed to be essential in the apical polarization of N-cadherin in dermomyotomal cells (Martins et al., 2009), thus maintaining dermomyotome integrity and epithelial state (Cinnamon et al., 2006). This state is thought to be crucial to keep muscle progenitors in an uncommitted and proliferative state. Muscle progenitors from the hypaxial regions of the dermomyotome lose their epithelial state and acquire mesenchymal characteristics in a process of epithelial to mesenchymal transition (EMT) that allow them to migrate through long distances. Prior migration, epithelial muscle progenitors detach from the dermomyotome losing their cadherin-based adhesion and secreting matrix metalloproteinase that lead to the dissociation of the epithelial structure. Activation of EMT has been associated with upregulation of focal adhesion kinases typical for migrating cells (Desiderio, 2007). The characteristics of the matrix encountered by migrating myogenic cells once they have become activated as well as the ECM interactions they build during migration are poorly characterized but seem to be crucial for the migration process. Antibodies against the hemophilic binding site of N-cadherin demonstrated that interactions between myogenic cells and mesenchymal cells are necessary for myogenic cell pathfinding through the limb bud mesenchyme (Brand-Saberi et al., 1996). The adaptability of the ECM-state during muscle formation has been better characterized in amphibians. Amphibians possess high regeneration capacities that allow them to regenerate whole appendages and are broadly used as a model to study the process of limb regeneration. During this process a transitional ECM accompanied the re-structured blastema. Collagens such as collagen type I and II are downregulated, while a matrix of hyaluronic acid, fibronectin and tenascin-C replace them to assure migration, myotube fragmentation and myoblast fusion in the regenerating area (Calve et al., 2010).

Furthermore, secreted factors bind to the ECM, which modulates their spatiotemporal activity and availability. The SLRP decorin is a well-characterized example how the ECM regulates ligand activity. Decorin binds to the soluble ligands of the transforming growth factor beta (TGF-β) signaling pathway and consequently modulates skeletal muscle formation (Brandan et al., 2008).

During the successive processes of splitting and segregation of muscle masses, new components of the ECM are secreted that delimit proliferation and differentiation of myogenic cells and at the same time provide a structure for the nascent myofibers. Connective

tissue cells secrete ECM-components and recent studies have highlighted the role of these cells establishing a prepattern for muscle formation and playing a key role in muscle patterning and maintenance (Kardon et al., 2003; Hasson et al., 2010; Mathew et al., 2011). However, neither the signaling molecules nor the rearrangement in the ECM necessary to fulfill correct muscle patterning have been identified.

As soon as multinucleated fibers are formed, these must be connected to the ECM and also to the tendons to allow force transmission. This requires a maturation of the ECM as well as the expression of specialized adhesion proteins by the myofibers. These adhesion proteins form the so-called costameres that physically couple the contraction complex in the sarcoplasm with the extracellular scaffold (Figure 8B). The sarcolemma contains transmembrane proteins as the dystroglycan complex and integrins that are coupled to the cytoskeleton at the inner side of muscle cells. On the outer side, the closest sheet of extracellular proteins is called the basal lamina that builds a continuous framework with the outer ECM. The costamere complexes tightly couple the myofibers to the basal lamina and hence to the ECM. Defective costamere proteins as well as components of the ECM have been involved in many distinct myopathies reflecting their critical role in muscle maintenance (Brandan et al., 2008; Ameye and Young, 2002; Bönnemann, 2011).

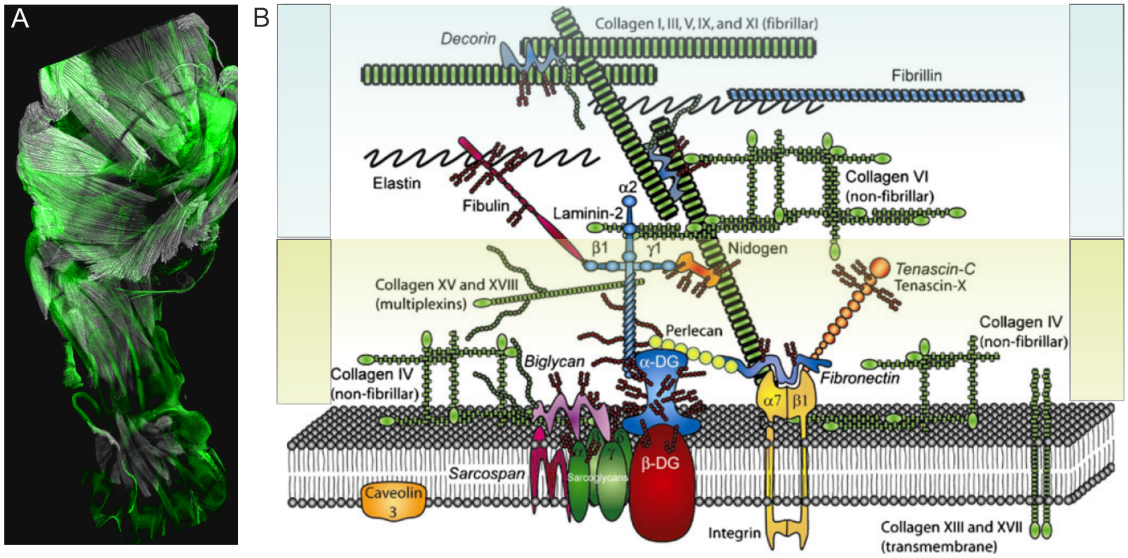

Figure 8: **ECM sustains muscle formation**. (A) 3D-representation after whole mount immunohistochemistry of E14.5 mouse forelimb revealing the interaction of the type XII collagen (green) with muscles (grey). Highly expressed in tendons and at lower levels in connective tissue, type XII collagen directly interacts with muscles at the interface muscle-tendon (B) Schematic representation of proteins involved in costamere formation. Transmembrane protein complexes such as dystroglycan and integrins complexes associate the sarcolemma with panoply of proteins outside the myofiber that create a structured scaffold. The closest extracellular matrix to the sarcolemma is the so-called basal lamina (e.g. Collagen IV, Laminins) that is via non-fibrillar components such as Collagen VI linked to the densely packed matrix of fibrillar collagens (e.g. Collagen I and III). β-DG, dystroglycan-beta. Modified from Nedergaard et al. (2013).

Lately, the ECM has regained increasing interest impinging on myogenic stem cell (satellite cell) maintenance. Myogenic progenitors acquire a satellite cell position, wedged within the basal lamina and the plasma membrane of the myofiber at late fetal stages in the mouse (MAURO, 1961). The Notch signaling pathway has been recently involved in the homing of satellite cells instructing them to build their own microenvironment, secreting their own basal lamina and adhering to the muscle fibers. Disturbing this process of homing and basal lamina assembly compromises the myogenic capabilities of satellite cells (Bröhl et al., 2012). The ECM is dynamically remodeled during regeneration (Goetsch et al., 2003) and it was shown that fibronectin plays a key role in satellite cell expansion via influencing Wnt7a signaling during this process (Bentzinger et al., 2013).

4.9 Aims of the study

Formation of complex systems in the body demands the precise coordination and connection of different tissues. Despite the important functions assigned to connective tissue, its characterization is still in its infancy due the lack of specific markers.

Previously, our group has characterized the dynamic expression pattern of the transcription factor OSR1 during chick development and postulated that OSR1 could be a novel connective tissue marker. Moreover the embryonic expression of *OSR1* in both chick and mouse strongly correlated with areas of active myogenesis indicating that this transcription factor might be involved in musculoskeletal system development. However, the *OSR1* functional relevance in muscle connective tissue and influence on musculoskeletal system patterning remain elusive.

The aim of the study was to unravel the influence of *Osr1* on musculoskeletal development using mouse genetic tools. The first aim was to characterize the *Osr1* expression pattern during limb formation in detail with special emphasis on its relation with muscle development. Second, a task was to shed light on the contribution of *Osr1* expressing cells to mouse embryonic tissues, i.e. to unravel the developmental potential of Osr1+ cells. The main aim however was to assess the importance of *Osr1* for musculoskeletal system formation using a mouse model lacking *Osr1* and further phenotypic characterization of musculoskeletal impairments using histological and biochemical methods. Special interest lay on the elucidation of downstream targets of *Osr1* to find candidates by which Osr1+ connective tissue cells might orchestrate musculoskeletal formation.

5 Material

5.1 Instruments

Table 1: Centrifuges

Name	Supplier
Microtiter plate centrifuge 5416	Eppendorf
Micro centrifuge 5415 D	Eppendorf
Chilling centrifuge 5417 R	Eppendorf

Table 2: Thermo cyclers

Name	Supplier
GeneAmp PCR System 2700	Applied Biosystems
GeneAmp PCR System 2720	Applied Biosystems
GeneAmp PCR System 9700	Applied Biosystems
ABIPrism HT 7900 Real-time Cycler	Applied Biosystems

Table 3: Microscopy

Name	Supplier
Microscope DMR	Leica
Camera AxioCam HRc	Zeiss
Camera AxioCam MRm	Zeiss
Stereo microscope MZ6	Leica
Stereo microscope MZ7-5	Leica
LSM700	Zeiss
LSM710 NLO	Zeiss

Table 4: Histology

Name	Supplier
Microtome Cool Cut HM355S	Microm
Microtome 2050 Supercut	Reichert-Jung
Cryotome H560	Microm
Embedding station EC 350-1&2	Microm
Dehydration stationTP 1020	Leica

Table 5: Other instruments

Name	Supplier
Plate reader Spectra Max 250	Molecular Devices
Nanodrop2000	Thermo Scientific
Bioruptor UCD-300	Diagenode
TissueLyser	Quiagen

5.2 Chemicals

Unless stated otherwise, chemicals were obtained from Merck (Darmstadt), Roth (Karlsruhe) or Sigma-Aldrich (Hamburg, Seelze, Schnelldorf and Steinheim).

5.3 Buffers

If not mentioned otherwise, all solutions were prepared according to Sambrook, et al. 2001.

5.4 Kits

The following kits were used according manufacturer's instructions to perform standard procedures, such as RNA purification, cDNA-synthesis, DNA-sequencing and protein concentration.

Table 6: Kits

Name	Supplier
NucleoSpin Plasmid	Macherey-Nagel
Nucleobond PC100	Macherey-Nagel
NucleoSpin Gel and PCR Clean-up	Macherey-Nagel
TaqMan Reverse Transcription Reagents	Roche/Applied Biosystems
BigDye Terminator v3.1 Sequencing Kit	Applied Biosystems
BCA Protein Assay Kit	Pierce
RNAeasy-Kit	Qiagen
SYBR Green qPCR Master Mix	life Technologies
GOTaq qPCR Master Mix	Promega

5.5 Plasmids

Table 7: Vector

Name	Application	Supplier
pTAgfp	sub cloning of PCR products	Dr. Jochen Hecht (MPIMG, Berlin)

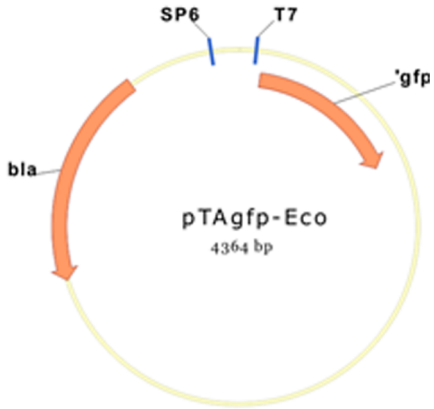

Figure 9: **Simplification of the pTAgfp plasmid**.

5.6 Antibodies

Table 8: Primary antibodies

Name	Host	Product number	Dilution	AR
Human-MyHC	Mouse	05-716	1:500	Yes(1,2)
GFP	Rabbit	TP401	1 μg/ml	No
GFP	Chicken	Ab13970	10 μg/ml	No
Human-Desmin	Goat	AF3844	0,2 μg/ml	No
Lbx1	Guinea pig	Provided*	1:20.000	No
Chick-Pax7	Mouse	Pax7	1:50	Yes(2)
Human-Col4a1	Goat	Ab769	10 μg/ml	No
panColVI	Rabbit	Ab6588	1 μg/ml	No
Human-a-SMA	Rabbit	Ab5694	2 μg/ml	No
Mouse Pecam1	Hamster	2H8	1:250	No
Human-Laminin	Chicken	Ab14055	5 μg/ml	No
Col12a1	Rabbit	Provided**	1:500	No
Col14a1	Rabbit	Provided**	1:500	No
anti-ColI	Goat	1310-01	1:100	No
anti-βTubulinIII	Mouse		1:200	No
Human-Vinculin(7F9)	Mouse	SC-73614	2 μg/ml	No
N-Cadherin	Rabbit	SC-7939	2 μg/ml	No
Human-TCF4	Rabbit	C48H11	0,2-2 μg/ml	No
Mouse-PdgfRa	Goat	BAF1062	4 μg/ml	No
MyoD(C20)	Rabbit	SC-304	2 μg/ml	No
Vimentin	Rabbit	SC-5565	1:100	No
MyoD	Rabbit	Provided*	1:4000	No
Fibronectin	Mouse	F0791	1:100	No
N-Cadherin	Rabbit	AB12221	1:100	No
Cleaved caspase3	Goat	9661(CS)	1:100	Yes(3)
anti-BrdU	Sheep	AB1893	1:50	Yes(3,4)
anti-p44/p42 MAPK	Rabbit	9101(CS)	1:100	No

Antibodies kindly provided by Prof. C. Birchmeier-Kohler* and Prof. Manuel Koch**. Performed antigen retrieval are described in the section 6.3.4.

Table 9: Secondary antibodies and conjugated molecules

Name	Host	Product number	Dilution
568, 488 and 680	Donkey	Anti-mouse	4 μg/ml
568, 488 and 680	Donkey	Anti-rabbit	4 μg/ml
568,488 and 680	Donkey	Anti-goat	4 μg/ml
565 and 488	Goat	Anti-hamster	4 μg/ml
568 and 488	Goat	Anti-guinea pig	4 μg/ml
565, 488 and 680	Goat	Anti-chicken	4 μg/ml
488-streptavidine			
Texas Red Phalloidin			

Alexa FLuor antibodies were purchased from life technologiesTM.

5.7 Bacteria

Table 10: Bacterial strains

Name	Application	Supplier
E. coli Top10	cloning	Invitrogen

5.8 Primer

All primers were synthesized by MWG Biotech AG (Ebersberg) and HPSF purified.

Table 11: Primer for RTqPCR

Primer name	Primer sequence 5' –> 3'
Gadphfw	CTGCACCACCAACTGCTTAG
Gadphrev	GGATGCAGGGATGATGTTCT
Osr1fw	GCACACTGATGAGCGACCT
Osr1rev	TGTAGCGTCTTGTGGACAGC
Osr2fw	CACACAGACGAGAGGCCATA
Osr2rev	GCAGCTGTAGGGCTTGATGT
Tcf4fw	AAGCCTCCAGAGCAGACAAA
Tcf4rev	TAAGTGCGGAGGTGGATTTC
Col3a1fw	CTAAAATTCTGCCACCCCGAA
Col3a1rev	AGGATCAACCCAGTATTCTCCACTC
Col6a1fw	CGTGGATGCGGTCAAGTA
Col6a1rev	CCAGGTGTTTGGCCTCATTT
Col6a2fw	TTCCCTGCCAAACAGAGC
Col6a2rev	ATATTGCAACAGAGCCATGC
Col6a3fw	AGGCCGTACTCAAGCTTTCC
Col6a3rev	AGCAAACATGGCAGGTAAGG
Col6a5fw	AGGCCGTACTCAAGCTTTCC
Col6a5rev	AGCAAACATGGCAGGTAAGG
Col6a6fw	AGGCCGTACTCAAGCTTTCC
Col6a6rev	AGCAAACATGGCAGGTAAGG
Col12a1fw	CAGAGGATATCATTTGAACTCACAC
Col12a1rev	AGCATCCTTGTATGTGACGTG
Col14a1fw	GCTCCACCCACAAGGTTAAG
Col14a1rev	CTGGCAGAAGGCCTTGAATA
Cxcl12fw	GCTCCACCCACAAGGTTAAG
Cxcl12rev	CTGGCAGAAGGCCTTGAATA
Sox9fw	GCTCCACCCACAAGGTTAAG
Sox9rev	CTGGCAGAAGGCCTTGAATA
Sox5fw	GCTCCACCCACAAGGTTAAG
Sox5rev	CTGGCAGAAGGCCTTGAATA
beta-actinfw	CTGTATTCCCCTCCATCGTG
beta-actinrev	GGAGAGCATAGCCCTCGTAG
Scxfw	CCTTCTGCCTCAGCAACCAG
Scxrev	GGTCCAAAGTGGGGCTCTCCGTGACT
Tnmdfw	AACACTTCTGGCCCGAGGTAT
Tnmdrev	AAGTGTGCTCCATGTCATAGGTTTT
Mkxfw	AGTAAAGACAGTCAAGCTGCCACTG
Mkxrev	TCCTGGCCACTCTAGAAGCG
Runx2fw	GGTCCCCGGGAACCAA
Runx2rev	GGCGATCAGAGAACAAACTAGGTTT

Table 12: Standard cloning primer

Primer name	Primer sequence 5' –> 3'
T3Promoter	TAATACGACTCACTATAGGG
T7Promoter	CATTTAGGTGACACTATAG
Sp6Promoter	AATTAACCCTCACTAAAGGG

Table 13: Primer for genotyping

Primer name	Primer sequence 5' –> 3'
Osr1-wt	GGATGACACAGTTTCTGTTTGG
Osr1-het	AGCCAGGAAGAGCACATCAC
Osr1-KO	CCATCGGTTCCATAACTTCG
mTmGfw	AAGCTGAGAGCCCTGTGTGT
mTmGrev	TTTTGCTGCACACCTGACTC

5.9 Imaging software

Table 14: Software

Application	Software	Developer
Microscopy imaging	Axio Vission Rel. 4.8	Axio Vision Application
Microscopy imaging	Zen 2010	Zeiss
Image processing	ImageJ	Wayne Rusband (NIH,USA)
Image processing	CoralDRAW X6	Corel
Image processing	Photoshop CS5	Adobe
Image processing	Illustrator CS5	Adobe
3D imaging	Amira 5	FEI visualization Sciences Group
3D imaging	FluoRender 2.13	University of Utah

5.10 Other software

Table 15: Other Software

Application	Software
Data analysis and text processing	Microsoft Office
RTqPCR analyses	SDS 2.1
FACS sorting	FACSDIVATM
FACS analyzing data	FlowJo
Statistical analyses	GraphPad Prism 5

5.11 Internet resources

Table 16: Internet resources

Resource	Address
UCSC Genome Browser	http://genome.ucsc.edu/
NCBI	http://www.ncbi.nlm.nih.gov/
Ensembl Genome Browser	http://www.ensembl.org/index.html
Eurexpress	http://www.eurexpress.org/ee/

5.12 Mouse lines

- ***Osr1***$^{GCE/ERT}$ **line**

  Created by homologous recombination in the lab of Andrew McMahon the *Osr1* line provided a useful genetic tool to study the importance of the transcription factor OSR1 (Mugford et al., 2008). The strategy used resulted in the insertion of the targeted vector eGFPCreERt2 (GCE) that replaced the start codon of *Osr1* positioned in the second exon (Figure10). This mouse line allowed:

  - Address *Osr1* expression in the mouse after visualization of the protein eGFP under the control of *Osr1* regulatory elements.
  - Temporal activation of the targeted Cre recombinase by Tamoxifen induction.
  - Inactivation of OSR1 activity and loss-of-function experiments.

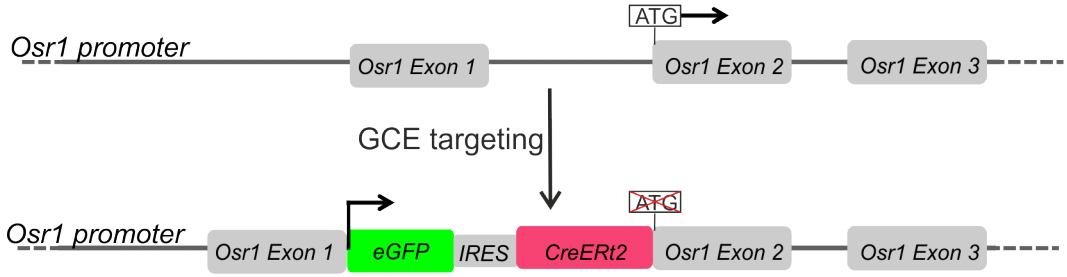

Figure 10: **Simplification of the genetic strategy used by Mugford and colleagues to create the Osr1^{GCE} mouse line**. Insertion of the GCE cassette and replacement of the ATG codon in the second exon of *Osr1* led to the expression of the protein GFP under the control of *Osr1* regulatory elements and simultaneously loss-of-function of OSR1. Adapted from Mugford et al. (2008).

- **R26mTmG line**

  The reporter line R26mTmG (Muzumdar et al., 2007) was used in combination with the above mentioned Osr1^{GCE} line to achieve lineage tracing of Osr1+ cells. In R26mTmG-animals a membrane-targeted Tomato protein (mT) is ubiquitous expressed under the control of the strong pCA regulatory elements. pCA consists of a chicken b-actin core promotor with a cytomegalovirus (CMV) enhancer. The mT excision achieve after recognition of flanked LoxP sites (Figure11) by Cre recombinases lead to cellular specific expression of the targeted-membrane GFP protein (mG).

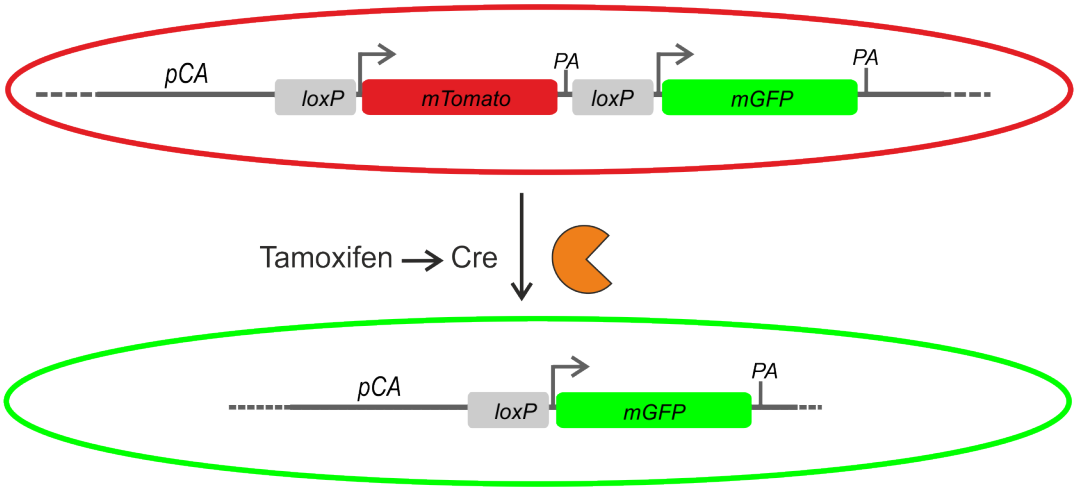

Figure 11: **Schematic representation of the double reporter cassette mTmG and further excision by Cre recombinases**. In R26mTmG-animals a membrane-targeted Tomato protein (mT) is ubiquitous expressed under the control of the strong pCA regulatory elements. pCA consists of a chicken β-actin core promotor with a cytomegalovirus (CMV) enhancer. The mT excision achieved after recognition of flanked LoxP sites (Figure11) by Cre recombinases lead to specific expression of the targeted-membrane GFP protein (mG). PA, polyadenilation signal sequence. Adapted from Muzumdar et al. (2007).

- ***Pax3^{GFP}* line**

  Kindly provided by Prof. Frédéric Relaix *Pax3*$^{+/+}$, *Pax3*$^{GFP/+}$ and *Pax3*$^{GFP/GFP}$

E11.5-E13.5 embryos were used to asses *Osr1* expression in limbs devoid of muscles (Relaix, 2006). Insertion of the reporter gene GFP in the *Pax3* locus allowed visualization of *Pax3* expression and loss-of-function experiments of the *Pax3* gene.

6 Methods

6.1 Molecular Biological Methods

Classic molecular biology experiments described in this section were performed following the handbooks "Molecular Cloning: A Laboratory Manual" (Sambrook, et al., 2012).

6.1.1 Isolation of genomic DNA

Determination of animal genotypes was achieved after genomic DNA extraction of small animal biopsies. Animal tissue was digested using two different methods. The first method includes tissue digestion overnight in 0.5 ml SDS-buffer with 200 μg/ml of the endopeptidase proteinase K at 55°C. The following day, 0.25 ml 5 M NaCl was added and incubated 10 min at RT. Directly after incubation samples were placed on ice for 10 min. Debris were spun down before for 10 min at 8000 rpm and 4°C. The supernatant was transferred into a new tube and 1 ml ice-cold ethanol was added. Precipitates were centrifuged for 10 min at 13000 rpm and 4°C discarding the supernatant. The pellet was washed twice with 500 μl 70% EtOH prior dissolving it in 100 μl of ddH_2O. The second method is based in the partially digestion of animal tissue with the compound QuickStract (QE09050). Animal biopsies were digested for 20 min at 68°C in 50 μl quickstract prior inactivation at 98°C during 2min.
SDS-buffer: 0.85% SDS, 17 mM EDTA; pH 8, 170 mM NaCl, 17 mM Tris; pH 7.5

6.1.2 Total RNA isolation

6.1.2.1 RNA extraction from tissue

Fresh isolated embryonic tissue was either directly processed for RNA-isolation with RNeasy kit (Quiagen 74104) or frozen in liquid nitrogen for longer storage. Following manufacture protocols, tissue was disrupted using a plastic pestle, which fitted to a 1.5 ml tube. After disruption RLT-buffer was immediately added and tissue was homogenizes passing at least 5 times through a 20-gauge needle fitted to a 1 ml syringe. The same volume of 70% ethanol was added to clear the lysate and provide appropriate binding conditions before the solution was filtered through an RNeasy spin column, which will bind the isolated RNA to its silica-based membrane. High-salt buffers allow RNA longer than 200 bases to bind to the column. RNA was eluted in 30 μl nuclease-free water.

6.1.2.2 RNA extraction from isolated cells

FACS sorting approaches were used to isolate fluorescence labeled cells. From this approaches only a limited amount of cells was obtained. Therefore RNA isolation was modified to ensure maximum RNA yields. Cells were directly collected in serum coated polylipren 4.5 ml tubes (BD biosystems). Sorted cells were concentrated by centrifugation at 1200 rpm. Prior disruption in RLT-buffer (RNeasy kit, Quiagen 74104), cells were resuspended in 1x PBS and centrifuged again at 1200 rpm. On-column RNA extraction followed as above described.

RNA was measured spectrophotometrically using Nanodrop 2000. Possible RNA-degradation and presence of genomic DNA was proofed loading 1μl of isolated RNA on 1% agarose gel or using 2100 Bioanalyzer System (Aligent technologies) in case samples followed next-generation sequencing.

6.1.3 cDNA synthesis

Taqman reverse transcription system (life technologiesTM N8080234) provides all the components for RNA reverse transcription on base of a Moloney murine leukemia virus retro-transcriptase. 1 μg of RNA from prepared tissue or 100-500 ng in the case of FACS isolated cells was used as template for each reaction. cDNA was synthesized following manufacturer instructions. Synthesized cDNA was accordingly diluted for subsequently PCR and RT-qPCR analyses.

6.1.4 Synthesis of digoxigenin labeled RNA-transcript

Every transcript was subcloned in the pTA-GFP plasmid, which contains T7 or T3 and SP6 binding positions at both sides of the inserted element. Thus, synthesized transcripts by PCR can be easily subcloned and sequenced. Sequence and orientation of the transcript was verified after sequencing using the following PCR with T7 or T3 and SP6 primers.

Amplification of the desired transcript using PCR-reaction, see tables 18and 17, was followed by DNA-extraction using Nucleo-spin Gel and PCR extraction from Macheray and Nagel. The RNA-polymerase will specifically recognize the antisense sequence (T7, T3 or SP6) and synthetizes using digoxigenin labeled nucleotide (DIG) a labeled antisense sequence of the transcript. The new synthetized RNA was protected from possible degradation by RNase adding 1 μl of RNA-inhibitor (Roche) to the 20 μl mix. Transcription was performed after 2 hours of incubation at 37°C or 40°C for SP6 polymerase. After incubation the volume was filled up until 100 μl with DEPC-water. Finally, the polymerase was heat-inactivated for 10 minutes at 96°C.

6.1.5 Polymerase chain reaction (PCR)

6.1.5.1 Amplification of DNA

Generally, genes were amplified from appropriate cDNA or plasmids with a Pfu/Taq-polymerase mixture and cloned into pTA-GFP plasmid if needed, where their sequence fidelity was determined by Sanger-sequencing. The reagents conataining a mixture of 1:10 Pfu/Taq-polymerase were pipeted, according to the described protocol in Table17, into a chilled 0.2 ml reaction tube and incubated in a thermo cycler as described in Table 18.

Table 17: Amplification PCR

Amount	Reagent
200 ng	DNA template
2.5 μl	10x reaction buffer (provided by the institute)
1.5 μl	dNTPs (1.25 mM, Fermentas)
1 μl	T7 or T3 Promoter (10 μM)
1 μl	SP6 Promoter (10 μM)
0.5 μl	DNA polymerase
add to 25 μl with ddH H_2O	

Table 18: Amplification PCR

Phase	Temperature	Time	Cycles
initial denaturation	95°C	5 min	
denaturation	95°C	30 sec	
primer annealing	58°C	30 sec	35 cycles
elongation (*Taq*/*Pfu*)	72°C	1 min	
final elongation (*Taq*/*Pfu*)	72°C 7 min		
end	94°C	∞	

PCR products were analyzed on 1.5% agarose gels.

6.1.5.2 Colony PCR

This method is an easy and quick variant of the amplification method to identify successful sequence insertion and its orientation in a plasmid. Bacterial colonies can be used directly as DNA templates. The colonies were picked with sterile pipette tips, streaked out on a replica-plate (LB-agarose) and dipped into a PCR tube containing standard PCR reaction mix.

6.1.5.3 Genotyping of *Osr1*$^{GCE/ERT2}$ animals

Extracted genomic DNA from either adult animals or embryos was used to determine *Osr1* genotype. Following the PCR protocols described below, amplification of two DNA fragments was expected. A fragment of 273 paired bases (pb) corresponding to the *Osr1* wild type allele or a fragment of 700 pb corresponding to the targeted GCE allele.

PCR products were analyzed on 1.5% agarose gels.

Table 19: PCR *Osr1* genotyping

Amount	Reagent
1 μl	DNA template
2.5 μl	10x reaction buffer (provided by the institute)
2 μl	dNTPs (1.25 mM, Fermentas)
2 μl	Osr1-het (10 μM)
1 μl	Osr1-WT (10 μM)
1 μl	Osr1-KO (10 μM)
0.5 μl	DNA polymerase
add to 25 μl with ddH H_2O	

Table 20: PCR *Osr1* genotyping

Phase	Temperature	Time	Cycles
initial denaturation	95°C	5 min	
denaturation	95°C	1 min	
primer annealing	56°C	1 min	35 cycles
elongation (*Taq*)	72°C	1 min	
final elongation (*Taq*)	72°C	10 min	
end	4°C	∞	

6.1.5.4 Genotyping of R26mTmG animals

Similarly as for *Osr1* genotyping PCR, mTmG genotyping proceeded as described below. Amplification of a 320 pb fragment was expected for wild the wild type and a 250 pb long fragment for the targeted allele.

PCR products were analyzed on 1.5% agarose gels.

Table 21: PCR R26mTmG genotyping

Amount	Reagent
1 μl	DNA template
2.5 μl	10x reaction buffer (provided by the institute)
2 μl	dNTPs (1.25 mM, Fermentas)
2 μl	mTmGF (10 μM)
1 μl	mTmGfw (10 μM)
1 μl	mTmGrev (10 μM)
0.5 μl	DNA polymerase
add to 25 μl with ddH H_2O	

Table 22: PCR R26mTmG genotyping

Phase	Temperature	Time	Cycles
initial denaturation	95°C	5 min	
denaturation	95°C	1 min	
primer annealing	56°C	1 min	35 cycles
elongation (*Taq*)	72°C	1 min	
final elongation (*Taq*)	72°C	10 min	
end	4°C	∞	

6.1.5.5 RT-qPCR

The expression level of desired genes can be quantifed via real-time quantitative PCR (RT-qPCR). The general use of fluorescent compounds that bind to double-stranded DNA have allowed standardized measurements of amplify DNA. During the PCR reaction, the rise in fuorescence due to the increase of PCR product is measured every cycle in the PCR-cycler. The reaction was carried out in 384 well plates in a total volume of 12 μl on an ABIPrism HT 7900 Real-time Cycler (Applied Biosystems). RT-qPCR was performed using extracted RNA from whole limb lysates or FACS sorted cells to compare expression levels of desired genes.

To achieve relative quantification standard curves were produced using serial dilutions of embryonic cDNA. Dilutions were made depending on the expected expression level, starting from 0.4-4 ng and decreasing down to 0.0125-0.125 ng cDNA. Relative quantifcation of every gene was calibrated by the levels of expression of at least two housekeeping genes, generally *Gapdh* and b-actin. Suitable primers (see Table12) were used in a final concentration of 1.5 pmol. Two different PCR master mix were used, SYBR Green PCR Master Mix (Applied Biosystems) or PCR master mix (Promega, M7505). If not denoted other-

wise, the here presented data are averages and standard error of the mean of triplicates of one representative experiment out of at least three. The data analysis was performed with the software SDS 2.1 (Applied Biosystems).

6.1.6 Sanger sequencing

Sequencing was performed by Mohsen Karbasiyan (Institute for Medical Genetics, Charite) on a ABI 3700 capillary sequencer (Applied Biosystems).The sequencing-PCR was set up using BigDye v3.1 (Applied Biosystems), according to the specifications of the manufacturer.

6.2 Preparation of animal tissue

Adult animals were killed by cervical dislocation and animals younger than 2 weeks were decapitated.

Embryos at the desired stage of development were isolated from pregnant mice after a small incision at the abdomen and directly transferred to PBS.

6.2.1 Fixation of prepared embryonic tissue

Embryos from stage 11.5-18.5 post-coitus were decapitated and the body was separated at the base of hip in two parts. Fixation of the tissue was performed at RT for 2 hours with a solution of 4% paraformaldehyde (PFA) dissolved in PBS. After fixation PFA was removed and tissues were washed 3x for 5 minutes with PBS. Tissue used in further *in situ* hybridization was similarly treated and fixed in 4% DEPC-PFA.

6.3 Histological methods

6.3.1 Paraffin embedding and sectioning

Following fixation, tissue was directly processed for paraffin embedding. Dehydration and paraffinization of the tissue was performed using the Tissue Processor (Leica TP1020). Tissue was embedded in the desired orientation with the help of embedding station EC 350-12. Paraffin sections were obtained with the microtome HM355S (Thermo scientific) and cut 6 μm thick. Sections were dried overnight at 40°C and placed at 4°C for storage.

Previous immunostaining, paraffin sections were deparaffinated using UltraClear and rehydrated using a descent gradient of ethanol baths.

6.3.2 Cryo-embedding and sectioning

PFA-fixed tissue was treated first with a solution of 15% sucrose dissolved in PBS and subsequently with a solution of 30% sucrose overnight to protect the tissue during cryo-embedding. Sucrose-treated tissue was immersed in Tissue-Tek OCTTM compound (Sakura Finitek) at RT for at least 20 minutes before final embedding using a chilled ethanol-dry ice bath.

Cryosections were 12 μm thick and obtained with the cryostat HM 560M Cryo-Star (Thermo scientific). Directly after sectioning, sections were warmed up for 40 minutes on a 37°C plate to avoid unwished wrinkles in the tissue and finally place in storage at -80°C.

6.3.3 *In situ* hybridization (cryosections)

In situ hybridization was performed on frozen sections using the designed probes for *Scx* (Schweitzer et al., 2001) and *Osr1* (Stricker et al., 2006).
Frozen sections were warm up at least 30 minutes at RT previous further processing. Sections were washed 3x for 5 minutes with diethylpyrocarbonate (DEPC) treated PBS. The following step of acetylation was performed to reduce background using a buffer containing triethanolamine (0.75%), hydrogen chloride 30% (0.15%) and acetic anhydride (0.2%) dissolved in DEPC-water. Acetic anhydride was added to the buffer solution just before the slides were immersed in acetylation buffer. Slides were thoroughly mixed in the buffer solution for the first 2 minutes. Acetylation buffer was washed out in 3 wash steps of 5 minutes with DEPC-PBS. Previous hybridization, sections were treated with a prehybridization buffer. Slides were positioned horizontally in a humidified chamber with PBS containing the prehybridization solution and incubated at least for 2 hours at RT.
RNA secondary structures were avoided warming up the solution at 80°C during 5 minutes. Before adding 100 μl of hybridization buffer containing DIG-labeled RNA-probe, prehybridization buffer was removed and the chamber was humidified with a solution of 50% Formamide and 5x SSC solution. Every slide was covered with a glass coverslip. Hybridization was performed at 65°C overnight.
After hybridization, coverslips were removed washing first 5 minutes in 2x SSC at RT. Not hybridized RNA-probe was removed washing the slides two times at 65°C during 30 minutes with 2x SSC. Two washing steps more of 30 minutes at RT with MABT prepared the tissue for the following blocking step. Slides were blocked adding 500 μl of blocking solution (MABT + 5% blocking reagent Roche 1109617001) and incubating them for 1 hour at RT in a PBS humidified chamber. An anti-DIG antibody (Roche: 11093274910) coupled to an alkaline phosphatase was dissolved 1:2000 in blocking reagent and incubate

overnight at RT for the specific detection of the DIG-labeled RNA-probe.
At the third day antibody solution was thoroughly washed with MABT five times during 30 minutes at RT. Slides were treated two times in NTMT for 10 minutes at RT before they were immersed in 200 ml of developing solution (NBT 5 μg and BCIP 2.6 μg in NTMT). Developing of the staining reaction was performed at 37°C in a light protected chamber till the signal of the alkaline phosphatase reaction achieved the desired intensity. Staining reaction was stopped washing the slides during 5 minutes in PBS. Sections were directly dehydrated in 100% ethanol and Ultraclear and mounted in HYDRO-MATRIX or further processed for immunostaining.
MABT: 100 mM Maleic acid pH 6, 0.1% Tween

6.3.4 Immunohistochemistry

Cryosections were warmed for at least 30 minutes at RT previous further processing. Antigen accessibility was improved via antigen retrieval for specific antibodies (see Table8). One of four different antigen retrievals were performed depending on the used antibody:

1. Heat-induced epitope retrieval. Sections were permeabilized during 6 minutes in -20°C chilled methanol and subsequently washed 3x with PBS for 5 minutes. Epitope retrieval consisted of a treatment with 1 mM EDTA at 95°C for 10 minutes.

2. Heat-induced epitope retrieval. Another faster variant of this method used the antigen retrieval solution DAKO pH 6, which was heated in the microwave at 750 W for 3 minutes. The retrieval solution was cooled for 5 minutes at RT prior immersion of the sections. Immersed sections were boiled in the microwave for 2 minutes. Finally sections were cooled at RT for 20 minutes.

3. Heat-induced epitope retrieval. During this antigen retrieval sections were washed 3x in PBS previous treatment with citrate buffer, 10mM sodium citrate pH 6, at 95°C for 10 minutes.

4. Hydrochloric acid (HCl) antigen retrieval. Detection of DNA-intercalated bromodeoxyuridine (BrdU) was improved using this antigen retrieval, which consisted in a treatment with 7.5% 1 N HCL dissolved in bdH_2O at 37°C during 30 minutes.

After antigen retrieval sections were washed 3x for 10 minutes with PBS. Thereafter, sections were covered with 200 μl of blocking solution (1x PBS, 3% horse Serum, 3% goat serum, 5 mg/ml blocking reagent (Perkin Elmer FP1012)) and 0.1% of Triton-100X and incubated for 1 hour at RT. First antibodies were dissolved in staining buffer (Blocking solution without blocking reagent (Perkin Elmer FP1012)) in according concentration

and incubated overnight at 4°C. At the next day, primaries antibodies were washed 3 times for 10 minutes with PBX (1xPBS, 0.1% Triton 100x). Secondary antibodies were dissolved in according concentration (See Table9) in staining buffer and incubated for 1 hour at RT. Addition of 1 mg/ml diamidino-2-phenylindole (DAPI) with the secondary antibodies was performed to counterstained nuclei on sections. Secondary antibodies were washed 3 times for 10 minutes with PBS previous mounting with an aqueous solution Fluoromount-G (Southern Biotech), which reduces fluorochrome quenching during fluorescence microscopy and provide semi-permanent seal for long storage.

6.3.5 Whole-mount immunohistochemistry

Using long process of permeabilization that prepares the whole limb for antibodies penetration is possible to adapt normal immunohistochemistry approaches to whole mount stainings. This method was adapted from the described protocol by Merrell et al. (2015).

Whole E14.5 embryos were fixed in 4% PFA overnight at 4°C. Embryos were washed at least 3x during 1 hour in PBS gently rotating. After washing embryos were carefully skinned prior bleaching using a mix of 1 part of hydrogen peroxide (H_2O_2) and 2 parts of Dent's fix (1 part DMSO and 4 parts Methanol). Separated limbs were rinsed 5 times with methanol previous permeabilization in Dent's fix rocking at 4°C for long periods (from several weeks to months).

After permeabilization limbs were rinsed in PBS during three long wash passages of 1 hour. After 1 hour of incubation in blocking solution, primary antibodies were diluted in staining solution and incubated for 3 nights at RT.

Secondary antibodies were diluted also in blocking solution and added after 5 wash passages of 1 hour. They were incubated for 3 nights at room temperature, keeping dark by covering with aluminum foil and gently rotating.

The last part of the whole mount immunostaining procedure differs to the normal immunostaining procedure by using an extra step of tissue clearing using Benzyl alcohol Benzyl Benzoate (BABB). After secondary antibodies limbs were rinsed in PBS 3x for 1 hour keeping them in dark by covering. The next steps of dehydration with methanol are critical to avoid precipitates what can interfere with further imaging. First, tissue was immersed in a solution of 50% PBS and 50% methanol for 5 minutes. Second, the tissue was incubated in methanol 3x during 20 minutes and finally a mix of 50% methanol and 50% BABB replaced the methanol during 10 minutes.

The last step of clearing consists of at least 20 minutes treatment with BABB. Limbs were cleared in the imaging chamber immersed in BABB and immediately imaged using a LSM700 confocal microscope.

6.3.6 Oil Red O staning

The dye Oil Red O was used to stain lipid droplets on frozen sections. For that propose sections were washed with PBS for 5 minutes prior staining. Sections were rinsed with 60% isopropanol for 10 minutes and immersed in Oil Red O staining solution for 15 minutes. After staining sections were rinsed again with 60% isopropanol for 10 minutes and washed with PBS. Immunofluorescence was performed after Oil Red O staining.
Oil Red O staining solution: 0.5 g Oil Red O (CL 26125) in 100 ml isopropanol.

6.4 Cell culture methods

6.4.1 Extraction and culturing of primary embryonic cells

6.4.1.1 Dense mouse limb extracts

Extraction

Limb extracts were isolated from E13.5 *Osr1*$^{+/+}$ and *Osr1*$^{GCE/GCE}$embryos to asses *in vitro* myoblast fusion. Embryos were decapitated and the tissue was enriched in skeletal muscle and muscle connective tissue removing all internal organs and paw. Remaining tissue was minced in 500 μl growth medium using a small scissor. Further enzymatic digestion of the tissue was performed using 10 mg/ml of Collagenase IV (Collagenase NB 4G proved grade 17465, SERVA ElectrophoresisTM) and under thoroughly shaking conditions 1400 rpm at 37°C during 40 minutes. After digestion, tissue extracts were washed 2x with PBS and resuspended in 100 ml growth medium.

Growth medium: DMEM (4,5 g glucose, 10% FCS (Biochrome), 1% L-glutamine and 1% penicillin/streptavidin (both Gibco))

Culturing

During the period of incubation high-density cultures were grown on a MatriGel-coated glass coverslip. 15 mm glass coverslips were coated with a solution of 10% MatriGel dissolved in growth medium. 50 ml drops were located in the middle of the coverslip and incubated for 2 hours prior adding 2 ml of growth medium per culture. Cultures were kept in a humidified incubator at 37°C and 5% CO_2 for 5 days and medium was changed every 2 or 3 days.
Growth medium: DMEM (4,5 g glucose, 10% FCS (Biochrome), 1% L-glutamine and 1% penicillin/streptavidin (both Gibco))

Differentiation

Myoblast differentiation was induced in limb extracts by culturing them under low serum conditions. Growth medium was replaced by a differentiation medium and cultures were incubated for at least five days under these conditions. Multinuclear myofibers were easily

identifiable under the microscope. If needed cultures were maintained in differentiation medium for longer periods.
Differentiation medium: DMEM (1 g glucose, 2% FCS (Biochrome), 1% L-glutamine and 1% penicillin/streptavidin (both Gibco))

6.4.1.2 Extraction of *Osr1*$^{GFP+}$ cells for FACS sorting

Pregnant females at day 11.5 and 13.5 post coitus were sacrificed as describe in (see section 6.2). To enrich samples in muscle connective tissue cells, only limbs including the shoulder region without the paw of *Osr1*$^{GCE/+}$ and *Osr1*$^{GCE/GCE}$ embryos were isolated and transfer to 200 μl of pre-warmed growth medium. Tissue was minced in 200 μl growth medium using a small scissor and additional 300 μl of growth medium was used to collect all tissue pieces. Further tissue enzymatic digestion was carried out using 10 mg/ml of Collagenase IV (Collagenase NB 4G proved grade 17465, SERVA ElectrophoresisTM) at 37°C in growth medium and under thoroughly shaking (1400 rpm) conditions for 50 minutes.

Digested limb extracts were filtered first throw a 100 μm strainer and washed twice with PBS before resuspension in sorting buffer (HBSS with 1% Gentamycin and 2 mM EDTA). Prior sorting, cells were filtered through a 35 μl filter. Calibration of the FACS Aria II machine previous sorting was performed in advance.

Cells were sorted directly in RLT buffer for RNA extraction (RNAeasy Mini Kit Quiagen) (20000 cells in 175 μl of RLT-buffer) or in medium coated tubes for further culturing.
Growth medium: DMEM (4,5 g glucose, 10% FCS (Biochrome), 1% L-glutamine and 1% penicillin/streptavidin (both Gibco))

6.4.2 Immunocytochemistry (ICC)

Expression of connective tissue markers in Osr1+ FACS sorted cells and myoblast fusion in culture were assessed by immunocytochemistry (ICC). For this purpose cells were cultured on round glass cover-slips in 12-well plates, where immunostaining was performed. Cultures were washed with PBS prior fixation with 4% PFA for 20 minutes. After fixation cultures were washed 3x in PBS for 5 minutes. PBS was replaced by a blocking solution, where cultures were incubated for 1 hour at RT. Suitable primaries antibodies, see table8 were diluted in 300 μl staining buffer and added to the wells containing the coverslips. Primary antibodies were incubated overnight at 4°C. The following day, cell cultures were washed thrice with PBX and incubated with appropriate secondary antibodies and DAPI for 1 h at RT. Finally, cultures were washed thrice with PBX for 10 minutes prior mounting. For mounting, coverslips were taken out from the 12-well plate and carefully placed

on a 40 μl drop of Fluoromount G.

6.5 Biochemical Methods

6.5.1 Total Protein isolation and protein concentration

Freshly prepared embryonic tissue was directly frozen in liquid nitrogen and stored until protein isolation. Frozen tissue was disrupted using a plastic pestle which perfectly fits to 1.5 ml tubes. Immediately after disruption 300 μl membrane lysis buffer were added to the tissue and it was kept at 4°C. The tissue was homogenized in a 2 ml tube using a metal ball via the TissueLyser device. Sonification for 8 cycles of 30 seconds at low power with the Sonifizer allowed further homogenization. The lysate was centrifugated for 10 minutes at 10000 rpm to eliminate debris. Only supernatant was used as protein template.

Protein concentration was measured using the colorimetric protein assay Micro BCATM Protein Assay Kit (Thermo scientific 23235). This method used bicinchoninic acid (BCA) as the detection reagent for Cu^{+1}, which is formed when Cu^{+2} is reduced in an alkaline environment. The water-soluble complex formed exhibits a strong absorbance at 562 nm that is linear with increasing protein concentration.

10 μl of the protein template and BSA standards in triplicates were added to a mix of BCA reagents and incubated for 2 hours at RT. Absorbance was measured at 562 nm using the device Plate reader Spectra Max 250. Protein concentration was calculated using the equation after lineal regression of BSA standard values.

6.5.2 SDS PAGE

6.5.2.1 Gel preparation (polyacrylamide)

Depending on the expected protein sizes, gels with appropriate percentages of acrylamide were prepared according to Sambrook, et al., 1989, using the Mini Protean II System (Biorad).

6.5.2.2 Sample preparation

The necessary amount of protein was calculated prior electrophoresis loading 20 μg of protein solution per lane. Loading-buffer was added to the samples, which were subsequently heated for 10 min at 98°C to achieve disruption of secondary and tertiary structures. Additionally, a pre-stained protein ladder (Fermentas) was loaded to the gel, in order to determine the molecular weight of detected proteins.

Loading-buffer: 2 ml 1 M Tris, 4 ml glycerine, 2 ml 20% (w/v) SDS, 400 μl 1% bromephenol blue, 600 ml ddH_2O, 1 ml 40x β-mercaptoethanol; pH 7.5

6.5.2.3 Electrophoresis

Gels were run under 80 V condition for 30 min, thereafter the voltage was increased to 100 V until the bromephenol blue reached the lower edge of the glass slides. For better separation of large proteins, the running time was elongated.

5x running-buffer: 25 mM Tris, 250 mM glycine, 0.1% (w/v) SDS

6.5.3 Western blot (WB)

6.5.3.1 Protein transfer

Separated proteins were transferred to a suitable peace of Polyvinylidene fuoride (PVDF) membrane. PVDF membrane was activated in methanol for a period of 2 minutes and equilibrated in transfer-buffer. Assembly of the gel-membrane sandwich was performed in wet conditions humidifying with transfer buffer. Transfection was carried out in a so-called wet chamber (BioRad), considering that proteins were SDS-coated. Blotting took place in the wet chamber at 100 V for 1 hour and at 4°C.

1x transfer buffer: 25 mM Tris, 192 mM glycine, 20% MeOH

6.5.3.2 Protein detection

After blotting, the membrane was washed 2x with TBST for 5 minutes and blocked in 5% milk powder dissolved in TBST (blocking solution) for at least one hour. The suitable antibody was incubated overnight at 4°C in blocking solution. The next day, the membrane was washed 3x in TBST for 5 min and incubated with a suitable HRP-coupled secondary antibody for at least 1 h at RT. Finally, the membrane was washed thrice and protein was visualized using enhanced chemo luminescence (ECL) solution (Rotilumin, Carl Roth). Protein signal was detected by the LAS 4000 Imaging System (Fuji) and quantified with ImageJ.

TBST: TBS, 0.02% Tween20

6.6 Statistical analyses

Immunostaning and RT-qPCR were performed using at least 3 embryos of each genotype. Quantifications obtained from at least 4 sections were performed in serial sections. Interval of confidence was calculated using two tailed Student's *t*-test. Statistical analyses were performed with GraphPad Prism5.

7 Results

7.1 Characterization of *Osr1* expression and cell lineage fate during mouse embryonic development

7.1.1 Expression pattern of *Osr1* during embryonic limb development

The expression pattern of the transcription factor OSR1 has been characterized mainly in the chick model. In early development *OSR1* is mainly expressed in the lateral plate mesoderm and intermediate mesoderm from stage HH6 (Hamburger-Hamilton) to HH16. Later on during development, *OSR1* presents a dynamic expression pattern in a broad number of embryonic tissues, and also in the limb mesenchyme, where it is expressed in irregular connective tissues (Stricker et al., 2006). To analyze *Osr1* expression in mouse limbs, I used the *Osr1*^{GCE} mouse model, developed by Andrew McMahon's laboratory. In this mouse line, a cassette containing an enhanced GFP (eGFP or simply GFP) followed by an internal ribosomal entry site and the coding sequence for an estrogen inducible Cre recombinase (CreERt2) was knocked into the endogenous *Osr1* locus, replacing the translational start site within exon 2 (Mugford et al., 2008). This mouse model allows us to perform *Osr1* expression analysis using GFP as an *Osr1* reporter.

Immunohistochemical analysis using an antibody against GFP confirmed *Osr1* (GFP) expression in the mouse limb mesenchyme at E11.5 (embryonic day 11.5), in close association with muscle progenitors, labelled with the transcription factors *Pax7* (Figure 40A, A'). Consistently with previous whole-mount *in situ* hybridization data (Stricker et al., 2006), the *Osr1* expression pattern presented different domains in the limb, where Osr1+ cells were partially embedding muscle progenitors of the ventral and dorsal premuscle masses in the mesenchymal tissue directly beneath the ectoderm. In proximal limb regions, strong *Osr1* expression was observed in presumptive muscles of the shoulder girdle (Figure 40A and A'), showing close spatial association between Osr1+ cells and Pax7+ myogenic progenitors in this region. At E12.5, Osr1+ cells were distributed in a regionalized manner. Split muscle masses labelled with an antibody against MyHC showed Osr1+ connective tissue cells surrounding first formed myofibers in the forelimb (Figure 40B, B'). Intriguingly, *Osr1* positive cells were not found associated with all muscles. In forelimbs, some muscles showed high *Osr1* expression in interstitial cells, while other muscle masses presented few Osr1+ connective tissue cells (Figure 40B, arrows). A similar regionalized pattern was seen in hindlimbs at E13.5, where muscles, such as the gastrocnemius muscle were surrounded by Osr1+ connective tissue cells. In contrast, other muscles such as the tibialis posterior muscle presented very few Osr1+ connective tissue cells (Figure 40C,

C' arrows). Despite the presence of Osr1+ cells in a similar pattern observed at E13.5, at E14.5 *Osr1* expression detected by GFP-antibody staining on hindlimb cross-sections started to decline in intensity in connective tissue of the gastrocnemius muscle, previously shown to be highly Osr1+ (Figure 40D, D'). Importantly, throughout the analyzed stages, *Osr1* was never found expressed within muscle progenitors, myoblasts or myofibers.

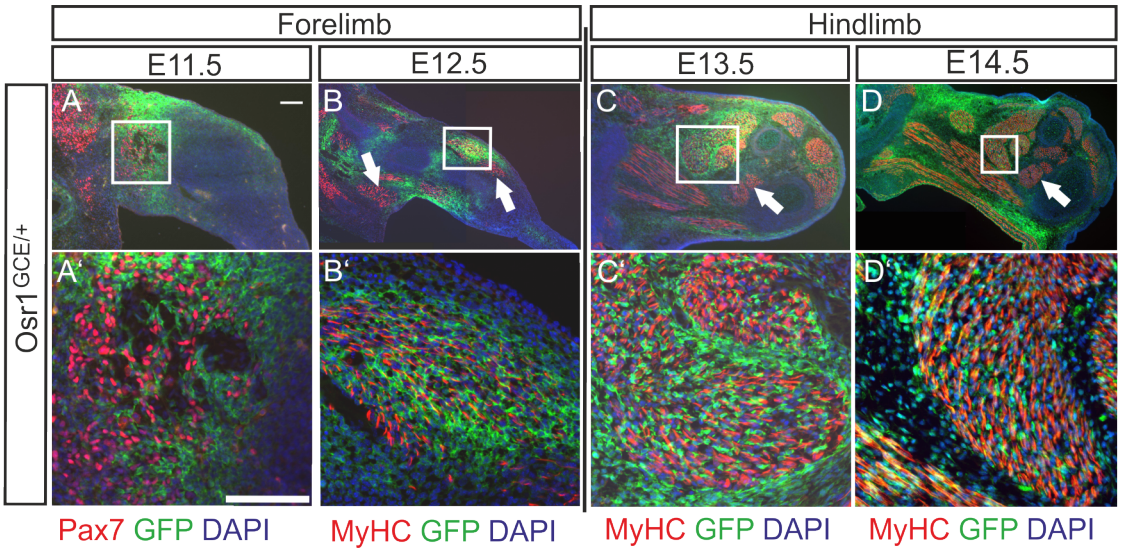

Figure 12: ***Osr1* expression during embryonic muscle development in mouse limbs.** Counterstaining with the muscle progenitor marker Pax7 at E11.5 showed close association of Osr1+ cells with muscle progenitors in the proximal limb (A and A'). In E12.5 forelimbs, as well as E13.5 and E14.5 hindlimbs, *Osr1* showed a regionalized expression in mesenchymal cells surrounding embryonic muscles and myofibers labelled by Myosin heavy chain (MyHC) in red (B-D'). Cytoplasmic GFP expression was visualized using an anti-GFP antibody. Scale bar 100 μm.

The transcription factor TCF4 is a downstream component of the β-catenin/Wnt signaling pathway. TCF4 is the first recognized marker for muscle connective tissue cells (Mathew et al., 2011). Immunohistochemistry analyses using an antibody against GFP and co-labelling for TCF4 protein using a specific antibody on cross-sections of forelimb and hindlimb heterozygous *Osr1*$^{GCE/+}$ embryos revealed partial co-expression of both transcription factors, but also distinct regions of exclusive expression of one of each factors during development. At E11.5 *Osr1* and *Tcf4* expression presented a dorsal and ventral domain in the mouse limb mesenchyme close to muscle progenitors. In these regions, Osr1+ cells were located closer to the skin than Tcf4+ cells and there was only a minor overlap of expression. Only few cells were co-expressing both factors at the interface of the *Osr1* and *Tcf4* expression domains (Figure 13A, B white arrow shows co-expression, orange arrows how cells expressing *Osr1* or *Tcf4*, respectively).

Later during development, at E13.5 expression of the two transcription factors was analyzed on hindlimb cross-sections. Co-labelling with specific antibodies against TCF4 and GFP revealed co-expression of both transcription factors in specific muscles (Figure

13C, D white arrows). In the ventral part of the lower leg *Osr1* and *Tcf4* were found to highly co-localized in connective tissue cells surrounding muscles of the gastrocnemius region (Figure 13D, white arrows). In contrast, muscles located in other regions such as gracilis muscles displayed a connective tissue enriched with Osr1+ cells and negative for Tcf4+ cells (Figure 13E, F white arrows), while connective tissue cells surrounding the muscle tibialis posterior were exclusively positive for *Tcf4* immunostaining (figure 13F, orange arrows).

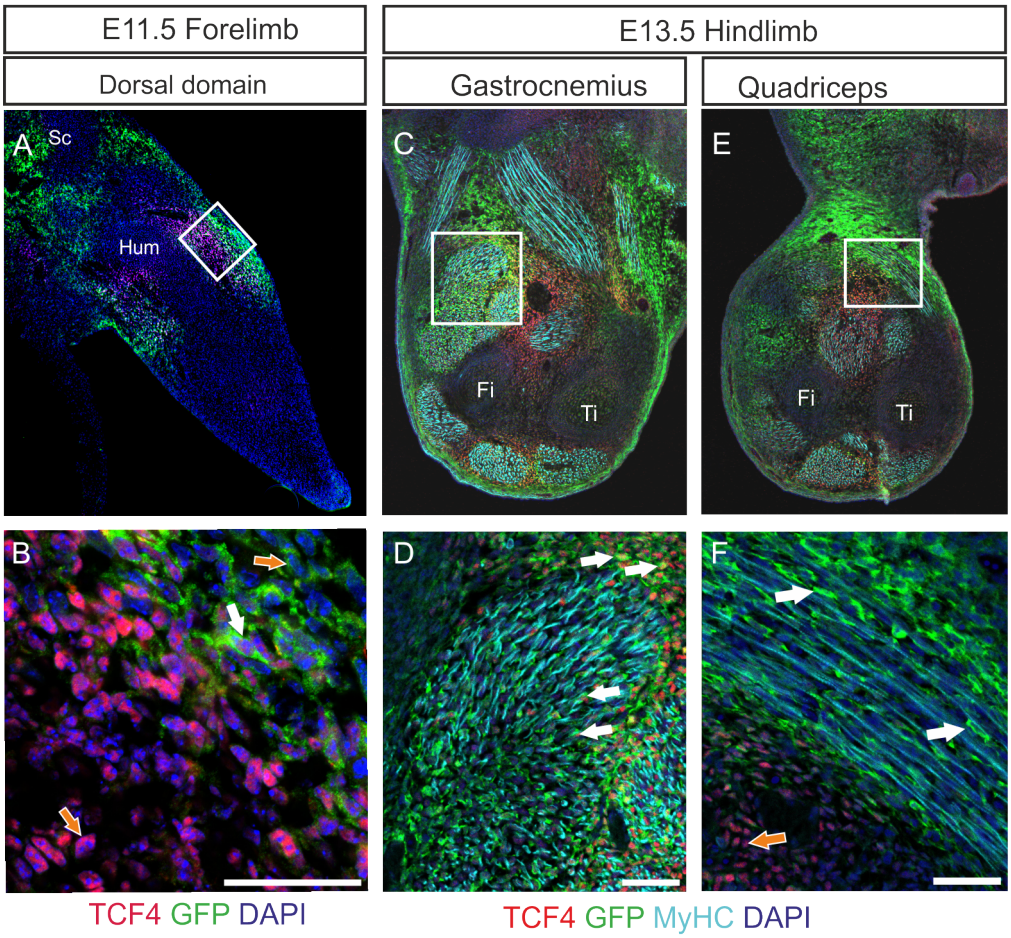

Figure 13: ***Osr1* is partially co-expressed with the transcription factor *Tcf4* in limb connective tissue during development**. Immunolabeling of cross-sections at E11.5 showed Osr1+ (GFP, green) cells in superficial layers and TCF4+ (red) cells in a more centralized regions. In both ventral and dorsal domains, only a small portion of the cells co-express both transcription factors (A, B). At E13.5, GFP+ and Tcf4+ domains of expression highly overlap in some regions (C, D arrows) while both transcriptions factors appear mutually exclusive in others (E, F arrows). Sc, scapula; Hum, humerus; Fi, fibula; Ti, tibia. Scale bar 20 μm.

To further characterize embryonic Osr1+ cells, cells were FACS-sorted using the reporter eGFP under the control of *Osr1* promotor at E13.5. Sorted Osr1+ cells were directly plated on glass coverslips and allowed to adhere for 12h before fixation and analyzed by immunolabeling for known connective tissue markers (Mathew et al., 2011).

Ratios of Osr1+ cells expressing each connective tissue marker were calculated counting four different regions of the plated cell culture. The intermediate filament vimentin, characteristic of muscle connective tissue fibroblasts (Zou et al., 2008) was present in the majority (90.1%) of Osr1+ cells (Figure 14A). In accordance with the expression data shown above (Figure 13A-C), only a moderate proportion (48.1%) of Osr1+ sorted cells expressed the transcription factor TCF4 (Figure 14B). Interestingly, at E18.5 the proportion of Osr1+ cells isolated from limb muscles co-expressing *Tcf4* was higher (87.8%) than at E13.5. In addition, the majority (94.7%) of Osr1+ sorted cells express the membrane receptor *PdgfRα* (Figure 14C), which is a widely used marker for fibroblasts, however not being specific for this cell type. Another marker of fibroblasts is type VI collagen (ColVI), previously shown to be uniquely synthesized at high levels by connective tissue fibroblasts (Zou et al., 2008). We observed that a high number (63.9%) of Osr1+ cells secreted high levels of collagen VI (Figure 14D). Similarly to *Tcf4* expression, an increased proportion of Osr1+ cells (91.3%) produced type VI collagen protein at E18.5.

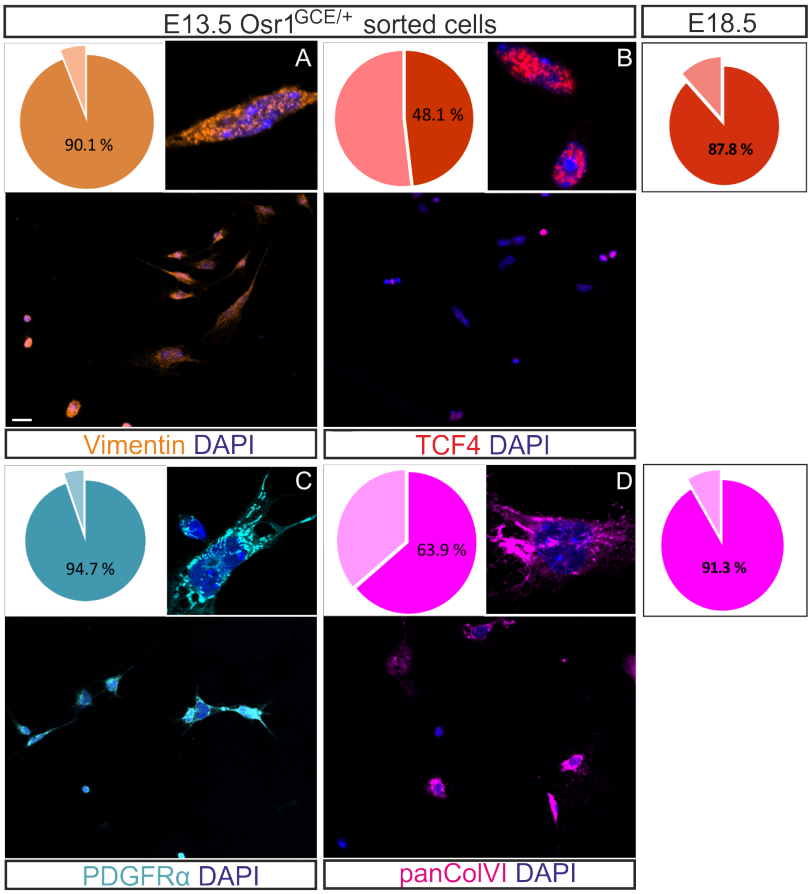

Figure 14: **Osr1+ cells GFP-FACS sorted from E13.5 and E18.5 *Osr1*$^{GCE/+}$ embryo limbs express several connective tissue markers in different proportions**. Immunolabeling of Osr1+ sorted cells after 12h in culture using antibodies against described connective tissue proteins: TCF4, vimentin, collagen VI and PDGFRα (A-D). Percentage values represent the proportion of cells expressing the corresponding marker obtained after counting four different regions of the cell culture. Scale bar 20 μm.

Differentiation and patterning of different limb tissues shows partial mutual interdependence (e.g. Kardon et al. (2002)). To determine whether *Osr1* expression is independent on the presence of muscle tissue, we took advantage of a *Pax3*^{GFP} knock-in allele, where the *Pax3* coding sequence has been replaced with GFP. Embryos devoid of *Pax3* show no migration of muscle progenitors into the limbs which has for consequences an absence of limb muscles. The pattern of *Osr1* expression was addressed by in situ hybridization using an *Osr1* probe on cryosections of muscleless limbs of *Pax3*$^{GFP/GFP}$ and control embryos at E11.5 to E13.5.

At E11.5 the *Osr1* expression pattern revealed by *in situ* hybridization (Figure 15) corroborated the GFP-based expression pattern presented above (Figure 40A, A'). Immunostaining of Pax3+ cells by an anti-GFP antibody taking advantage of the inserted GFP allele, labelled Pax3+ muscle progenitors that showed close association with *Osr1* dorsal and ventral domains of expression, in control *Pax3*$^{GFP/+}$ embryos. At E11.5, the ventral and dorsal domains of *Osr1* expression appeared normal in muscleless limbs of *Pax3*$^{GFP/GFP}$ embryos (Figure 15A, A' and 15D, D'). At E12.5 muscles start to split, visualized by immunolabeling for MyoD. *Osr1* expression was found associated with the areas of muscle formation, an overlapping pattern was seen in *Pax3*$^{GFP/GFP}$ limbs (Figure 15B, B'; 15E, E' and white arrows). From E12.5, successive splitting steps of limb muscle masses lead to the separation of most limb muscles at E13.5. Expression of *Osr1* showed a similar pattern in controls and *Pax3*$^{GFP/GFP}$ forelimb sections. Regions of *Osr1* expression in the connective tissue surrounding single muscles resembled muscle shapes even in the absence of muscles in E13.5 *Pax3*$^{GFP/GFP}$ mutant embryos (Figure 15C, C'; 15F, F', white arrows). Altogether this suggests that the regionalized expression pattern of *Osr1* in the limb is initiated independently of muscles.

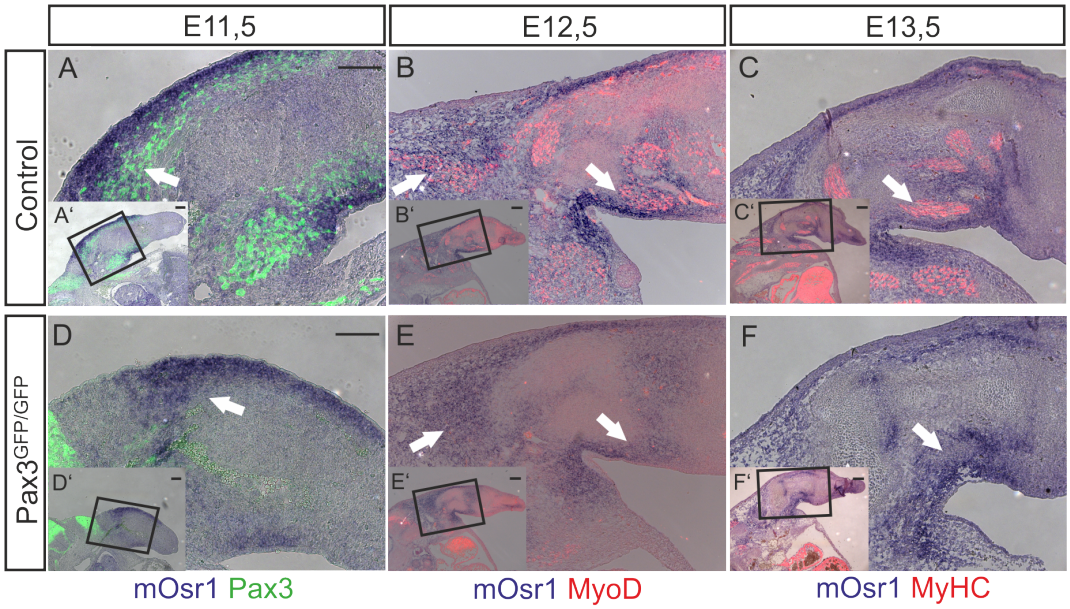

Figure 15: ***Osr1* expression pattern determined by *in situ* hybridization is not affected in muscleless limbs of *Pax3*$^{GFP/GFP}$ embryos**. At E11.5, counterstaining with an anti-GFP antibody (green) allowed visualization of Pax3^{GFP} cells (A, A' and D, D'). Similar to stage E11.5 no changes in *Osr1* expression pattern were observed on forelimb cross-sections at the stages E12.5 (B, B' and E, E') and E13.5 (C,C' and F, F') using antibodies against MyoD (red) and MyHC (red) to counterstain myoblast and myofibers, respectively. Arrows point to similar *Osr1* expression areas on control and *Pax3*$^{GFP/GFP}$ sections. Scale bar 200 μm.

Taken together the results obtained by *in situ* hybridization and GFP reporter analyses allow us to postulate that *Osr1* is a connective tissue marker and displays a conserved expression with the chick model. Interestingly, *Osr1* is only partially co-expressed with the known connective tissue marker TCF4 in limb mesenchyme. However, most of Osr1+ cells expressed *PdgfR*α. Culture of Osr1+ cells indicated their potential to differentiate into fibroblasts (Figure 14), however the in vivo cell fate of Osr1+ cells remains unknown.

7.1.2 Contribution of *Osr1* cells to limb tissues

Mouse genetic tools developed to trace cell pools expressing a specific gene have demonstrated their value to elucidate the origin of many cell types. Spatial-temporal genetic labelling of cells can be achieved by combining a CreERt system and a Cre-sensitive reporter mouse such as the mTmG line. This mouse line constitutively expresses a ubiquitous membrane targeted Tomato (mT), which in the presence of Cre is excised switching the cell to membrane GFP (mG) expression (Muzumdar et al., 2007). I aimed to genetically label Osr1+ cells at different embryonic stages and subsequently trace their fate during development taking advantage of the CreERt2 contained in the *Osr1*^{GCE} allele. For this purpose, *Osr1*$^{GCE/+}$ males were crossed to homozygous mTmG females, which

were Tamoxifen induced at desired time points via intraperitoneal injection.

Osr1+ cells were genetically labelled at E11.5 and E15.5 by Tamoxifen injection and their fate was analyzed at stage E18.5.

Cross-sections of the upper part of the body (forelimb and trunk) were used for immunohistochemistry analyses. Osr1+ derived cells were found to contribute in high numbers to dermal fibroblasts, secreting proteins of the extracellular matrix such as type I collagen, independently of the stage of induction (Figure 16A, B). A considerable number of Osr1+ derived cells were located in close proximity to hair follicles (Figure 16A, B white arrows) but these cells were never found in the epidermis of the skin. Surprisingly I found a contribution of Osr1+ derived cells to embryonic brown fat tissue counterstained with the lipid dye Oil red O. Between stages E11.5 and E15.5 the number of Osr1+ cells giving rise to interscapular brown adipocytes steeply declined. At stage E15.5 barely any *Osr1* descendant cell was found to become a brown adipocyte (Figure 16D, white arrow).

Furthermore, lineage tracing experiments revealed a contribution of *Osr1*-expressing cells at E11.5 and E15.5 to the alpha smooth muscle actin (α-SMA) rich media layer and the close adventitia layer of blood vessels. Blood vessels-associated myofibroblasts differentiate and form a muscle layer enriched for the protein α-SMA. Co-staining of forelimb cross-sections at E18.5 with an anti-α-SMA and anti-GFP antibodies revealed Osr1+ derived cells predominantly outside of the ring of cells enriched by α-SMA protein. At early stages of induction Osr1+ derived cells were also found to partially form part of the ring of cells highly producing α-SMA protein (Figure 16E, F white arrows).

We observed that *Osr1*-expressing cells labelled between E11.5 and E15.5 become muscle interstitial fibroblast-like cells at E18.5 that reside outside of the muscle basal lamina stained with an anti-laminin antibody (Figure 16G, H).

Quail-chick and chick-quail chimera experiments already showed that the connective tissues of peripheral nerves (epineurium, perineurium and endoneural fibroblasts) are not from a neural crest origin, but are derived from limb bud mesodermal cells (Haninec, 1988). This raises the question whether Osr1+ mesenchyme cells have the potential to give rises to peripheral nerve connective tissue. Nerves were labelled using an antibody against the microtubule protein β-Tubulin III, known to be highly exclusive for nerves, on forelimb cross-sections. β-Tubulin III positive axillary peripheral nerves were ensheathed by Osr1+ derived cells at the different layers of nerve connective tissue (Figure 16I), as was observed at E18.5 after Cre induction at E11.5. After Cre induction at E15.5 a lower the number of Osr1+ derived cells were found surrounding peripheral nerves and labeled cells appeared more distant from the nerve (Figure 16J, white arrow).

In addition, Osr1+ cells provided a source to a broad number of mesenchyme-derived cells in close association with endoderm-derived tissues. One example is the lung mes-

enchyme, where traced Osr1+ cells appeared preferentially close to blood vessels independently of time of induction (Figure 16K, L white arrows). At early time of induction (E11.5) Osr1+ derived cells were present in the lung stroma and partially co-expressing the mesodermal marker PdgfRα (figure 16K, L orange arrows). This contribution was significantly reduced at later stages (figure 16L, arrows).

In addition, rarely *Osr1* descendants were observed within tendons labeled for type XII collagen (Figure 17A). Cartilage and skeletal elements of forelimbs were easily identifiable by differential interface contrast microscopy (DIC), and similarly to tendons displayed rare Osr1+ derived cells (Figure 17C). Nevertheless, joints present exhibit an interestingly high amount of GFP labelled Osr1+ derived cells in concordance with the already reported expression of *Osr1* in the joint interzone in early development (Stricker et al., 2006; Gao et al., 2011) (Figure 17B, white arrows).

Of special interest was the observation that Osr1+ cells never contributed to the myogenic pool since mG labeling was never found within myofibers at E13.5. This was the case for limb muscles as well as for trunk muscles. A representative picture for limb muscles is shown in Figure 17C (white arrows). Immunostaining using an anti-GFP antibody labelled Osr1+ derived cells in the muscle interstitium in close proximity to fibers with a fibroblast like shape. Also compare Figure 16G,H, Osr1+ cells were never found beneath the basal lamina of myofibers.

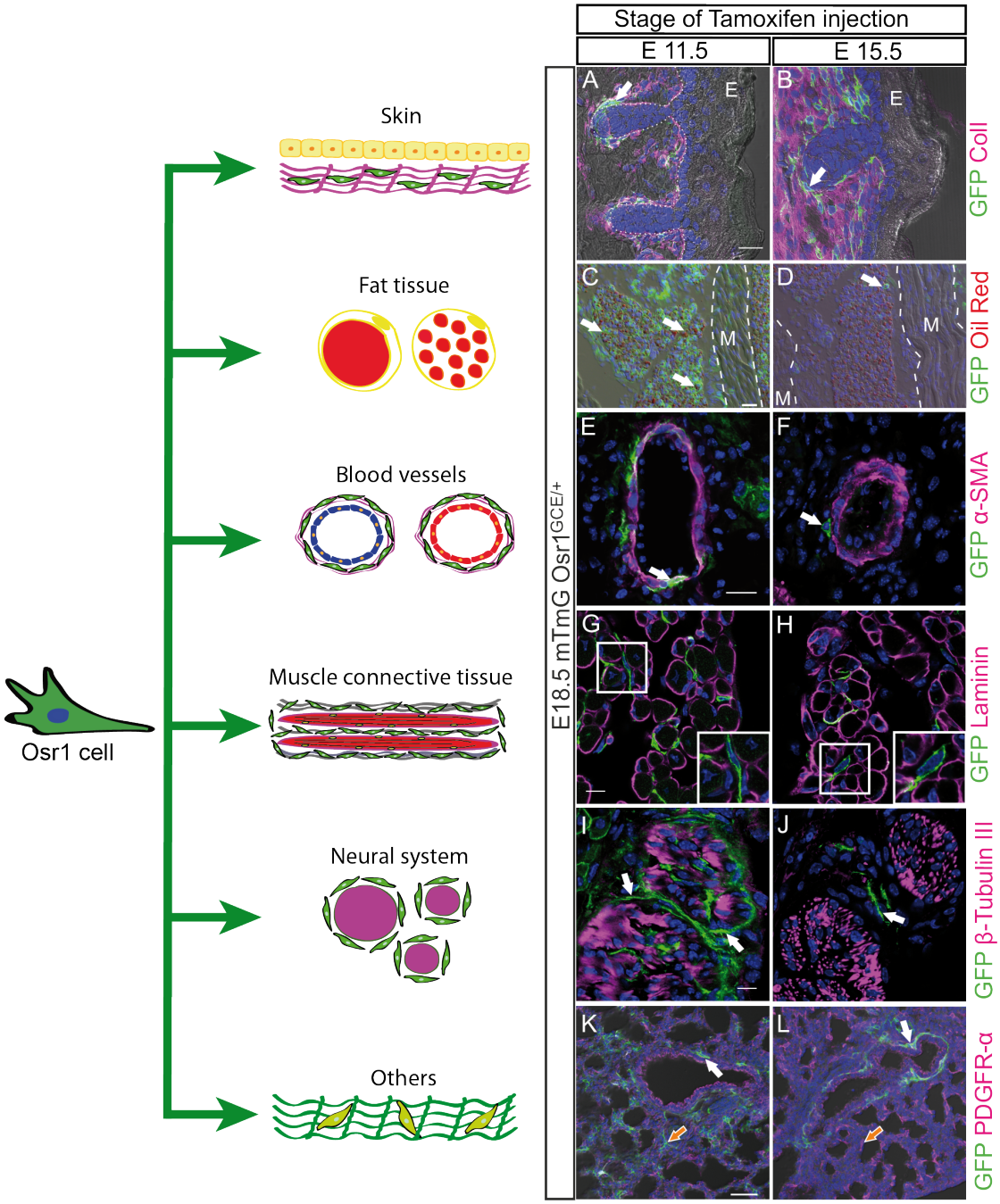

Figure 16: **Osr1+ cell lineage contributes to a broad number of lateral plate derived tissues**. Immunohistochemical staining of E18.5 forelimb and trunk cross-sections were used to reveal Osr1 contribution to different embryonic tissues. Tracked cells expressing *Osr1*(GFP, green) at E11.5 and E15.5 contribute to hypodermic fibroblasts embedded in a matrix of type I collagen (A,B), brown and white adipose tissue assessed by Oil Red O staining (red) (C,D), adventitia and αSMA-media layers of blood vessels by co-staining with anti-αSMA antibody (E,F), interstitial muscle connective tissue fibroblasts outside of the muscle basal lamina labelled by laminin (G,H), connective tissue of peripheral nerves stained with an antibody against the protein β-Tubulin III (I,J) and stromal lung fibroblasts and lung blood vessel associated fibroblasts partially co-expressing the mesenchymal marker alpha type platelet-derived growth factor receptor (PdgfRα). Em, Epidermis; Mu, muscle; scale bar 10 μm (I, J); 20 μm (A-H, K, L).

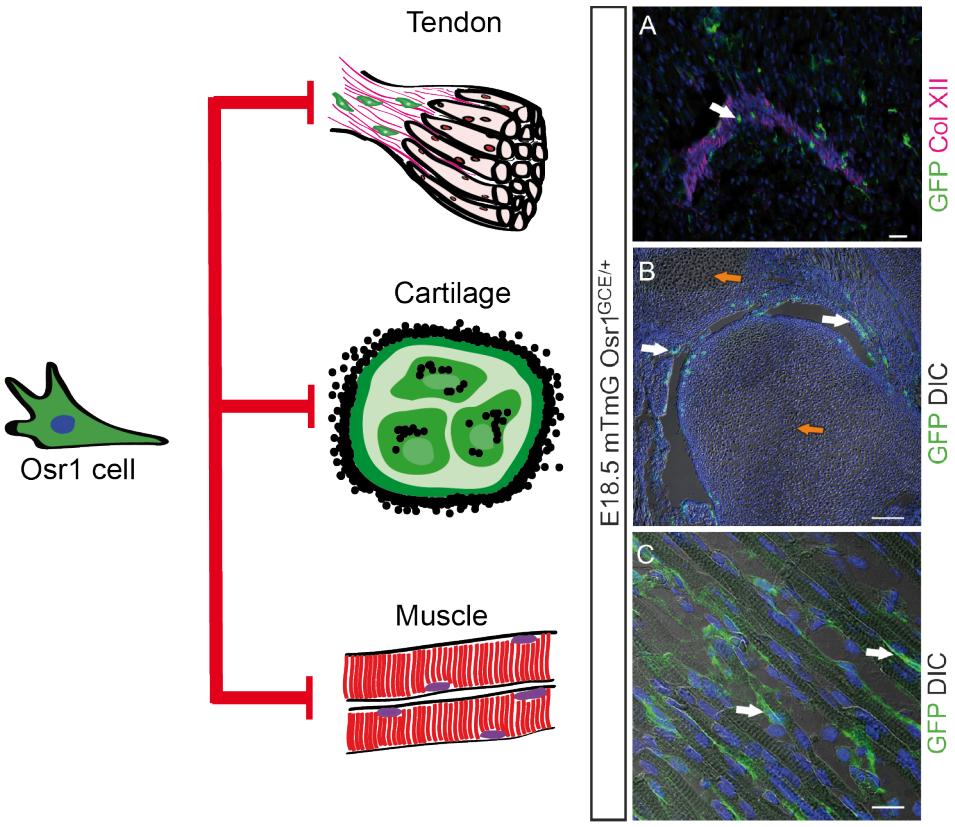

Figure 17: **Osr1+ cells do not contribute to muscle linages and rarely to tendons, cartilage and skeletal elements**. Tracking Osr1+ cells at embryonic stages E11.5 and consequent immunohistochemistry analysis of E18.5 cross-sections revealed very few numbers of these labelled cells within collagen XII labeled tendons on cross sections of the shoulder region (A). Differential interface contrast (DIC) microscopy of GFP-immunostained sections was used to highlight cartilage, skeletal structures and myofibers (B, C). In (B) mG positive cells can be seen within the cartilage of scapula and humerus, but mainly in the joint lining cells and synovial membrane. Scale bar 50 μm.

Linage tracing as well as GFP-reporter approaches confirmed Osr1+ cells as a source of different types of connective tissues. During the phase of limb embryonic myogenesis (E11.5-E14.5) these cells are in constant close association with muscle progenitors and muscle fibers. These results together with an expression pattern independent of muscle formation strongly suggested Osr1+ cells as a model to study the influence of connective tissue in muscle patterning. To decipher the role *Osr1* might have in muscle development we took advantage of the *Osr1* knockout mouse model *Osr1*$^{GCE/GCE}$ (Mugford et al., 2008).

7.2 Lack of *Osr1* in *Osr1*$^{GCE/GCE}$ mutants leads to muscle defects

7.2.1 Muscle patterning defects in *Osr1*$^{GCE/GCE}$ embryos

To visualize muscle defects, we first performed an exhaustive analysis of paraffin sections covering the complete E13.5 hindlimbs and forelimbs using an antibody against myosin

heavy chain (MyHC) as a marker to label muscle fibers. Overview images of whole limb sections were aligned and stacked to compare defects in different sections between *Osr1*$^{+/+}$ and *Osr1*$^{GCE/GCE}$ embryos using AMIRA. Thus, a more comprehensive and comparable analysis of muscle defects was obtained. This first readout reported that all muscles of hindlimb and forelimb were present in E13.5 *Osr1*$^{GCE/GCE}$ embryos. However, it also highlighted striking changes in general muscle patterning and muscle shape of limbs and girdle regions (Figure 18A, B).

A good example of affected muscles was the gastrocnemius muscle, depicted in Figure 18A and 18B. Comparable cross-sections of *Osr1*$^{+/+}$ and *Osr1*$^{GCE/GCE}$ embryos exhibit a remarkable loss of normal muscle shape after immunostaining using an anti-MyHC antibody. The gastrocnemius muscle is formed by two muscle heads with an L-like-shape, the so-called medial and lateral heads. In *Osr1*$^{GCE/GCE}$ mutant embryos the medial head of this muscle appeared wrongly located below its lateral head (Figure 18A, B). Additionally, muscle fibers in the medial part of the muscle grew in a disarranged frayed manner (figure 18B, orange arrow and 18D blue arrow).

In order to improve the visualization of muscle defects, I aligned limb cross-sections to reconstruct 3 dimensional (3D) muscle shapes in selected muscles. Volume rendering using the program Amiraő created a reconstruction of the muscle shape (Figure 18C and D). 3D reconstructions allowed visualization of muscle shapes in 3D that resemble more closely to the in vivo situation. As previously observed on sections (Figure 18A and B), 3D reconstructions of the gastrocnemius muscle confirmed the wrong location of the whole medial head in E13.5 *Osr1*$^{GCE/GCE}$ mutant embryos. Thus, this part of the muscle is separated from its presumptive tendon attachment at the head of femur (Figure 18C, D and green arrows). To assess the effect of this severe muscle patterning impairment in the formation of the tendon connecting the medial head of the gastrocnemius muscle with the femur, cross-sections of the region in hindlimb *Osr1*$^{+/+}$ and *Osr1*$^{GCE/GCE}$ embryos were used to address *Scx* expression. *In situ* hybridization revealed the loss of *Scx* expression in the presumptive tendon structure on E13.5 *Osr1*$^{GCE/GCE}$ hindlimb cross-sections, where mislocated muscle fibers counterstained by an anti-MyHC antibody were not found at their normal location at the muscle/tendon attachment (Figure 18E, F).

This approach provided first insights in muscle impairments of *Osr1*$^{GCE/GCE}$ knock out embryos, but only remarkable changes such as for the gastrocnemius muscle became apparent due to a low resolution of the volume-rendered 3D model. Therefore, I decided to take advantages of a different technique to image whole embryos or organs using immunofluorescence followed by confocal stacking and 3D reconstruction. This approach had the advantage, compared to the previous, to use whole intact tissue (not sectioned) allowing a higher fidelity in the 3D shape of imaged objects. Furthermore, in combination

with immunofluorescence this allowed to use more than one tissue marker facilitating observations of tissue interactions. Using E14.5 *Osr1*$^{+/+}$ and *Osr1*$^{GCE/GCE}$ embryos, we could assess muscle defects of fully patterned limb muscles. Embryos were carefully skinned before bleaching and subjected to a long permeabilization period to enhanced antibody penetration. Limbs were cleared with a compound of benzyl alcohol and benzyl benzoate after immunolabeling and before imaging. An inverted confocal microscope was used to create Z-stack images of whole limbs. Images were analyzed using the program FluoRender (Wan et al., 2012) specialized on fluorescence 3D reconstructions.

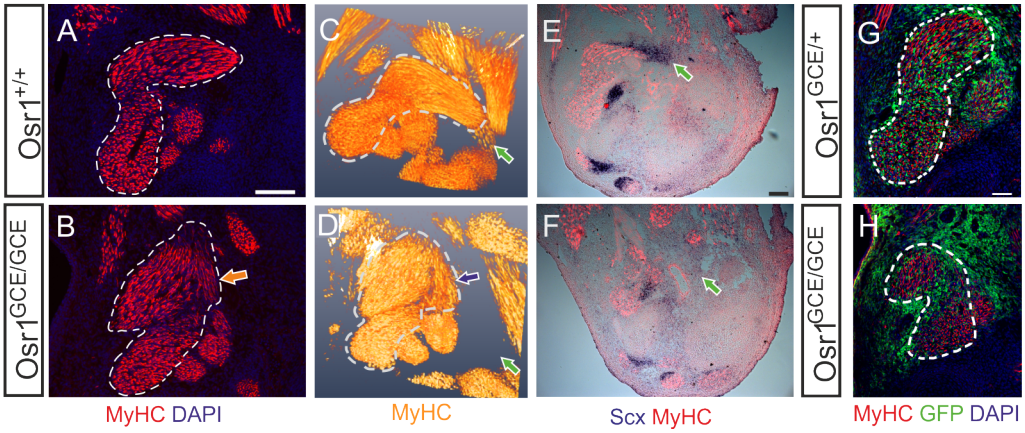

Figure 18: ***Osr1***$^{GCE/GCE}$ **embryos show muscle patterning defects in the limb**. Immunostaining on paraffin sections of E13.5 hindlimbs using an antibody against MyHC revealed muscle shape impairments at the gastrocnemius region (A, B). Muscle immunostaining of consecutive paraffin sections were used in volume rendering models generated by the program Amira to visualize affected muscles in E13.5 *Osr1*$^{+/+}$ and *Osr1*$^{GCE/GCE}$ embryos (C, D). *In situ* hybridization on cryo-sections revealed loss of *Scx* expression at the tendon attachment zone of the gastrocnemius muscle (E, F). Cryo-sections of E13.5 hindlimb embryos were stained against GFP and MyHC proteins to visualize *Osr1* expression in *Osr1*$^{GCE/+}$ and *Osr1*$^{GCE/GCE}$ embryos in the same gastrocnemius region (G, H). Scale bar 100 μm (A), 50 μm (E).

3D models obtained with this technique revealed a more accurate reconstruction of muscles with much higher resolution allowing the observation of changes in patterning of all limb muscles. (Figure 19A, B; 19E, F). Detailed comparison of 3D reconstructions from hindlimb and forelimb muscles revealed that muscles were differentially affected. Although the majority of the affected muscle in *Osr1*$^{GCE/GCE}$ showed reduced size (Figure 19C, D; 19G-J), diversity in muscle shapes presented along the affected muscles was noticeable. I found that in severe affected long muscles, muscle fibers were severely shortened reducing the longitudinal size of the muscle, while their width remains mostly unchanged (Figure 19G-L). Consistent changes were observed in muscles, where only a part of the muscle has not correctly developed or was missing, while the rest of the muscle was not severe changed (e.g. Figure 19C, D). Furthermore, other affected muscles displayed a serious impairment in muscle shape affecting the whole muscle and disrupting its original shape

(Figure 19I-L). In contrast, other muscles did not appear to be severely affected showing only a minor shortening of their length. These muscles often were slightly shorter at the attachment zones to tendons, seemed to be flattened and broader in the middle part of the muscle.

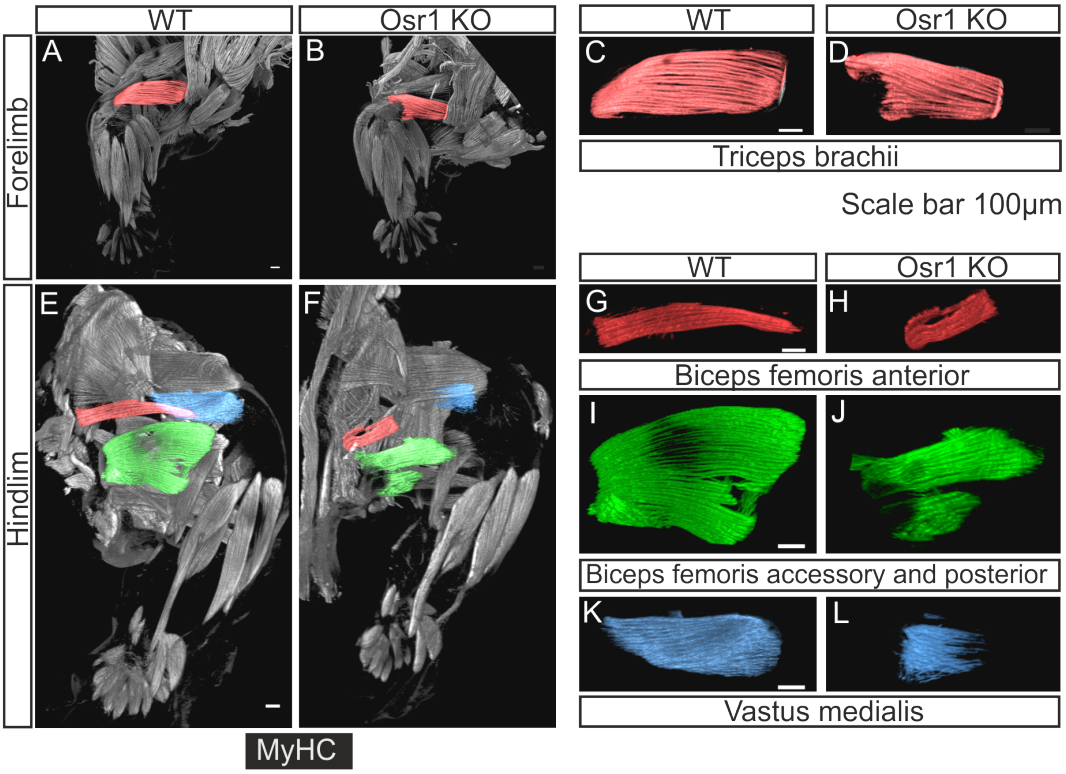

Figure 19: **Muscle patterning defects revealed after 3D reconstruction of E14.5 *Osr1*$^{+/+}$ and *Osr1*$^{GCE/GCE}$ limb muscles.** Whole mount immunostaining was performed to achieve muscle staining of hindlimbs and forelimbs. 3D reconstructions were created using the program FluoRender after previous Z-Stacks confocal images (A, B; E,F, left). For better comparison, single muscles from whole limbs 3D reconstructions were extracted (right). Examples of muscles of forelimb (C, D) and hindlimb (G-L) showing severe muscle patterning impairments. Scale bar 100 μm.

In summary, the combination of these two approaches allowed characterization of local distinct defects in limb muscle pattern that would be mostly not recognizable via common 2D section immunostaining.

7.2.2 Myofiber disorganization in *Osr1*$^{GCE/GCE}$ embryos

Every muscle of the limb contains a specific number of fibers, the orientation of which assure function of the muscle. One general characteristic observed in *Osr1*$^{GCE/GCE}$ muscles was a loss in myofiber organization. The subscapularis muscle of the upper forelimb represents an example of this impairment. This muscle is formed by intricate muscle fascicles that are tightly delimitated by connective tissue and connected at one side to tendons of the shoulder blade and in the other side to tendons of the humerus head. Muscle fibers

of this muscle were often misaligned with a frayed aspect, as observed in E14.5 3D reconstructions (Figure 20A, B). Muscle fiber misalignment was already observed at the stage E13.5. Cross-sections of the subscapularis muscle area revealed fusion of muscle fascicle and an invasion of likely fascia tissue (Figure 20D orange arrow). Myofibers in the different muscle fascicles of E13.5 *Osr1*$^{+/+}$ subscapularis muscle follow the same direction as the muscle was cross-sectioned and immunostained using an anti-MyHC antibody to label muscle fibers (Figure 20C, white arrows). In contrast, in E13.5 *Osr1*$^{GCE/GCE}$ embryos, myofibers of the same fascicle appeared orientated in a different direction and therefore sectioned in a different angle (Figure 20D, white arrows). Other muscles exhibited more drastic changes in muscle fiber orientation than frayed appearance of fibers. Some muscles presented completely mislocated fibers in a portion of the muscle, growing in a wrong direction, completely un-functional for muscle contraction as previously observed in the middle part of the gastrocnemius muscle (Figure 18D, arrow), proximal region of biceps femoris and vastus medialis muscles (Figure 19J, L).

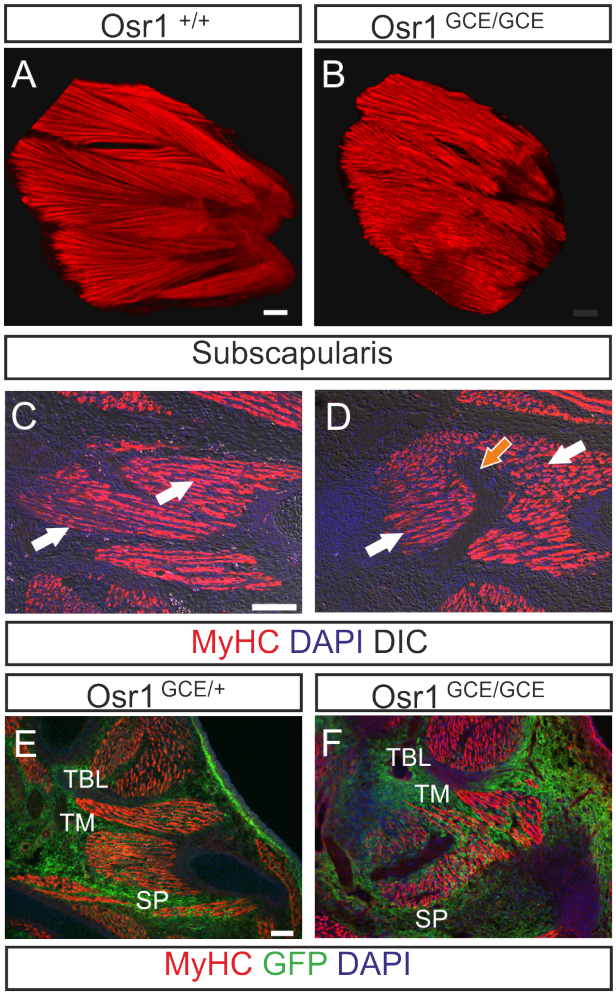

Figure 20: **Muscle fibers presented a general disorganization and frayed alignment in muscles of *Osr1*$^{GCE/GCE}$ embryos**. 3D reconstruction of the subscapularis muscle at the stage E14.5 showed the normal intricate alignment of fibers in *Osr1*$^{GCE/+}$ forelimbs and their disorganization in *Osr1*$^{GCE/GCE}$ embryos (A, B). Immunostaning of the same muscle region at the stage E13.5 using MyHC merged with DIC microscopy brightfield image showed muscle fiber arrangements in *Osr1*$^{+/+}$ and *Osr1*$^{GCE/GCE}$ (C, D). White arrows point to similar regions of the subscapularis muscle, whilst orange arrow point to ectopic fascia tissue only found in *Osr1*$^{GCE/GCE}$ embryos. Immunohistochemistry on E13.5 forelimb cross-sections using anti-GFP and anti-MyHC antibodies showed *Osr1* expression pattern in subscapularis region (E, F). Scale bar 100 μm (A-D), 50 μm (E, F). SP, subscapularis muscle; TBL, triceps brachii long head; TM, teres major

7.2.3 Formation of ectopic muscles and ectopically located muscle progenitors in *Osr1*$^{GCE/GCE}$ embryos

Interestingly, at several parts of the limb, ectopic formation of muscle fibers was observed. This was seen at few places, but consistently in several *Osr1*$^{GCE/GCE}$ animals. An example is the small bundle of muscle fibers growing apart in the distal portion of the muscle extensor digitorum longus (EDL) between this muscle and the flexor digitorum quarti (FDQ) observed in 3D reconstruction (Figure 21A, B). These muscle fibers were

also observed in cross-sections of E13.5 hindlimbs (Figure 21C, D) connecting both muscles. Immunohistochemistry using *MyoD* as a marker for myoblast demonstrated that in the same region myoblasts were ectopically located (Figure 21E, F). These results were suggestive of a dislocation of muscle progenitors followed by myogenic differentiation in wrong places.

As previously reported, blood vessels have an important function delimitating muscle edges (Tozer et al., 2007). We aimed to observe impairments in blood vessel formation using an antibody against the endothelial protein platelet endothelial adhesion molecule (PECAM1). General blood vessel patterning appeared unaffected in E13.5 $Osr1^{GCE/GCE}$ mutant embryos. However, formation of capillaries labelled by PECAM1 was impaired in the region where muscle fibers were growing ectopically between EDL and FDQ muscles (Figure 21G, H, arrows).

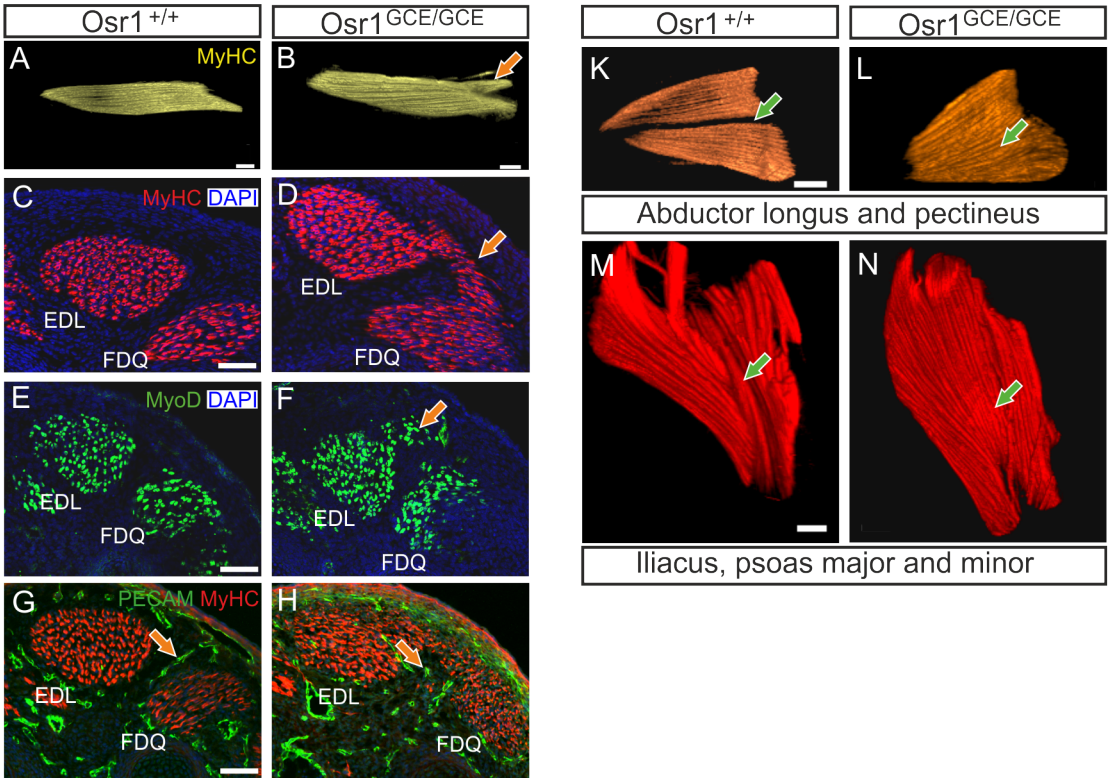

Figure 21: **Ectopic formation of muscle fibers close to the hindlimb muscle EDL together with aberrantly located muscle precursors**. 3D reconstruction of the EDL muscle at the stage E14.5 shows ectopic bundle formation after MyHC whole mount immunostaining (A, B). Further immunochemistry analysis at the stage E13.5 of the same region revealed ectopic myoblast location after immunostaining using an anti-MyoD antibody (C-F). Labeling for PECAM1 showed defective blood vessel formation in the same region in the mutant (G, H). Additionally, 3D reconstruction of hindlimb muscles revealed fusion of specific muscles in E14.5 *Osr1* mutant embryos (K-N). EDL, extensor digitorum longus; FDQ, flexor digitorum quarti. Scale bar 100 μm.

Further analysis of E14.5 whole limb 3D reconstructions highlighted also a defect in

separation of specific muscles in total or in part, consequently leading to the fusion of these muscles in *Osr1*$^{GCE/GCE}$ mutant embryos. A clear example of this muscle impairments are the abductor longus and pectineus muscles of the upper hindlimb. These two muscles similar in shape exhibit loss of muscle interspace and consequent fusion of muscles (Figure 21K, L). Similarly, the three muscles of the hip, iliacus, psoas major and minor presented a loss of muscle edges, impeding recognition of each single muscle limits in 3D reconstructions of E14.5 *Osr1*$^{GCE/GCE}$ mutant embryos (Figure 21M, N).

7.2.4 Correlation of *Osr1* expression with phenotypic changes in muscle patterning

Comprehensive phenotypical analysis of muscle defects of forelimbs and hindlimbs reported differentially affected muscles in *Osr1* mutant mice. This observation together with the regionalized expression of *Osr1* in connective tissue suggested a correlation between the expression pattern of *Osr1* and the muscle defects observed in the mutants. Closer observation of *Osr1* expression on cross-sections of *Osr1*$^{GCE/+}$ and *Osr1*$^{GCE/GCE}$ E13.5 embryos after immunohistochemistry using an anti-GFP antibody to label Osr1+ cells and anti-MyHC to label myofibers reported high correlation of affected muscles with high levels of *Osr1* expression. Affected hindlimb muscles (Figure 18G, H) as well as forelimb muscles (Figure 20E, F) exhibited strong *Osr1* expression in the surrounding as well as interstitial connective tissue.

This has a second implication. Osr1+ cells were obviously present in the connective tissue of *Osr1*$^{GCE/GCE}$ mutants despite lack of OSR1 protein. Osr1+ cells surrounded affected muscles in null mutants in a similar manner as in *Osr1*$^{GCE/+}$ embryos. Therefore, the muscle defects in *Osr1*$^{GCE/GCE}$ mutant cannot be explained by an absence of Osr1+ cells in *Osr1*$^{GCE/GCE}$ muscle connective tissue. Rather, it suggests that the Osr1+ cells deprived of OSR1 activity are functionally defective, e.g. via aberrant expression or downregulation of signaling factors.

7.3 Transcriptome analysis of embryonic Osr1+ cells

Quantifying gene expression levels provides an useful readout about the transcriptional state of cells or tissues at the moment of RNA extraction. Microarray technology has taken this analysis to a genome-wide level, however a more accurate and comprehensive analysis of transcriptional level of all the genes can be achieved by massively parallel sequencing approaches (next generation sequencing, NGS).

7.3.1 RNA-sequencing of Osr1+ sorted cells

RNA-sequencing (RNA-Seq) was chosen to measure genome-wide changes in gene expression levels at the stage E13.5. At this stage, mouse limb muscle patterning is not completely finished and Osr1+ cells, as previously described, are located in the connective tissue surrounding individualized muscles and between muscle fibers (Figure 40C, C'). Fluorescence-activated cell sorting (FACS) was used prior RNA-seq to specifically obtain a transcriptomal analysis of limb Osr1+ cells. Consequently, transcriptome analysis was designed to compare *Osr1*$^{GCE/+}$ and *Osr1*$^{GCE/GCE}$ cells.

To obtain cell suspension of limbs and shoulders, E13.5 embryos of each genotype were dissected as described in section (Figure 11A). Cell extracts were used for FACS sorting based on GFP fluorescence. A wild-type cell suspension was used to set up scatter configuration and thresholds for GFP intensity. GFP-positive cells built a new clearly identifiable cloud of cells with a GFP-intensity signal in *Osr1*$^{GCE/+}$ and *Osr1*$^{GCE/GCE}$ extracts clearly distinguishable from *Osr1*$^{+/+}$ GFP-negative cells (Figure 22B). Out of all extracted cells, Osr1+ cells constituted on average 15.9% in *Osr1*$^{GCE/+}$ limb cells and 33.5% in *Osr1*$^{GCE/GCE}$ limb cells (Figure 22B).

RNA extracted from 2 independent *Osr1*$^{GCE/+}$ and *Osr1*$^{GCE/GCE}$ embryos were sequenced using Next-generation sequencing on the Illumina HiSeq 2500 platform. Bioinformatic analysis of output data after sequencing was performed by Mickael Orgeur. Briefly, sequencing reads of each biological replicate were mapped by using TopHat2 [PMID: 23618408] against the genome of mus musculus (version mm9) and the corresponding RefSeq gene annotation downloaded from the UCSC browser. Read counts were estimated by using the python framework HTSeq [PMID: 25260700] and analyzed by using the R package DESeq2 [PMID: 25516281]. Hierarchical clustering was first performed on the gene expression levels between each biological replicate to assess the sample-to-sample distances (Figure 22C). Replicates belonging to the same genotype, *Osr1*$^{GCE/+}$ or *Osr1*$^{GCE/GCE}$, were closer to each other than any replicate of the other genotype. Expression level differences between each biological replicate were thus dependent on the genotype and read counts could be further analyzed. 511 genes were considered as being differentially expressed according to a false-discovery rate of 5% and a Benjamini-Hochberg adjusted p-value below 0.1. As observed in the volcano plot representation (Figure 22D), the 511 differentially expressed genes were similarly distributed between up-regulated and down-regulated genes.

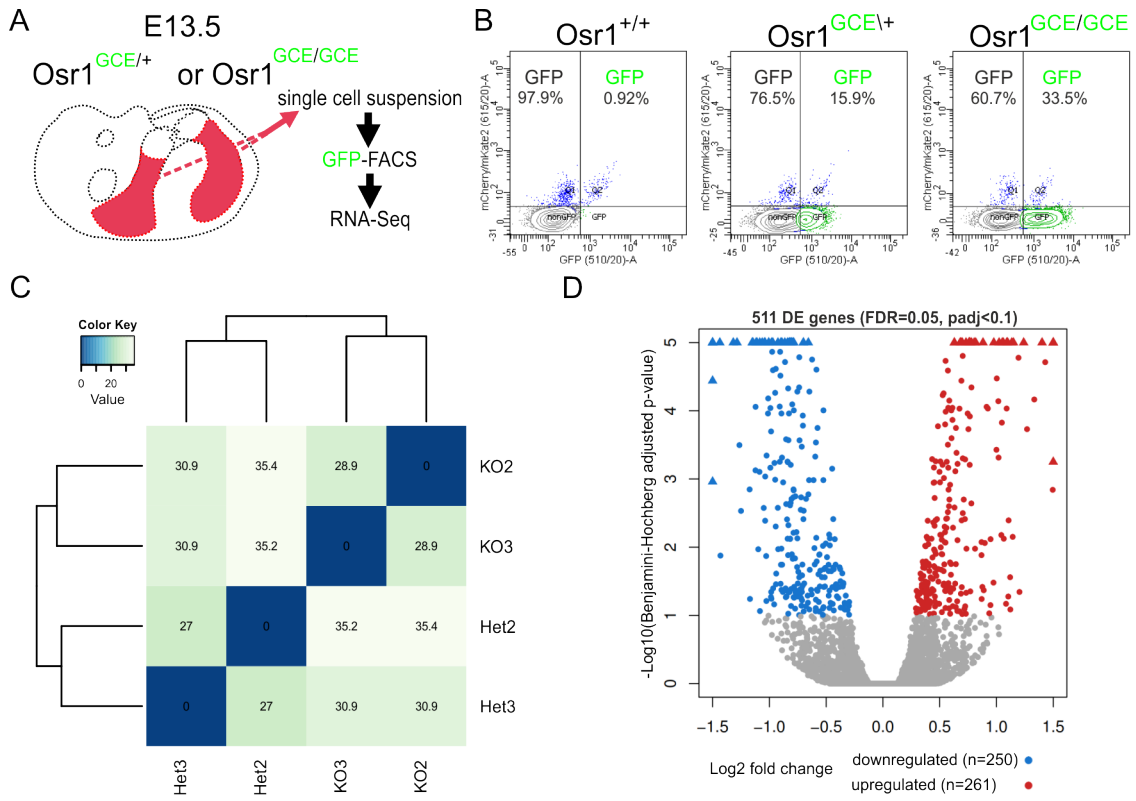

Figure 22: **Transcriptome of E13.5 *Osr1*$^{GCE/+}$ and *Osr1*$^{GCE/GCE}$ FACS sorted cells using RNA-seq**. Procedure of Osr1+ cell isolation from E13.5 limbs and shoulder regions (A) and cell populations based on mCherry and GFP emission signals visualized by FACSDivaTM software(B). Sample-to-sample distance heat map between E13.5 *Osr1*$^{GCE/+}$ (Het) and *Osr1*$^{GCE/GCE}$ (KO) cells based on their gene expression levels (C). Volcano plot representation of the 511 deregulated genes obtained after RNA-Seq data analysis (D). This double logarithmic representation plots depicted the significance (y-axis) versus the gene expression fold-change (x-axis) between the *Osr1* heterozygous and knock out samples. Genes with expression value and/or significance beyond the axes scale are represented as triangles. DE, differentially expressed, FDR, False Discovery Rate; padj, adjusted p-value.

7.3.2 Gene ontology analysis of deregulated genes

Gene ontology (GO) is a bioinformatics approach developed in the attempt to classify and standardize genes or gene products attributed to a certain biological context. With the aim to clarify the importance of the deregulated genes found in Osr1-deficient cells in different biological contexts, we used the DAVID online tools [PMID: 19131956]. We asked whether the deregulated genes in *Osr1* knock out cells are represented into specific GO terms within the categories related to biological processes, cellular compartments and signaling pathways.

The cellular component GO category describes locations at the level of subcellular structures of protein complexes. GO analysis for cellular components highlighted genes coding for extracellular proteins (GO term "extracellular region", Figure 23A) as over-represented among the differentially expressed genes. In addition the extracellular region

subcategories "extracellular matrix" and "proteinaceous extracellular matrix" were enriched (Figure 23A). Within the deregulated extracellular matrix (ECM) genes, down and up-regulated genes were equally distributed as shown by heat-map representation (Figure 23B).

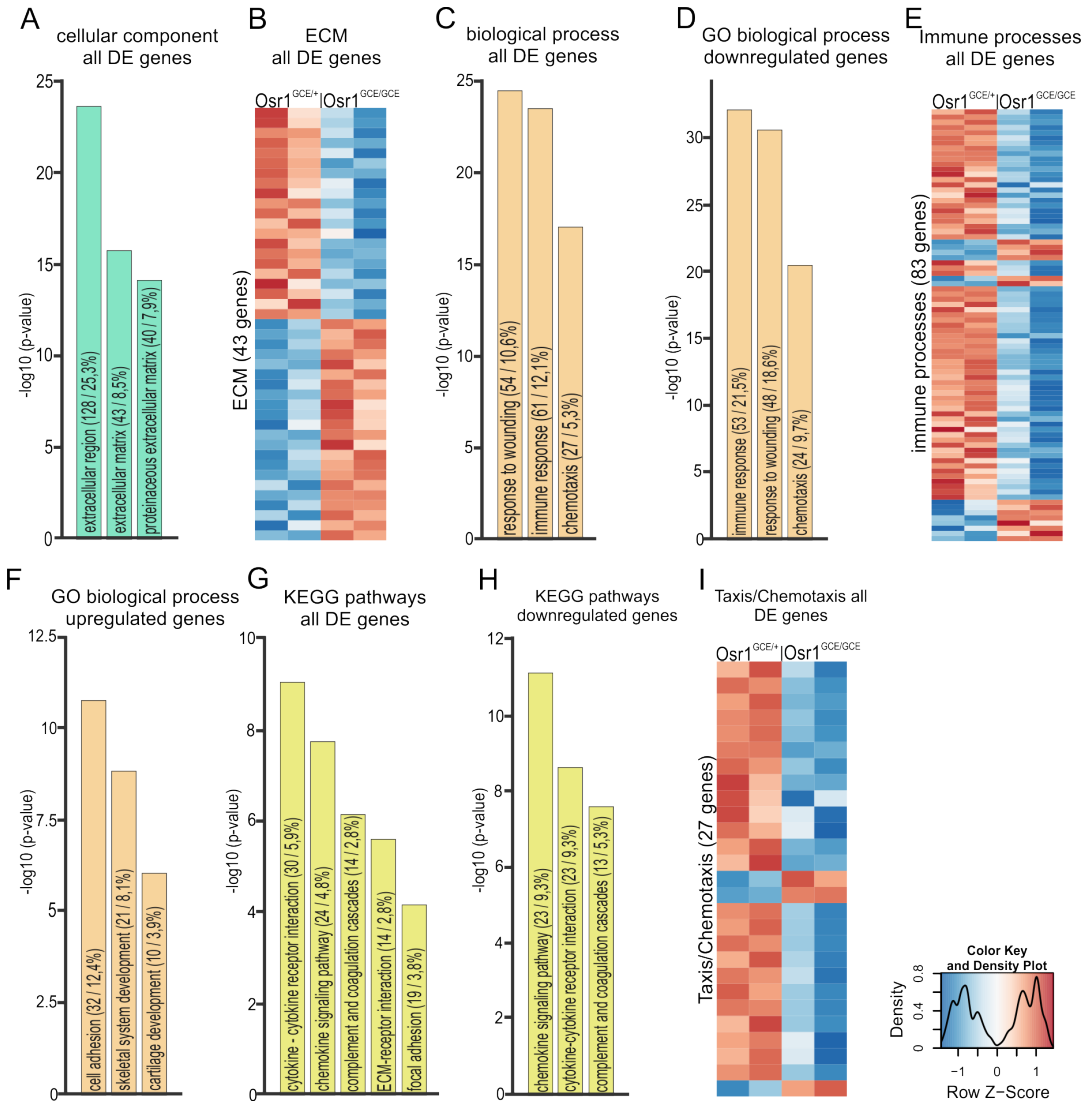

Figure 23: **Gene ontology (GO) analysis of deregulated genes revealed strong enrichment for genes coding for extracellular proteins and for proteins involved in the immune response**. GO analysis of the domains "biological processes" and "cellular components" as well as KEGG pathway analysis using the annotation tool DAVID (Database for Annotation, Visualization and Integrated Discovery) were performed on all deregulated as well as specifically on up- and down-regulated genes (A, C, D, F, G, H). Heat-map of selected gene ontology compartments for deregulated genes, up- (red) and down-regulated (blue) genes (B, E and I). P-values are displayed in - based Log10.

Interestingly, gene ontology analysis of all deregulated genes for biological processes highlighted genes relating to immune processes such as the GO terms "response to wounding", "immune response" or "chemotaxis" (Figure 23C). Further analysis of genes belong-

ing to these GO categories showed that they contain genes not only involved in immune processes (albeit this is a prominent role), but a more general role in cellular communication. The vast majority of genes related to immune processes were down-regulated (Figure 23E). Therefore, GO analysis of down-regulated genes for "biological processes" showed a high significance in terms of p-values and percentage of genes in each immune response compartment (figure 23D). Conversely, GO analysis of upregulated genes for "biological processes" showed enrichment for "cell adhesion" (Figure 23F). Surprisingly, "skeletal system development" and "cartilage development" were highlighted (Figure 23F), despite the minimal contribution of Osr1+ derived cells to those tissues (Figure 17A-C).

KEGG (Kyoto Encyclopedia of Genes and Genomes) pathway analysis of differentially expressed genes in *Osr1* knock out cells highlighted signaling pathways that were usually involved in the immune system, such as cytokine-cytokine receptor interaction, chemokine signaling pathway or complement and coagulation cascades (Figure 23G), in agreement with GO analysis for "biological process"(Figure 23C-E). Similarly, the majority of genes belonging to these pathways were down-regulated in *Osr1*$^{GCE/GCE}$ cells, as exemplified in a heat-map representation of genes belonging to the GO compartment taxis and chemotaxis (Figure 23I). Consistently, KEGG pathways analysis performed for down-regulated genes yielded higher significance compared with the analysis of all deregulated genes (Figure 23H).

In summary, genome wide approaches allowed us to elucidate the transcriptional status of E13.5 Osr1+ cells heterozygous vs. null for *Osr1*, and indicated an important pool of secreted components of the extracellular region produced by Osr1+ cells. These components apparently are composed of both, structural ECM components and signaling molecules.

7.4 *Osr1* is required for connective tissue identity in the embryo

Cells derived from Osr1+ progenitors in the limb mesenchyme were barely observed to give rise to tendon or skeletal elements (see section 8.1.2). However, GO analysis of "biological processes" in up-regulated genes of E13.5 *Osr1*$^{GCE/GCE}$ cells highlighted a significant enrichment of genes belonging to the categories "skeletal development" and "cartilage development", indicating that genes involved in these processes were normally repressed by *Osr1* during normal development. This result together with published data about the *Osr1* inhibiting function of cartilage and bone differentiation of bone marrow mesenchymal stromal cells (BMSCs) (Stricker et al., 2012) strongly supported the idea of *Osr1* being a master regulator gene that maintains cells in a connective tissue state.

To further investigate the transcriptional changes due to lack of *Osr1* activity in Osr1+

connective tissue cells, we performed a more comprehensive analysis of the RNAseq data for genes known to be involved in cartilage and tendon formation or showing a predominant expression in either of these tissues (Eurexpress database, Havis et al. (2014)). All the genes selected on this basis were upregulated in *Osr1*-deficient cells (Figure 24A).

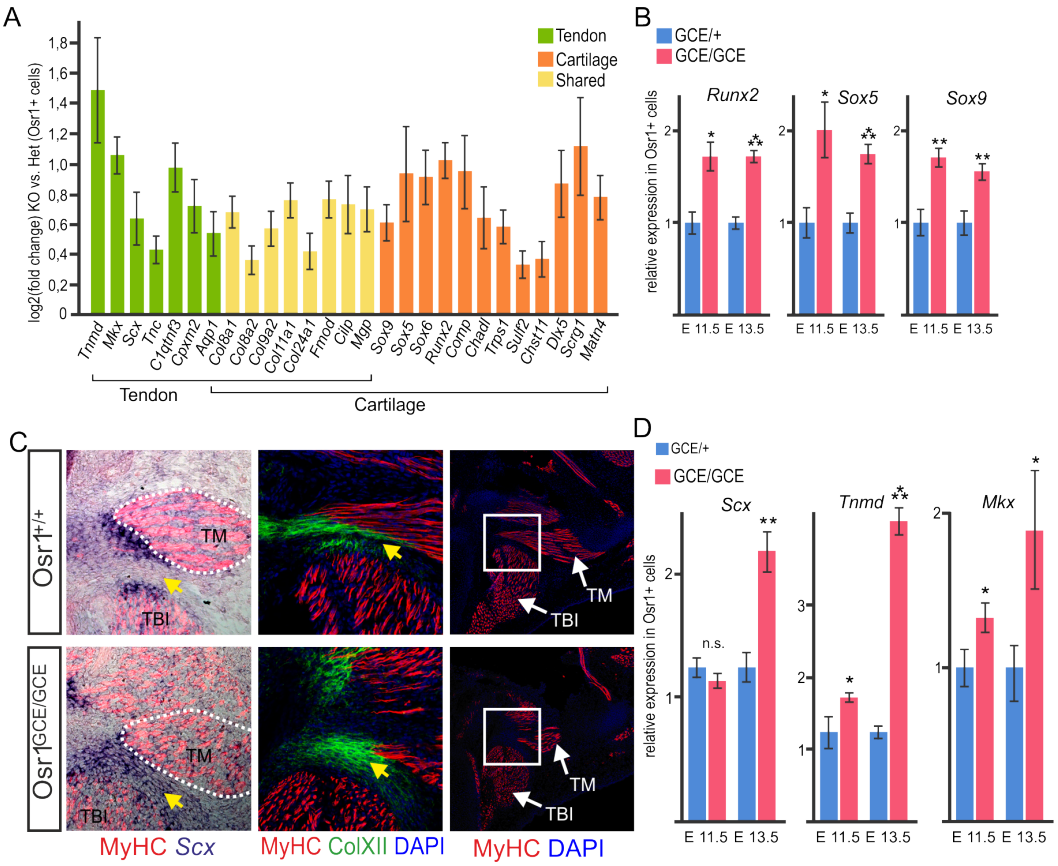

Figure 24: ***Osr1* is a marker for connective tissue identity**. At the transcriptional levels, lack of *Osr1* in $Osr1^{GCE/GCE}$ cells leads to an up-regulation of tendon and cartilage related genes (A). 0 is the level of the $Osr1^{GCE/+}$ cells (A). Up-regulation of cartilage and tendon genes was assessed by RT-qPCR using RNA isolated from $Osr1^{GCE/+}$ and $Osr1^{GCE/GCE}$ cells at the stages E11.5 and E13.5 (B, D). Immunohistochemical analysis of tendons of the forelimb muscle teres major using an antibody anti-ColXII (tendon) and anti-MyHC (muscle). *In situ* hybridization revealed ectopic expression of *Scx* in E13.5 In situ mutants compared to control E13.5 $Osr1^{GCE/+}$ (C). TBI, triceps brachii long head; TM, teres major. Scale bar 50 μm (A-D), 100 μm (E-H). Scale bar represent SEM, $*$ $p<0.05$; $**$ $p<0.001$; $***$ $p<0.0001$.

We found that the main transcription factors related to tendon development, scleraxis (*Scx*) and mohawk (*Mkx*), as well as genes encoding structural proteins and induced after tendon differentiation such as tenomodulin (*Tnmd*), tenascin c (*Tnc*) and aquaporin1 (*Aqp1*) were upregulated in sorted E13.5 $Osr1^{GCE/GCE}$ cells compared to E13.5 $Osr1^{GCE/+}$ cells (Figure 24A, green). Among all up-regulated genes a significant portion of genes were found to be associated with cartilage development in GO analysis (10 genes, 3.9% of all up-regulated genes). Transcription factors implicated in cartilage formation

such as *Runx2*, *Sox9*, *Sox5* or *Sox6* were up-regulated together with many cartilage associated proteins (Figure 24A, orange). In addition, common cartilage and tendon genes, showed an increase in their transcriptional levels in E13.5 *Osr1*$^{GCE/GCE}$ cells (Figure 24A, yellow). RT-qPCR analysis was performed to confirm the changes of mRNA expression levels of selected tendon and cartilage genes in E13.5 *Osr1*$^{GCE/GCE}$ cells (Figure 24B, D).

Comparison of the transcriptional levels of selected cartilage and tendon genes between *Osr1*$^{GCE/GCE}$ in addition to *Osr1*$^{GCE/+}$ sorted cells at E11.5 and E13.5 was performed to provide deeper insight into the developmental period the transcriptional switch Osr1+ cells occurs in. Interestingly, the up-regulation of cartilage gene expression was already observed in E11.5 *Osr1*$^{GCE/GCE}$ limb bud cells (Figure 24B). In a similar manner, albeit weaker, the expression of tendon related genes was upregulated in E11.5 *Osr1*$^{GCE/GCE}$ cells. The up-regulation at the transcriptional levels of tendon genes was confirmed at E13.5 being clearly more pronounced at this stage.

In situ hybridization using a *Scx* probe on E13.5 *Osr1*$^{+/+}$ and *Osr1*$^{GCE/GCE}$ forelimb cross-sections revealed ectopic expression of *Scx* in a layer of connective tissue that separates tendon structures between the teres major (tm) and triceps brachii long head (tbi) muscles. Immunohistochemical analysis using antibodies against MyHC and type XII collagen, confirmed the physical separation of both tendons by a thin portion of connective tissue in E13.5 *Osr1*$^{GCE/+}$ (Figure 24C, yellow arrows). In contrast, in the same region of E13.5 *Osr1*$^{GCE/GCE}$ embryos, fibers of type XII collagen are not separated by connective tissue and are merged in a unique bundle of type XII collagen (Figure 24C). Altogether this confirms a role for *Osr1* in maintaining connective tissue cell identity in mouse limb mesenchymal cells as previously postulated in the chick model.

7.5 Extracellular matrix impairment in *Osr1*$^{GCE/GCE}$ embryos

7.5.1 *Osr1* is required for the correct production and organization of structural components of the extracellular matrix

The extracellular matrix (ECM) commonly refers to the structural components secreted by cells that provide support to the surrounding cells. Despite this definition, ECM has acquired a more complex role than simply serving as a scaffold.

The transcriptome analysis of Osr1+ cells indicated defective expression of ECM genes in *Osr1*-deficient cells. Since Osr1+ cells are at a muscle interstitial position, it is likely that a considerable part of the muscle ECM might be secreted by muscle connective tissue cells. Comparison of relative transcript levels (normalized read count in RNA-Seq) of structural collagens such as type I, III, V or VI collagens were amongst the highest

expressed genes in Osr1+ cells indicating such a function for Osr1+ cells. Among the ECM genes found to be deregulated in E13.5 *Osr1*-deficient cells, connective tissue collagen genes as well as genes encoding associated extracellular matrix proteins, such as small leucine rich-proteoglycan (SLRP) or other matrix associated proteins were found to be downregulated in E13.5 *Osr1*$^{GCE/GCE}$ sorted cells (Figure 25A). Selected candidate genes were confirmed by RT-qPCR at E13.5 in *Osr1*$^{GCE/+}$ as well as *Osr1*$^{GCE/GCE}$ cells. In addition, RT-qPCR was also performed on FACS isolated cells from E11.5 embryos to assess whether the deregulation of these candidates started before the onset of an apparent muscle phenotype in *Osr1* mutants. RT-qPCR analysis confirmed the transcriptional down-regulation of structural collagens such as type III and V collagens as well as downregulation of genes encoding three different chains of type VI collagen in E13.5 *Osr1*$^{GCE/GCE}$ cells (figure 25B). At E11.5, only transcriptional downregulation of *Col6a3* was found significant among the analyzed structural collagens (figure 25B).

In addition to transcriptional changes of ECM components, we aimed to address ECM defects at the protein levels using antibodies against the ECM-proteins type VI collagen (COLVI) and fibronectin (FN1). At E11.5, defects in ECM formation were already visible. ECM embedding LBX1+ muscle progenitors showed a reduction in type VI collagen fibers as well as a decreased abundance of fibronectin (Figure 25K-L).

At E13.5, COLVI protein was detectable in muscle connective tissue of *Osr1*$^{GCE/GCE}$ hindlimb muscles (Figure 25C, D). Nevertheless, closer observation of affected muscles showed a significant reduction of protein abundance (Figure 25E, F). Connective tissue surrounding muscle fibers of the gastrocnemius muscle display a clear example of COLVI protein reduction (Figure 25E, F). Within the reported muscle impairments, fusion of muscles due to the loss of muscle interspace represented an interesting model to observe the role of connective tissue delimitating regions of muscle growth. The hindlimb muscles, semimembranosus and quadratus femoris showed on cross-sections a tight spatial association. Immunostaining using MyHC to label muscle fibers and COLVI revealed loss of a structural ECM separating both muscles as COLVI immunostaining decreased in this region. Muscle fibers grew through the border of the semimembranosus muscle leading to the fusion of this part of the muscle (Figure 25G, H).

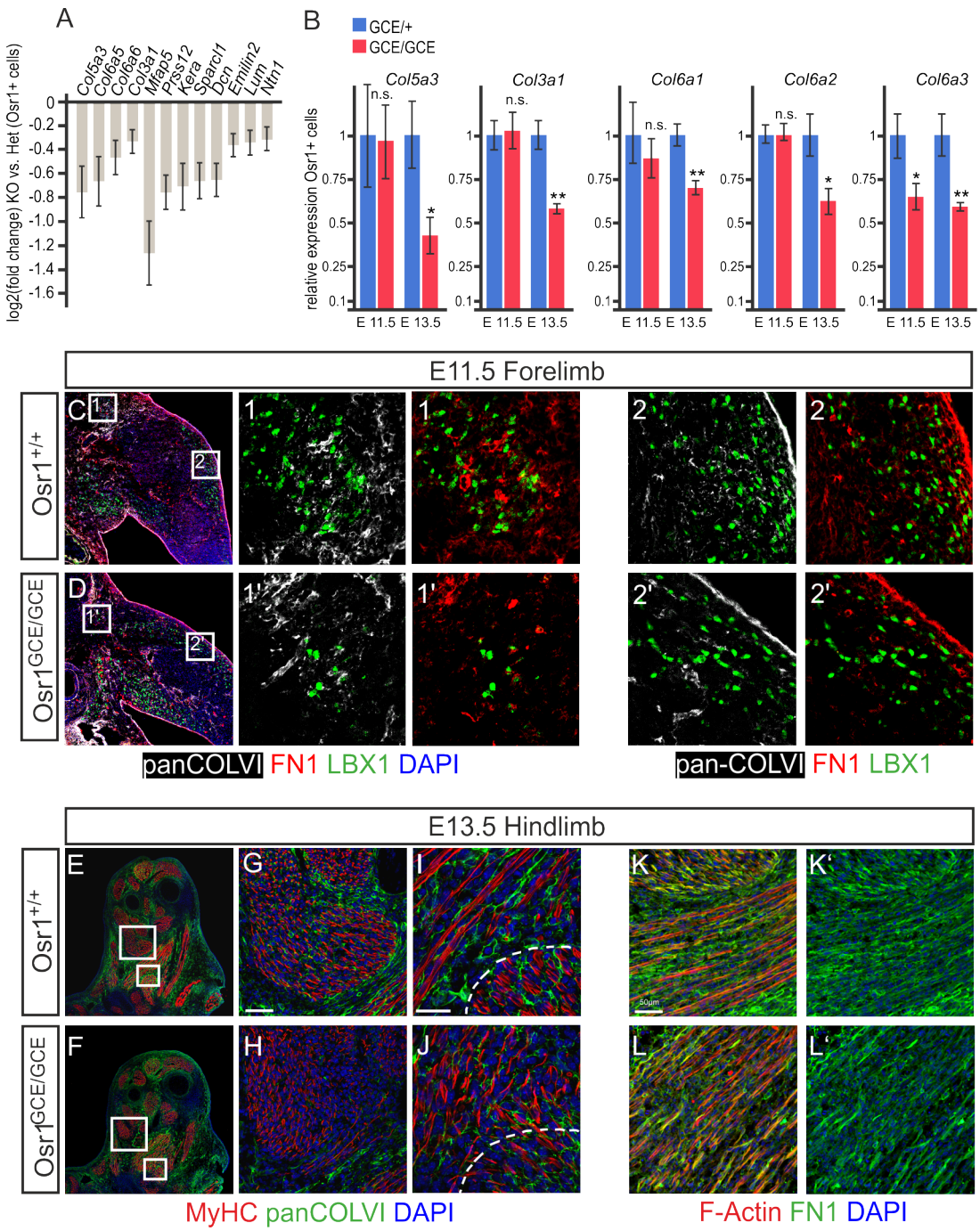

Figure 25: **Expression analysis for ECM genes and immunolabeling on sections highlighted changes in ECM structural components in *Osr1*$^{GCE/GCE}$ mutant embryos**. (A) Several structural proteins associated with muscle connective tissue were significantly down-regulated in E13.5 *Osr1*$^{GCE/GCE}$ limbs cells. Values of -log2 fold change of every gene were represented after RNA-seq. (B) RT-qPCR of E11.5 and E13.5 Osr1+ sorted cells was performed to confirm transcriptional changes of candidates genes. Expression values were calculated referring to expression in heterozygous. Immunohistochemistry analysis of E13.5 hindlimb and E11.5 forelimb cross-sections were used to visualize ECM proteins using antibodies against type VI collagen (panCOLVI) and fibronectin (FN1) and possible impairments in mutant embryos. Muscle fibers were labelled at E13.5 with an antibody against MyHC (red), at E11.5 muscle progenitors were labeled for LBX1. Error bars represent SEM and $*$ $p<0.05$, $**$ $p<0.01$. Scale bar 50 μm E, F; I-J' 20 μm G, H.

Fibronectin is a structural glycoprotein and one of the principal constituents of young ECM as well as highly expressed in many types of connective tissue. Fibronectin and type VI collagen were used as a marker to reveal structural changes in ECM. Antibody staining of E13.5 hindlimb cross-sections revealed a reduced abundance of fibronectin protein in the connective tissue of *Osr1*$^{GCE/GCE}$ embryos (figure 25I-J'). Furthermore, arrangement of fibronectin fibers in muscle connective tissue displayed an impaired organization, as shown for the semimembranosus muscle (Figure 25I', J').

7.5.2 Basal lamina disruption in muscles fibers of *Osr1*$^{GCE/GCE}$ embryos

Transmembrane proteins and glycoproteins of the muscle fiber membrane, the sarcolemma, are anchoring striated muscle fibers to structural ECM collagens through specialized protein complexes called costameres. The first sheet of specialized proteins bridging anchor proteins and ECM is formed by the basal lamina. Disruption of ECM structure could lead to basal lamina impairments.

Using an antibody against the basal lamina protein type IV collagen (COLIV) demonstrated changes in structure and protein level of the basal lamina. E14.5 hindlimb cross-section highlighted impaired basal lamina formation in affected muscles as gastrocnemius or semimembranosus. Levels of type IV collagen protein were decreased in the basal lamina of fibers belonging to gastrocnemius and semimembranosus muscles (Figure 26A-H). Furthermore, longitudinal sections of the semimembranosus showed a discontinuous production of type IV collagen protein along the disorganized muscle fibers of this muscle (Figure 26E-H).

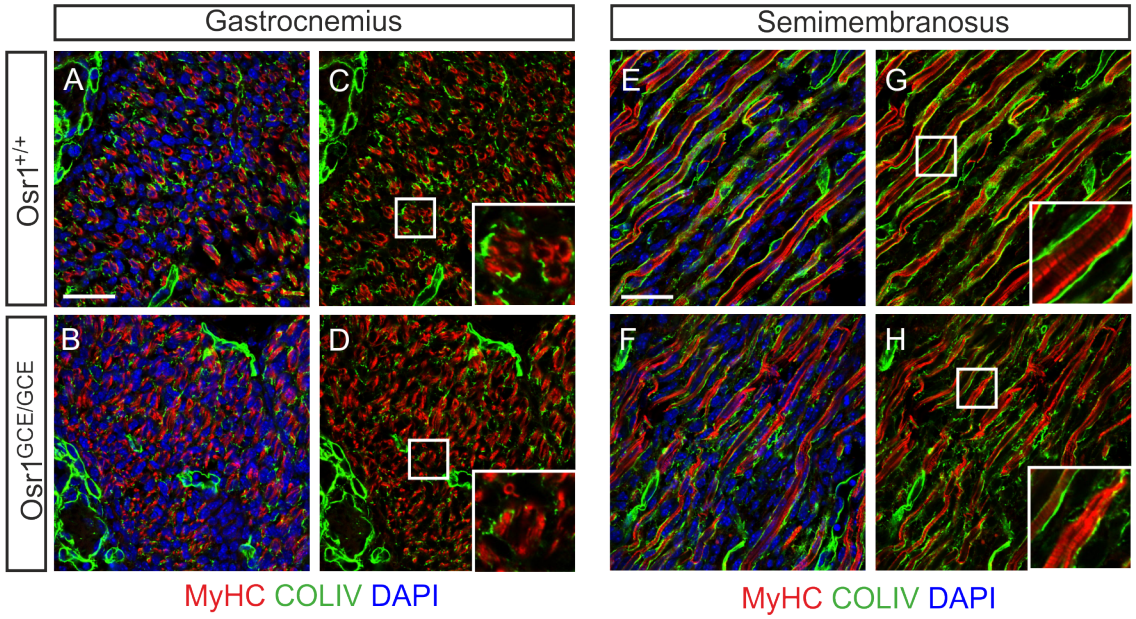

Figure 26: **Defects in the basal lamina of *Osr1*$^{GCE/GCE}$ muscles**. Immunostaining using an antibody against type IV collagen (COLIV) revealed lower level of this protein on cryosections of E14.5 *Osr1*$^{GCE/GCE}$ hindlimb muscles (A-B'). Longitudinal sections of the muscle semimembranosus using the same immunohistochemical approach showed a discontinuous production of type IV collagen along-muscle fibers of E14.5 *Osr1*$^{GCE/GCE}$ embryos. Scale bar 20 μm A, E.

Focal adhesions are protein complexes where cells establish physical contacts with the ECM. Vinculin is a structural component of focal adhesions and can be used to visualize their formation. Immunohistochemistry analysis of E13.5 hindlimb cross-sections using an anti-vinculin antibody showed a general decrease in vinculin abundance in *Osr1*$^{GCE/GCE}$ embryos compared to control embryos (Figure 27A, B). Myofibers establish correct contacts with their neighbor ECM where straight arrange line of myonuclei are organized. ECM interaction revealed by vinculin immunostaining showed discontinuous production of the protein along the poorly organized myofibers (Figure 27A', B'). Myofibers labelled by an antibody against MyHC showed disorganization in the same semimembranosus region (Figure 27C, D).

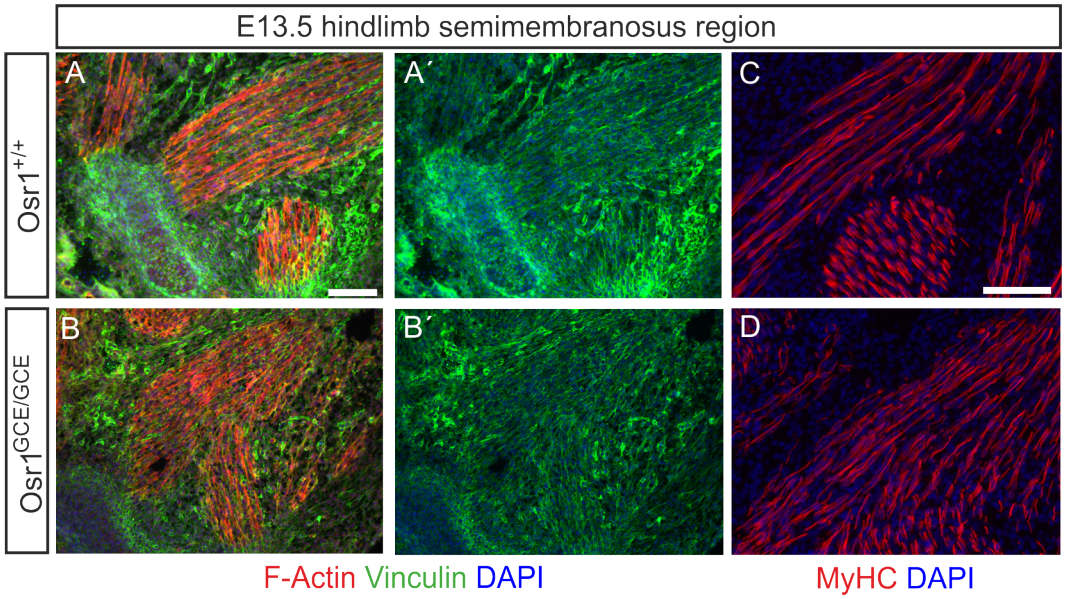

Figure 27: **Lower abundance of the focal adhesion protein vinculin in tissues of E13.5 *Osr1*$^{GCE/GCE}$ embryos**. Hindlimb cross-sections of E13.5 *Osr1*$^{GCE/GCE}$ embryos exhibited lower levels of the protein vinculin and disorganized formation of focal adhesions shown by immunolabelling with an anti-vinculin antibody (A-D). Disorganized myofibers in the semimembranosus region revealed after immunostaining labelling the protein MyHC (E, F). Scale bar 100 μm.

7.6 *Osr1*$^{GCE/GCE}$ embryos display defects in tendon formation

Force generated by muscle contraction is transmitted to the connective tissue ECM enveloping muscle fibers and muscles via protein complexes anchored in the sarcolemma. Connective tissue ECM is connected to the dense fibrillary collagen structure of tendons via the myotendinous junction and tendons are linked to the skeletal elements.

Although the induction of limb tendons is independent of muscle, their maintenance requires the presence of muscles. The muscle and ECM defects I observed likely lead to a failure of muscle function that could impede tendon maintenance. Immunostaining analysis was performed on cross-sections of hindlimbs and forelimbs E13.5 *Osr1*$^{+/+}$ as well as *Osr1*$^{GCE/GCE}$ embryos. First, it was aimed to address improper ECM formation in connective tissue surrounding tendons close to muscles of *Osr1*$^{GCE/GCE}$ embryos, as already reported for MCT (section). The proximal part of the semimembranosus muscle in hindlimbs is connected to the hip and the distal part to a tendon connecting it to the medial condyle of the tibia. At the distal end of this muscle, ECM-organization surrounding the tendon was revealed after immunostaining using an antibody against type VI collagen. The expression level of COLVI was not severely reduced in this area but the organization of COLVI was disarranged at muscle tips (Figure 28A, B). Hindlimb cross-sections were used to visualize focal adhesion formation at the tibial side of the semimembranosus using an antibody against vinculin. Immunohistochemistry analysis showed a strong decrease of

vinculin in tendon and the myotendinous junction in *Osr1*$^{GCE/GCE}$ E13.5 embryos (Figure 28C, D). Note that vinculin was virtually absent especially surrounding the tips of more peripheral muscle fibers (Figure 28C, D arrows).

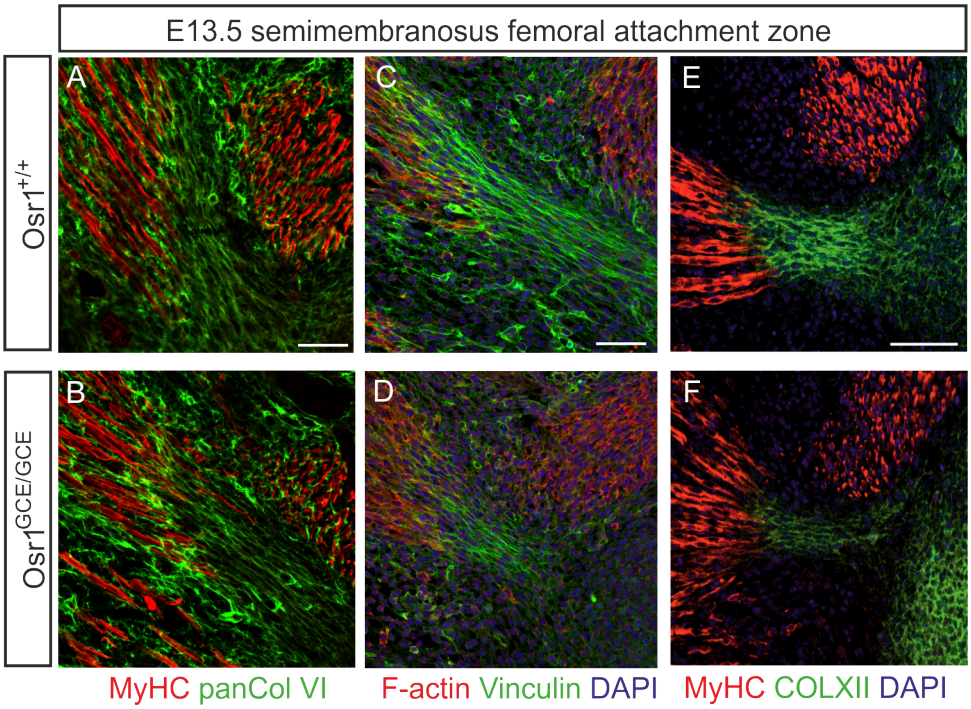

Figure 28: **Impairment in myotendinous junction formation in *Osr1*$^{GCE/GCE}$ mutants**. Cross-sections of E13.5 hindlimbs were analyzed by immunohistochemistry to reveal tendon defects on the tibia side of the semimembranosus muscle. Defects in connective tissue ECM was assessed using an antibody against type VI collagen (A, B). Cell contacts stained by anti-vinculin antibody highlighted loss of interaction between muscle and tendon cells in this region (C, D). Tendon precursors are not able to produce sufficient tendon collagens, revealed by type XII collagen immunostaining (E, F). Scale bar 50 μm.

Ultimately, tendon precursor cells start to secrete high amounts of specific collagens allowing the formation of dense bundles of ECM proteins connected to the ECM at the tip of muscles. Type XII collagen is richly secreted by tendon precursors as they start to differentiate. An antibody against the protein type XII collagen (COLXII) was used to visualize the tendon ECM. This revealed a strong decrease in COLXII protein at the semimembranosus tendon attachment in *Osr1*$^{GCE/GCE}$ embryos. Furthermore, the tendon COLXII network was connected to all myofibers in E13.5 Osr1+/+ embryos (Figure 28E). In contrast, peripheral fibers had lost tendon matrix contact in E13.5 *Osr1*$^{GCE/GCE}$ embryos (Figure 28F).

As muscle impairments were addressed in the majority of the muscle of the hind and forelimb, forelimb tendons were also analyzed. The same immunohistochemical approach allowed us to visualize tendons of forelimb muscles. As already reported the subscapularis muscle showed impairment in muscle shape and serious myofiber disorganization.

Comparable to the semimembranosus muscle in the hindlimb, the COLXII network did not connect all the fibers of this muscle to the tendon in E13.5 *Osr1*$^{GCE/GCE}$ embryos (Figure 28A, B).

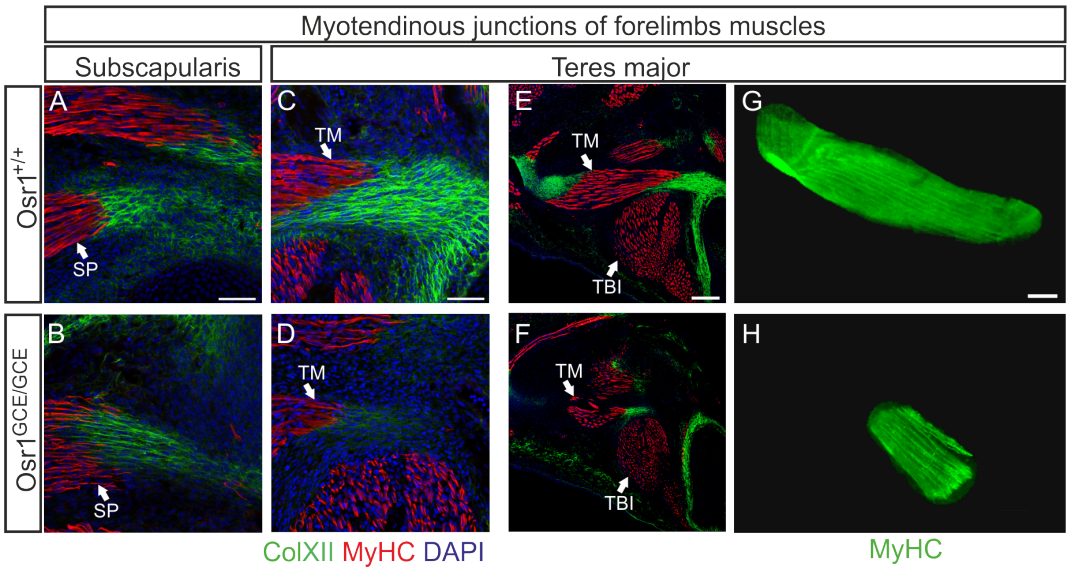

Figure 29: **Impairment in tendon formation in *Osr1*$^{GCE/GCE}$ forelimb muscles**. Cros-sections of E13.5 forelimbs were used in immunohistochemistry analysis to reveal impairment of tendon formation. Tendons were addressed by type XII collagen immunostaining and myofibers using an antibody against MyHC (A-F). 3D representation of the forelimb muscle teres major after whole mount immunostaining in E14.5 *Osr1*$^{+/+}$ and *Osr1*$^{GCE/GCE}$ embryos (G, H). SP, subscapularis; TBI, triceps brachii long head; TM, teres major. Scale bar 50 μm (A-D), 100 μm (E-H).

An interesting model to observe the effects in tendon formation of severe shortened muscle was the teres major muscle of the forelimb. As highlighted after 3D reconstruction, this muscle presented a strong reduction in muscle size in E14.5 *Osr1*$^{GCE/GCE}$ mutant embryos (Figure 29G, H). At the humerus side co-labelling with antibodies against MyHC and COLXII revealed a striking fact. Protein levels of type XII collagen were not only severely reduced as found in other tendon attachment sites, but the tendon structure connecting between tips of the muscle fibers and the head of the humerus was disconnected (Figure 29C, D). COLXII levels were reduced at the tendon attachment sites (Figure 29D), moreover the tendon structure connecting between tips of the muscle fibers and the head of the humerus was completely disconnected (Figure 29E, F).

In summary, this demonstrates that tendons in several hind and forelimb muscles presented severe impairments in muscle-tendon attachment of *Osr1*$^{GCE/GCE}$ embryos. Thus the importance of correct muscle formation for proper tendon development is highlighted.

7.7 Impaired Cxcl12/Cxcr4 axis in muscle progenitors of *Osr1*$^{GCE/GCE}$ embryos

RNA-seq analysis reported downregulation of diverse cytokines at the transcriptional level in *Osr1*$^{GCE/GCE}$ sorted cells compared to *Osr1*$^{GCE/+}$ cells (see section 7.3.1). Among those, the chemokine *Cxcl12* awoke special interest. *Cxcl12* is expressed in the limb mesenchyme during mouse development (Vasyutina et al., 2005). Furthermore, *Cxcl12* has been involved in muscle progenitor migration and maintenance (Vasyutina et al., 2005; Rehimi et al., 2010). *Cxcl12* transcript levels were assessed by RT-qPCR analyses performed on RNA isolated from E11.5 and E13.5 *Osr1*$^{GCE/+}$ as well as *Osr1*$^{GCE/GCE}$ sorted cells. This confirmed a significant reduction of *Cxcl12* expression already at stage E11.5 in *Osr1*$^{GCE/GCE}$ sorted cells becoming more pronounced at stage E13.5 (Figure 30A).

Activation of the *Cxcl12* receptor *Cxcr4* triggers the activation of the extracellular signal-regulated kinases (ERK)/ mitogen-activated protein kinase (MAPK) pathway in myoblast cultures (Hunger et al., 2012). Furthermore it was shown that CXCR4 is expressed in muscle progenitors during their migration into the limb (Vasyutina et al., 2005). In order to reveal an impairment in the CXCL12/CXCR4 axis in muscle progenitors, activation of the MAPK/ERK pathway in LBX1+ muscle progenitors was assessed via immunolabeling for phosphorylated ERK (pERK). pERK was observed at this stage mainly in subregions of dorsal (Figure 30B, C) and ventral muscle masses of the limb. This expression pattern is similar to the expression of CXCR4 in muscle progenitors reported by (Vasyutina et al., 2005). In E11.5 *Osr1*$^{GCE/GCE}$ embryos ERK phosphorylation was severely diminished in muscle progenitors of the dorsal (Figure 30B, C) and ventral muscle masses.

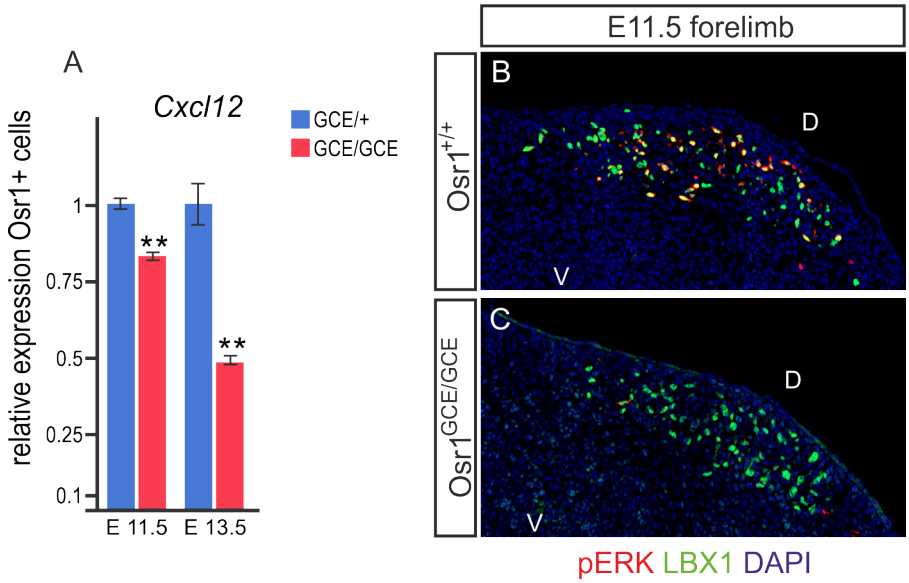

Figure 30: **Transcriptional down-regulation of the chemokine *Cxcl12* in the limb *Osr1*$^{GCE/GCE}$ sorted cells was accompanied by a reduction of the protein pERK in muscle progenitors of *Osr1*$^{GCE/GCE}$ forelimbs**. Transcriptional downregulation of *Cxcl12* at stages E11.5 and E13.5 after RT-qPCR analyses on *Osr1*$^{GCE/+}$ vs. *Osr1*$^{GCE/GCE}$ sorted cells (A). Immunostaining using antibodies against pERK (red) and LBX1 (green) proteins on forelimb cross-sections of E11.5 *Osr1*$^{+/+}$ and *Osr1*$^{GCE/GCE}$ embryos revealed severe reduction of pERK specifically in muscle progenitors (B, C). D, dorsal; v, ventral. ** p<0.001.

7.8 Reduced proliferative capacities of muscle progenitors cells in *Osr1*$^{GCE/GCE}$ mutants

Reduction of pERK protein specifically in muscle progenitors and defects in ECM production and assembly (see sections 7.5 and 7.7) pointed to possible proliferation and/or survival defects in myogenic cells. Proliferation was assessed by labeling cells in the S-phase of the cell cycle with the thymidine analogue, bromodeoxiuridine (BrdU). During a time period of 1 hour, pregnant female mice were treated with BrdU. Tracking proliferating cells that were BrdU+ labeled in this time window was performed via immunolabeling with and anti-BrdU antibody. Forelimb cross-sections of E11.5 *Osr1*$^{+/+}$ and *Osr1*$^{GCE/GCE}$ embryos were used to address proliferation capacities of Pax7+ and MyoD+ cells. In the proximal part of the forelimb highly proliferative muscle progenitors were labelled by an antibody against PAX7 protein (Figure 31A, B). A proliferation rate of muscle progenitors in *Osr1*$^{+/+}$ and *Osr1*$^{GCE/GCE}$ embryos was obtained quantifying the percentage of Pax7+ BrdU+ cells versus the entire population of Pax7+ cells in this area. The percentage of Pax7+BrdU+ cells was significantly reduced in proximal muscle masses of *Osr1*$^{GCE/GCE}$ mutant embryos indicating a lower proliferation rate of Pax7+ progenitors (Figure 31C). Proliferation of committed myoblasts expressing MyoD

was also addressed after immunohistochemistry analyses using antibodies against MYOD and BrdU. In the same proximal region of the forelimb MYOD+ cells proliferated with a lower rate in *Osr1*$^{GCE/GCE}$ embryos compared to *Osr1*$^{+/+}$ littermates (Figure 31D-F).

In addition, the proliferation rate of Pax7+ cells was decreased in hindlimb muscles at E13.5 (Figure 31D-G). Significantly reduced proliferation of Pax7+ cells was observed in the gastrocnemius (GC) and biceps femoris (BF) muscles (Figure 31H) demonstrating that the proliferation defect is not a transient feature.

In summary, these results highlighted a decreased proliferation of Pax7+ and MyoD+ cells at stage E11.5 that is maintained, at least for the Pax7+ population, until stage E13.5 in *Osr1*$^{GCE/GCE}$ embryos.

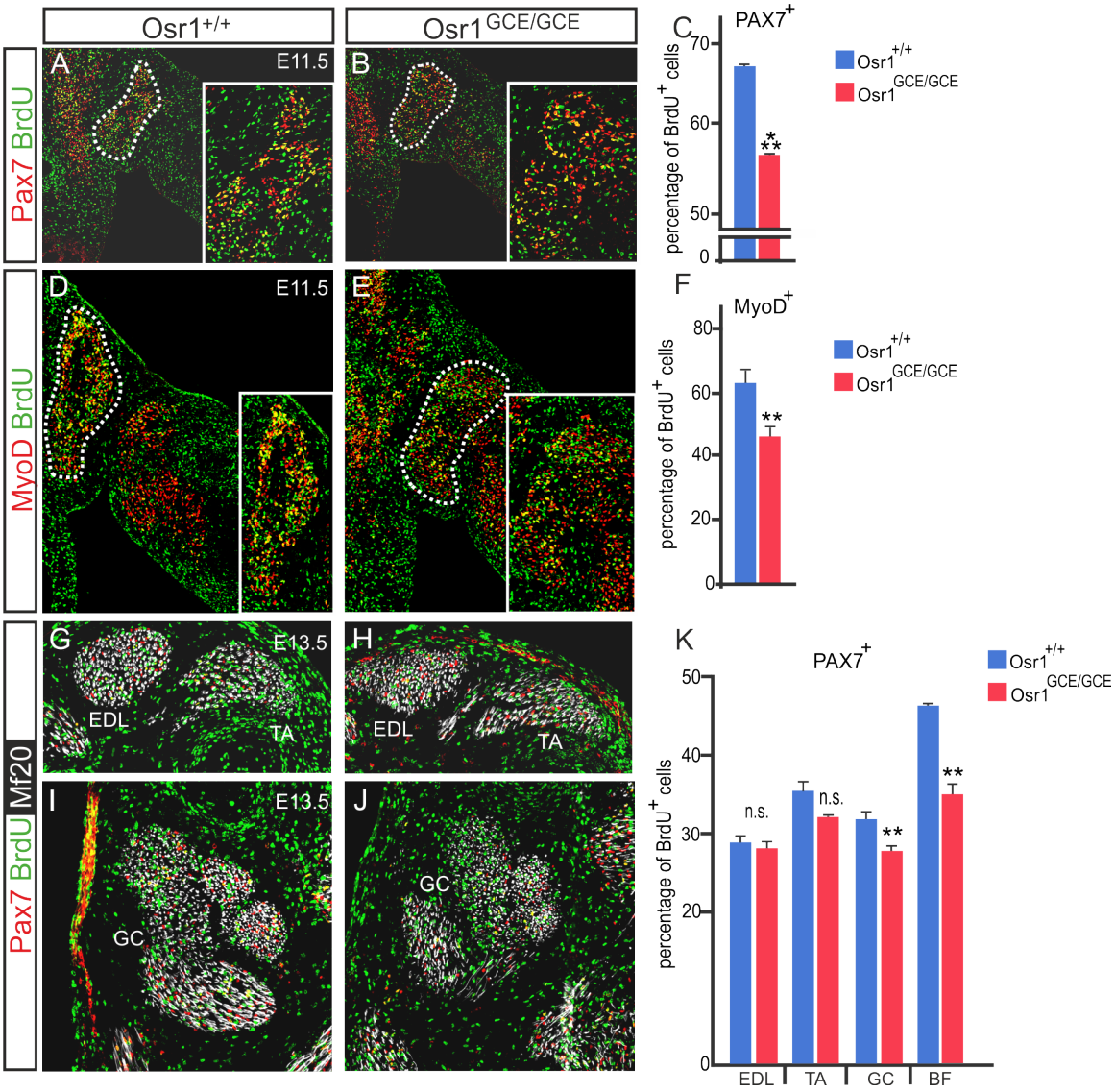

Figure 31: **Decreased proliferation of myogenic cells in *Osr1*$^{GCE/GCE}$ mutants**. 1h BrdU labeling was performed to label cells in the S-phase of the cell cycle. E11.5 forelimb and E13.5 hindlimb cross-sections were used forimmunohistochemistry analyses. Anti-Pax7 and anti-MyoD antibodies (red) in combination with an anti-BrdU antibody (green) were used to label proliferative myogenic cells (A, B; D, E). A significant reduction in the percentage of BrdU+ Pax7+ and MyoD+ BrdU+ cells was observed after quantification of the whole proximal part of the limb (C, F). At the stage E13.5 proliferation of Pax7+ cells was addressed in the whole muscle area of the extensor digitorum longus (EDL), tibialis anterior (TA), gastrocnemius (GC) and biceps femoris (G-J) muscles of the hindlimb. Percentage of BrdU+ Pax7+ cells in the entire muscle area revealed a decrease in proliferation of Pax7+ cells in GC and BF muscles (K). Muscle fibers were counterstained using an anti-Mf20 antibody (white). Ns, not significant, ** $p<0.001$ and *** $p<0.0001$.

7.9 Increased apoptosis of myogenic cells in the limb of *Osr1*$^{GCE/GCE}$ embryos

Apoptosis is a mechanism of programed cell death, which plays an important role during tissue organization in multicellular organisms. This process must be fine-tuned, as aberrant apoptosis is a frequent cause for derailment of developmental processes. Interestingly, increased apoptosis was observed in *Cxcr4*$^{-/-}$ animals in premuscle masses (Vasyutina et al., 2005). **C**ysteine-dependent **as**partate-directed prote**ases** (**Caspase**) are proteins that play an essential role as "executioner" during the process of apoptosis. Measurements of caspase-3 activation have been regularly used as a marker for apoptotic signaling (Montero and Hurlé, 2010). Immunohistochemistry analysis for cleaved caspase 3 was performed to assess the ratios of apoptotic myogenic cells in E11.5 *Osr1*$^{+/+}$ and *Osr1*$^{GCE/GCE}$ embryos. An antibody against cleaved caspase-3 allowed labeling of apoptotic cells that appeared very sparse on cross-sections of E11.5 mouse embryos. Specific co-labelling of myogenic cells was achieved using antibodies against PAX7 and MYOD proteins, which label muscle progenitors and differentiated myoblast, respectively, (Figure 32A, B). Increased apoptosis was mostly observed in the proximal muscle mass of forelimbs. In these regions, cleaved caspase-3+ cells appeared more abundant in *Osr1*$^{GCE/GCE}$ embryos (Figure 32A, B). Quantification of myogenic cells observed in this region expressing the apoptotic marker caspase-3 revealed a significant increase of apoptosis in myogenic cells of E11.5 forelimb *Osr1*$^{GCE/GCE}$ embryos compared to *Osr1*$^{+/+}$ littermates (Figure 32C).

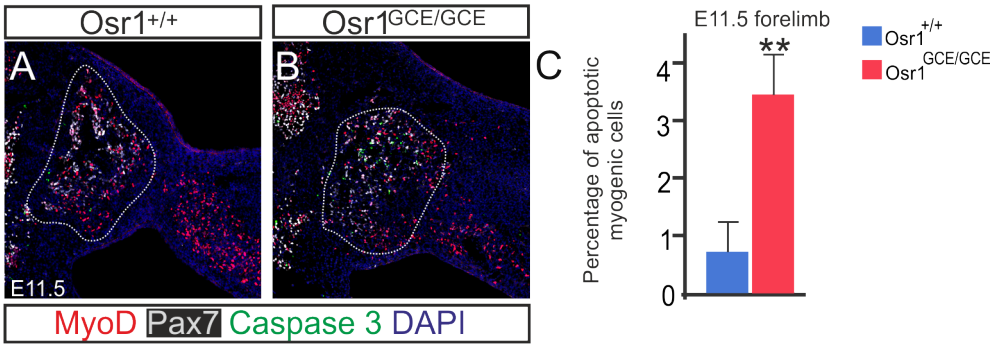

Figure 32: **Increased apoptosis of myogenic cells in the proximal forelimb muscle mass of E11.5 *Osr1*$^{GCE/GCE}$ embryos**. Immunohistochemistry analyses were performed on E11.5 forelimb cross-sections of *Osr1*$^{+/+}$ and *Osr1*$^{GCE/GCE}$ embryos to assess apoptosis in myogenic cells. Antibodies against the proteins PAX7 and MYOD were used to label myogenic cells in combination with an anti-cleaved caspase-3 antibody to address apoptosis (A, B). Percentage of myogenic cells co-labeled by a caspase-3 was calculated in the proximal region of E11.5 *Osr1*$^{+/+}$ and *Osr1*$^{GCE/GCE}$ forelimb (C). Error bar represent SEM, $**$ p$<$0.001.

7.10 Reduced number of myogenic cells in the limb of *Osr1*$^{GCE/GCE}$ embryos

A precise balance between proliferation and differentiation during muscle development is necessary to maintain populations of myogenic cells in order to achieve correct muscle growth. Immunohistochemistry analysis of E11.5 forelimb cross-sections were used to asses the number of muscle progenitors and myoblasts at this stage. Muscle masses in limbs were divided into three different regions (proximal muscle mass giving rise to the shoulder muscles, dorsal muscle masses and ventral muscle masses) to provide a comprehensive analysis of differentially affected regions. Antibodies against the transcription factors MYOD, LBX1 and PAX7 were used to label myogenic cells in the limb at E11.5 (Figure 33A-F). The number of Lbx1+ cells (migrating progenitors) was not significantly reduced in the proximal area, however in the dorsal and ventral muscle masses the number of Lbx1+ cells showed a reduction of about 25% in limbs of *Osr1*$^{GCE/GCE}$ embryos versus control limbs (Figure 33C). Additionally, populations of MyoD+ cells in the three different regions of the forelimb diminished in E11.5 *Osr1*$^{GCE/GCE}$ embryos with an approximate reduction of 25% (Figure 33D). At this stage, muscle progenitors of the proximal part of the limb already express *Pax7*. Immunostaining for PAX7 and MYOD on cross-sections of E11.5 *Osr1*$^{+/+}$ and *Osr1*$^{GCE/GCE}$ embryos provided a readout about the balance between muscle progenitors and differentiated myoblasts in this region of the limb (Figure 33E, F). Quantification of total numbers of MyoD+ or Pax7+ cells in several consecutive sections of proximal muscle masses reported a significant and similar reduction in the numbers of Pax7+ muscle progenitors and MyoD+ myoblasts in E11.5 *Osr1*$^{GCE/GCE}$ embryos (Figure 33G). Ratios of Pax7+/MyoD+ cells were not significantly changed as both populations were similarly reduced in *Osr1*$^{GCE/GCE}$ mutants. Similarly, ratios of MyoD and Pax7 co-expressing cells versus total numbers of Pax7+ cells appeared unchanged between *Osr1*$^{+/+}$ and *Osr1*$^{GCE/GCE}$ embryos (Figure 33H) indicating that there is no change in the pace of progenitor-to-myoblast differentiation in *Osr1* mutants.

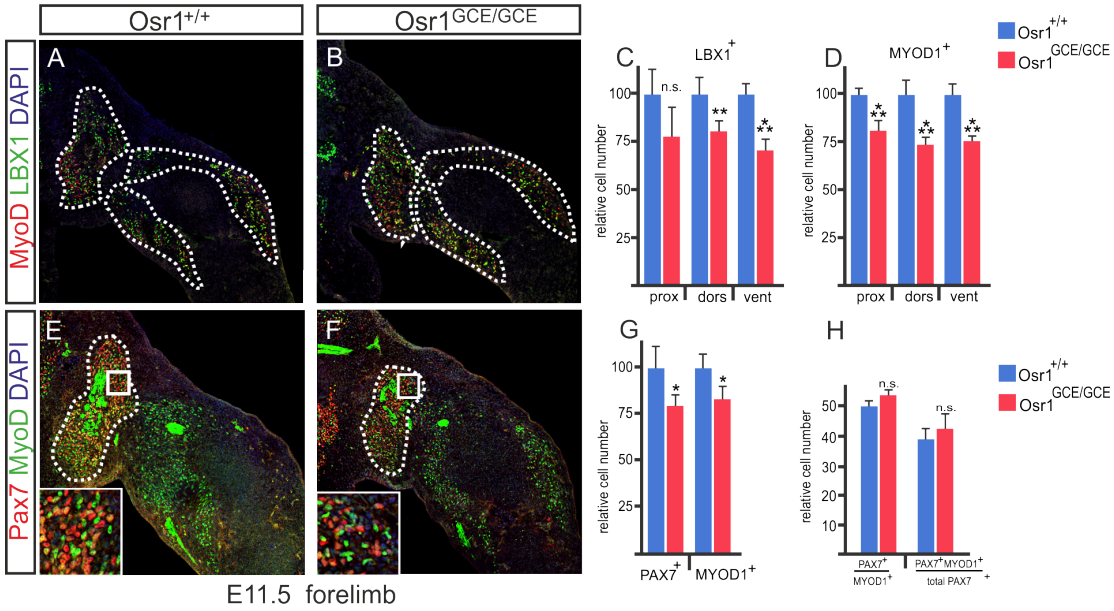

Figure 33: **Reduced numbers of myogenic cells in the forelimb of E11.5 *Osr1*$^{GCE/GCE}$ embryos**. Immunohistochemistry analysis for LBX1 and MYOD (A, B) or PAX7 and MYOD (E, F) was performed on E11.5 forelimb cross-sections to assess the number of myogenic cells at this stage. Relative numbers of MyoD+ or Lbx1+ cells are shown in (C, D), relative numbers of Pax7+ or MyoD+ cells in the proximal muscle mass are shown in (G) demonstrating a reduction in the number of myogenic cells in all muscle masses analyzed. Ratios of Pax7+ vs. MYOD+ cells (PAX7+/MYOD+) or the number of PAX7 and MYOD double positive cells relative to all PAX7 cells (PAX7+MYOD+/total PAX7) in the proximal region shows no significant difference (H). Error bars represent SEM. Not significant, ns; $*$ p<0.05; $**$ p<0.001 and $***$ p<0.0001.

Thus, at E11.5 there is a clear reduction in the number of myogenic progenitors in limb muscle masses, which can be traced back to a combined defect in myogenic progenitor proliferation and survival. Next, it was analyzed whether the effect of this early reduction in the myogenic pool was propagated to later stages or whether this was compensated. For this purpose quantification of myogenic progenitors was performed at E13.5 to provide a deeper insight about the dynamic changes in muscle progenitor and myoblast maintenance during the process of embryonic muscle formation.

Cross-sections of E13.5 hindlimbs were used to perform immunolabelling for MYOD and PAX7 (Figure 34A, B). Quantification of Pax7+ and MyoD+ cells in several muscles of hindlimbs revealed a differential impairment in myogenic cell numbers in different muscles. Pax7+ progenitors showed less abundance in all *Osr1*$^{GCE/GCE}$ muscles analyzed. TA and EDL muscles in *Osr1*$^{GCE/GCE}$ embryos showed a reduction of approx. 20% of Pax7+ cells, while GC and BF muscles exhibited an approximate 45% decrease (Figure 34C). Additionally, quantification of MyoD+ cells in EDL and TA muscles similarly showed reduced numbers of committed myoblasts in E13.5 *Osr1* knock out animals (Figure 34D).

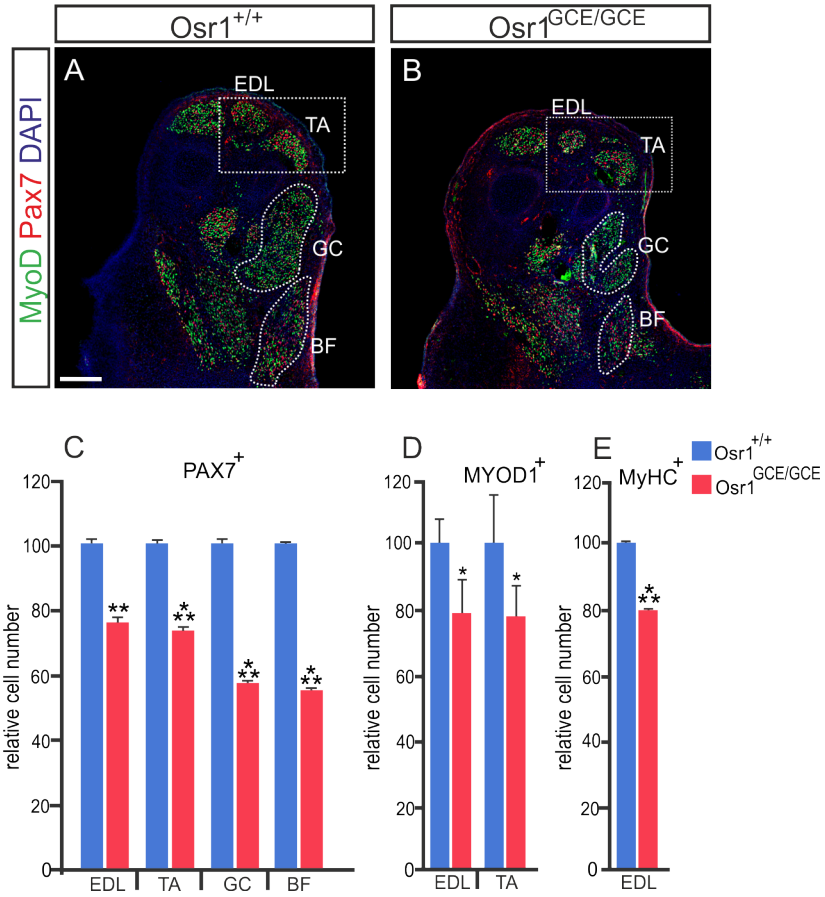

Figure 34: **Reduced numbers of myogenic cells in hindlimb muscles of E13.5 *Osr1*$^{GCE/GCE}$ embryos.** Antibodies against MyoD and Pax7 were used to label myogenic cells in the hindlimb muscles extensor digitorum longus (EDL), tibialis anterior (TA), gastrocnemius (GC) and biceps femoris (BF) of E13.5 *Osr1*$^{+/+}$ and *Osr1*$^{GCE/GCE}$ embryos (A, B). Quantification was performed on consecutive E13.5 hindlimb cross-sections. Numbers of Pax7+ cells in *Osr1*$^{GCE/GCE}$ animals quantified in the whole muscle area for each muscle were normalized to total numbers quantified in *Osr1*$^{+/+}$ littermates (C). Similarly, MyoD+ cells were quantified for EDL and TA muscles (D). At least 8 consecutive cross-sections of E13.5 *Osr1*$^{+/+}$ and *Osr1*$^{GCE/GCE}$ embryos were used to assess myofiber numbers in the EDL muscle (E). Error bars represent SEM. Not significant, ns; $*$ p<0.05; $**$ p<0.001 and $***$ p<0.0001. Scale bar 200 μm.

Phenotypic characterization of *Osr1*$^{GCE/GCE}$ muscles already reported reduced muscle size in almost all analyzed hindlimb and forelimb muscles. However, the number of myofibers remained uncharacterized. At least 8 consecutive cross-sections of E13.5 hindlimbs were used to assess myofibers in the entire area of the EDL muscle, which is the most suitable for quantification due to the fact that it has an equal number of myofibers along almost its complete length. Quantification analysis of MyHC+ myofibers of the EDL showed an approximate 20% reduction in E13.5 *Osr1*$^{GCE/GCE}$ embryos compared with E13.5 *Osr1*$^{+/+}$ embryos.

Altogether this highlighted a reduction in the number of muscle progenitors and differentiated myoblasts in the limb of *Osr1*$^{GCE/GCE}$ mutant embryos during the first wave

of myogenesis that were accompanied by reduced numbers of myofibers, and, as shown before, shortened myofibers.

7.11 Myoblasts exhibit impaired terminal differentiation in *Osr1*$^{GCE/GCE}$ mutants

Committed myoblasts are arranged in organized stripes allowing contacts with adjacent myoblasts to allow fusion to ultimately form multinucleated myotubes. One of the first proteins produced by myoblasts during the differentiation process is the intermediate filament protein desmin. Production of desmin appears in the limb from the stage E12.5 onward. Desmin subsequently forms an important part of the sarcomere (Capetanaki and Milner, 1998).

Immunohistochemistry analyses on E13.5 hindlimb cross-sections using the antibodies against the MYOD and desmin proteins revealed a general decrease of desmin abundance in myoblasts and myotubes in hindlimb muscles (Figure 35A, B). The general decrease of desmin abundance was confirmed by western blot from whole limb protein lysates of *Osr1*$^{GCE/GCE}$ embryos compared to E13.5 *Osr1*$^{+/+}$ embryos (Figure 35E). Higher magnification images of the EDL muscle highlighted that myoblast and myotube nuclei appeared rarely surrounded by desmin protein in their cytoplasm in *Osr1*$^{GCE/GCE}$ embryos (Figure 35C, D). Accordingly, myofibers were often observed with a frayed and thinner aspect of MyHC in *Osr1*$^{GCE/GCE}$ mutants compared to control embryos as as already observed in 3D reconstructions (See section 7.2.2), indicating an impaired terminal differentiation (Figure 35F, G).

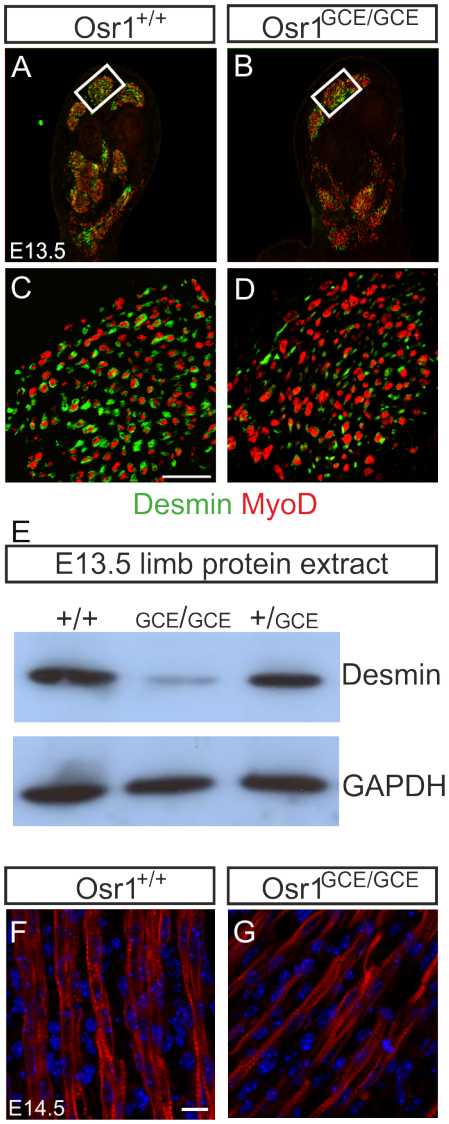

Figure 35: **Impaired terminal myogenic differentiation in *Osr1*$^{GCE/GCE}$ embryos**. Immunohistochemistry analysis showed reduced production of the intermediate filament protein desmin (green) in myoblasts and myotubes labeled for MyoD (red) on cross-sections of E13.5 hinlimbs (A, B). Content of desmin protein is severely diminished in E13.5 *Osr1*$^{GCE/GCE}$ whole limb lysates compared to *Osr1*$^{+/+}$ and *Osr1*$^{GCE/+}$ littermates (E). At the stage E14.5 cross-sections of the hindlimb revealed thinner muscle fibers of the semimembranosus muscle after immunolabeling for MyHC (F, G). Scale bar 50 μm (A), 20 μm (F).

7.12 Differential fusion impairments of myogenic cells in *Osr1*$^{GCE/GCE}$ embryos *in vitro* and *in vivo*

Fusion of committed myoblasts is a crucial step to achieve multinuclear myofibers. In culture, primary myoblast freshly extracted from embryos can be cultivated in a dense mix culture of limb extracts. Under low serum conditions, myoblasts fuse with nearby myoblasts forming multinuclear myofibers. Myoblasts isolated from E13.5 *Osr1*$^{+/+}$ and

Osr1$^{GCE/GCE}$ embryos were used to assess myoblast fusion in culture. After five days in a low serum medium, cultures were fixed and immunocytochemistry analyses were subsequently performed using antibodies against MYOD and desmin (Figure 36A, B). Quantification of myoblasts (1 nucleus) or myotubes with 2, 3 or more nuclei, however, appeared in similar proportions in cultures from *Osr1*$^{+/+}$ and *Osr1*$^{GCE/GCE}$ embryos (Figure 36C) excluding an intrinsic fusion defect in myoblasts derived from *Osr1* mutants.

To assess myoblast fusion *in vivo*, long term BrdU labelling (24h) was performed making use of the fact that committed myoblasts exit the cell cycle before becoming fusion competent. Thus, proliferating muscle progenitors were labelled by BrdU before being committed and fusing to myofibers. Immunohistochemistry analysis on hindlimb cross-sections of E13.5 *Osr1*$^{+/+}$ and *Osr1*$^{GCE/GCE}$ embryos were performed using an anti-MF20 antibody and BrdU-incorporated nuclei (Figure 36D, E). Counting BrdU+ nuclei within MF20+ fibers normalized to the total number of myofibers was used to calculate a fusion index. This experiment revealed a significant decrease of myonuclei that fused to myofibers during the 24h labeling phase in *Osr1* mutants (Figure 36F). This indicates that myoblasts of *Osr1* mutants are per se fusion competent, but lose this competence in the *Osr1* mutant environment.

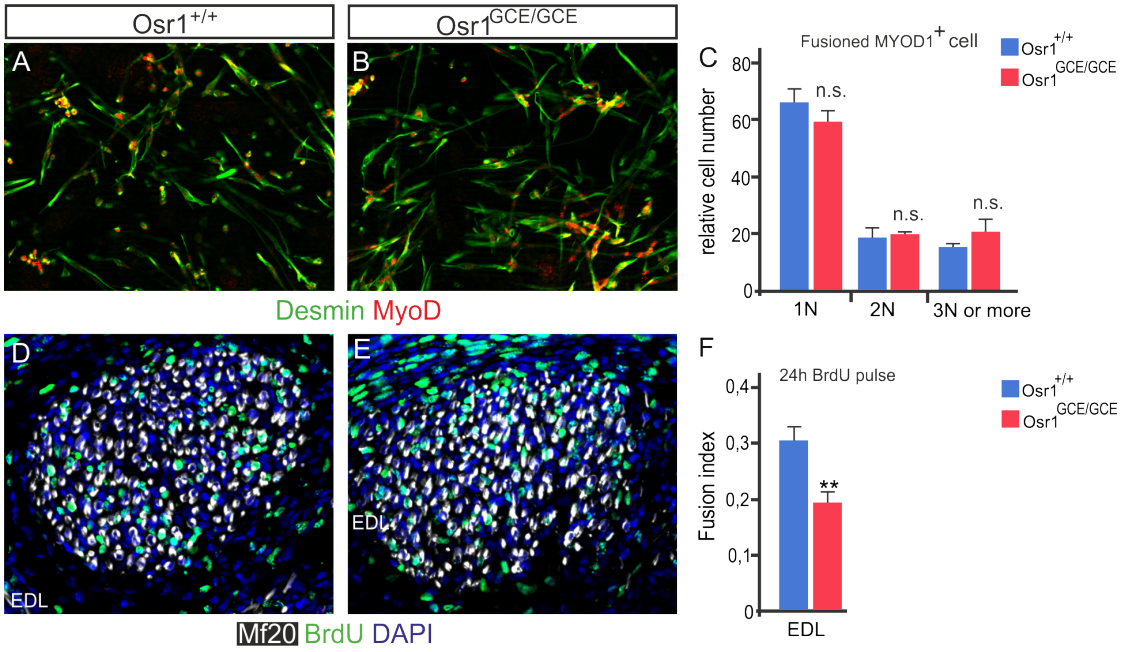

Figure 36: **Myoblast fusion analyses showed distinct defects in vitro and in vivo**. Cultures of myoblasts isolated from E13.5 *Osr1*$^{+/+}$ and *Osr1*$^{GCE/GCE}$ embryos were used to assess myoblast fusion in culture. Immunolabeling for desmin and MYOD was used to stain committed myoblasts or multinucleated fibers (A, B). Quantification of myoblasts (1 nucleus) or of nuclei within myotubes in cell cultures of E13.5 *Osr1*$^{+/+}$ and *Osr1*$^{GCE/GCE}$ embryos (C). *In vivo*, 24h pulse of BrdU treatment was used to address incorporation of myonuclei into muscle fibers. Fusion index was calculated by quantifying the amounts of incorporated myoblasts (BrdU+ nuclei within Mf20+ fiber) normalized to fiber number in the entire cross section area of the EDL muscle (F). Error bar represent SEM, n.s. not significant, $**$ p$<$0.001.

7.13 Patterning defects are preceded by muscle progenitor mislocation

The disruption of muscle patterning and muscle fiber organization observed at E13.5 / E14.5, i.e. towards the end of embryonic myogenesis, together with the above described early defect in myogenic progenitor migration, proliferation and maintenance in *Osr1*$^{GCE/GCE}$ mutant embryos prompted me to analyze whether the mispatterning phenotype would be visible already at early stages before E13.5.

Immunolabelling for PAX7 and MYOD indeed revealed first defects in the arrangement of myogenic cells in E11.5 *Osr1*$^{GCE/GCE}$ embryos. In wild type embryos, myogenic cells in proximal muscle masses exhibited an organized distribution of compact cells delineated by a sharp border. In contrast, in *Osr1*$^{GCE/GCE}$ mutants, myogenic cells in proximal muscle masses were disorganized being spread over a wider area leading to decreased myogenic cell density and an obvious breakdown of the border normally delineating muscle masses (Figure 37A, B, arrows).

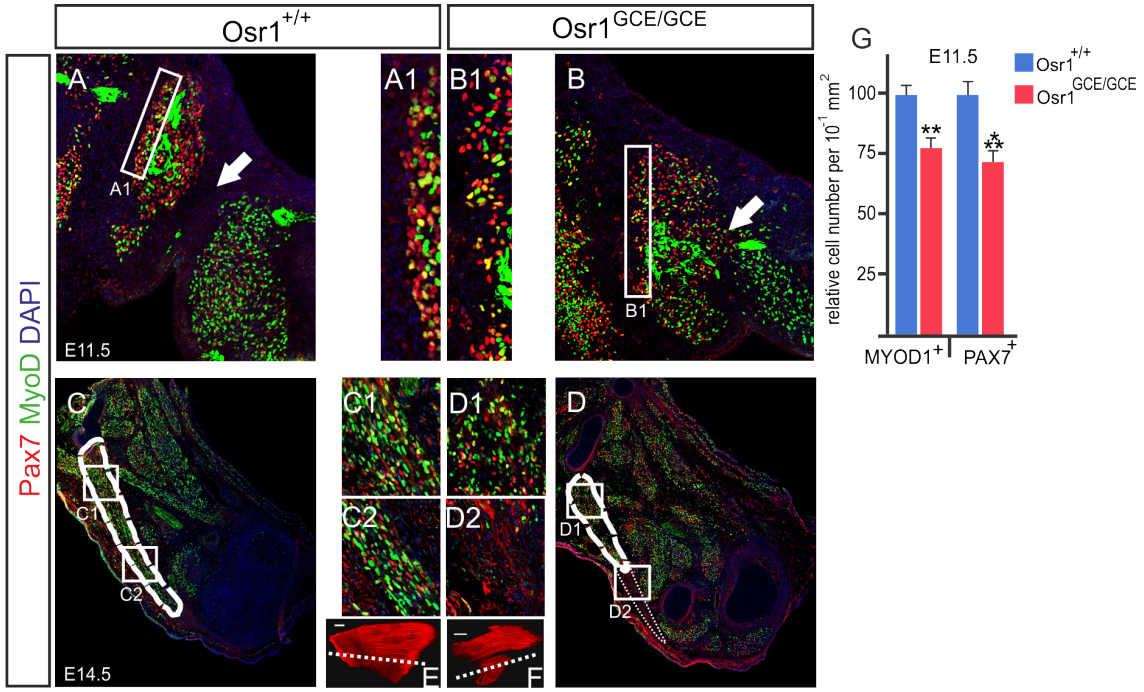

Figure 37: **Myogenic cells exhibit incorrect location leading to muscle patterning defects in *Osr1*$^{GCE/GCE}$ embryos**. Immunolabelling for PAX7 and MYOD on E11.5 forelimb and E14.5 hindlimb cross-sections revealed altered myogenic cell distribution. At E11.5 MyoD+ and Pax7+ cells showed diffuse spreading and disorganized distribution within muscle masses of *Osr1*$^{GCE/GCE}$ forelimbs compared to the compact organization in *Osr1*$^{+/+}$ (A-B1). Similarly, at E14.5 in hindlimbs Pax7+ and MyoD+ progenitors can be found over the complete area a single muscle covers, as for the muscle biceps femoris, the section plane is illustrated in (E, F). Longitudinal sections through the b. femoris (C,D) shows disorganization of myogenic cells in the area where the muscle are formed in the mutant (C1, D1) and a complete absence of myogenic progenitors in the area where the distal part of the B. femoris failed to form in the mutant (C2, D2). Reduction of MyoD+ and Pax7+ cells density in E11.5 Osr1 mutant embryos quantified in a 10^{-1} mm^2 area of in the forelimb proximal region (G). Error bar represent SEM. $**$ p$<$0.001 and $***$ p$<$0.0001. Scale bar 100 μm.

Muscle progenitors and myoblasts are well detectable at E14.5 delineating individualized differentiated muscles. In hindlimbs, the Biceps femoris is severely affected showing a misalignment and wrong orientation of myofibers as well as a severe distal truncation (Fig. 24 E, F). Labeling for PAX7 and MYOD (Fig. 24C, D) showed a highly organized arrangement of Pax7+ and especially MyoD+ cells in *Osr1*$^{+/+}$ embryos, which contrasted with the disorganized distribution of myogenic cells in *Osr1*$^{GCE/GCE}$ mutants (Figure 37C1, D1). Importantly, in wild type embryos, labeling for myogenic progenitors can be observed along the full length on the B. femoris muscle, while in *Osr1* mutants myogenic cells are virtually absent in the distal (truncated) region (Figure 37C2, D2). The analysis was performed on consecutive sections covering the full B. femoris muscle in wild-type and mutant embyros to exclude section artefacts. This rules out the possibility that muscle truncations are the consequences of disrupted myogenic differentiation at places where fibers should form, but rather indicates that myogenic cells are unable to reach their

allocated positions in *Osr1* mutants. Together with data presented above (Figure 37), where myogenic cells apparently appear at positions they should not reach normally, this indicates that myogenic cells show an overall misdistribution in limbs of *Osr1* mutants. This misdistribution apparently starts at E11.5 with myoblasts not adhering to the "border" muscle masses show in wild-type embryos and, together with a reduced number of myogenic progenitors leads to the muscle patterning phenotype presented above.

8 Discussion

Limb formation requires the interaction of tissues from different developmental origins with variable dependency on external cues. Myogenic cells have been described as, to some extent, naïve cells relying on instructive signals that guide their arrangement (Chevallier et al., 1977; Christ et al., 1977; Kieny and Chevallier, 1979). Although characterization of the intrinsic molecular mechanisms that govern myogenesis have seen a breakthrough in the last decades, the identity of extrinsic signals and their exact influence orchestrating muscle patterning remain poorly understood.

Derived from the lateral plate mesoderm, resident connective tissue cells in the limb have been poorly characterized and their role during limb morphogenesis has been hindered by the lack of specific markers that facilitate their analysis. Characterization of muscle connective tissue cells and their potential has just begun and suggests to influence muscle development and maintenance via manifold mechanisms (Kardon et al., 2003; Mathew et al., 2011; Hasson et al., 2010; Murphy et al., 2011).

8.1 *Osr1* expression and potential during mouse development

8.1.1 *Osr1* labels connective tissue cells associated with skeletal muscle during mouse limb development

Although well characterized during chick limb development (Stricker et al., 2006), the expression pattern of *Osr1* in mouse limbs was only partially described. Reporter gene systems are powerful and widely used in mouse genetics to address expression patterns with (or at) a cellular resolution. I used the *Osr1* reporter line *Osr1*$^{GCE/+}$ (Mugford et al., 2008) that constitutively produced an enhanced-GFP protein under the control of the *Osr1* promotor to address *Osr1* expression during mouse embryonic development with a special emphasis on its relation to myogenic cells. During development between E11.5 and E14.5, the limb premuscle masses segregate and form the pattern of more than 40 limb muscles. I found *Osr1* expression in connective tissue closely associated with muscle progenitors and differentiated muscle fibers, similar to previous chick results (Stricker et al., 2006, 2012). Osr1+ cells were found in close proximity to myogenic progenitors and in cells interstitial to myofibers. Importantly, *Osr1* expression was never found to be co-expressed with myogenic markers in the limb during this period. In agreement, in the lineage analysis (see below) a contribution of Osr1+ cells to the myogenic lineage was never seen. In contrast to the previously characterized connective tissue marker *Tcf4* (Kardon et al., 2003; Mathew et al., 2011), expression of *Osr1* has not been observed in tendon structures, skeletal elements, with the exception of the joint interzone, or in

myogenic cells. Thus, the highly specific expression in connective tissue in both chick and mouse embryos identified *Osr1* as a valuable connective tissue marker and provides us with a tool to study the function of this poorly characterized embryonic tissue of the musculoskeletal system during development.

Expression analyses of *Osr1* developed within the scope of this work were mainly based on the visualization of the reporter protein GFP. This green fluorescence protein has an approximated half-life in mammalian cells of 26h (Corish and Tyler-Smith, 1999). Proteins involved in transcriptional regulation, as transcription factors, usually possess a rather short half-life both at the transcriptional and protein level (Schwanhäusser et al., 2011). Despite its long half-life compared to the rapid and dynamic changes in expression of transcription factors during development, GFP expression pattern on *Osr1*$^{GCE/+}$ embryos was very similar to the previously described *Osr1* expression pattern in chick and mice (Stricker et al., 2006) that was based on mRNA *in situ* hybridisation. Additionally, *Osr1* expression pattern during E11.5-E13.5 (see section 7.1.1) confirmed previous results and underpinned the use of the *Osr1*$^{GCE/+}$ reporter line to describe *Osr1* expression during mouse development.

Interestingly, *Osr1* was not uniformly expressed embedding every single muscle mass or muscle. This regionalized expression in limb mesenchyme was also reported for *Tcf4* (Mathew et al., 2011), where *Tcf4* was expressed surrounding specific muscle masses in mouse limbs. The expression of both transcription factors combined with the data from Osr1+ sorted cells show that *Osr1* and *Tcf4* have partially overlapping expression domains between E11.5-E13.5. This strongly supports the idea that they label two populations of lateral plate mesoderm-derived cells that give rise to connective tissue cells in different areas of the limb and, in part, also in different muscles. The hypothesis that both populations label all precursors of muscle connective tissue remains to be confirmed.

OSR1 and its paralogue *OSR2* are expressed in chick limb mesenchyme in mostly exclusive domains with partial overlaps (Stricker et al., 2006). *OSR2* is also expressed in muscle connective tissue in the chick limbs (Stricker et al., 2012), and *Osr2* also labels muscle connective tissue progenitors in mouse embryos (Malcolm Logan, King's College London, personal communication). During limb bud initiation, the transcription factors T-box 4 and 5 (*Tbx4/5*) are expressed homogenously in lateral plate derived mesenchyme in hindlimbs and forelimbs, respectively, (Hasson et al., 2007; Naiche and Papaioannou, 2007). As limbs develop, restricted expression of *Tbx5* has been observed in specific skeletal and tendon elements, as well as other connective tissues (Hasson et al., 2007). Therefore *Tbx4* and *Tbx5* transcription factors label a lateral plate mesoderm-derived cell population that contributes to but is not specific for MCT.

Thus it seems likely that limb muscle connective tissue progenitors do not express a

single marker but have regionalized "codes" of transcription factor expression profiles. Complementary expression of *Osr1*, *Osr2*, *Tcf4* and maybe other transcription factors therefore might have to be taken into account to cover the full spectrum of MCT progenitors in limbs.

Neither *Tcf4* nor *Osr2* or *Tbx4/5* seemed to exert a compensatory effect at the transcriptional level in *Osr1*$^{GCE/GCE}$ cells, as they were not found within the up-regulated genes in *Osr1* knockout cells after RNA-seq analysis. *In situ* hybridization analyses of those transcription factors on *Osr1*$^{GCE/GCE}$ embryos will confirm these results and provide a better understanding of the transcriptional changes on the described connective tissue markers after lack of Osr1.

The preferential expression of *Osr1* in connective tissue surrounding specific muscles in limbs suggests a differential dependency for this transcription factor. Each limb muscle is characterized by its position, where it exerts its function. Therefore, requirements of connective tissue vary according to limb muscles depending on the required muscle contractile function. Hence, we could hypothesize that during muscle patterning differential requirement for MCT cells and therefore *Osr1* expression (and other transcription factors in connective tissue) are needed to accomplish final muscle shape. In contrast to its regionalized expression at E13.5, *Tcf4* appears to be homogenously expressed in all MCT at neonatal stages (Mathew et al., 2011). In agreement, I found that at E18.5 a high proportion of Osr1+ cells co-express *Tcf4*, suggesting that muscle connective tissue at late fetal stages assumes a uniform identity that loses the regionalized embryonic signature. These results could also imply similar functions of both transcription factors in MCT at late developmental stages.

The signaling pathway involved in the regulation of *Osr1* expression remain poorly characterized. During *Drosophila* embryogenesis *Odd* genes act as a repressor of other pair-rule genes or as an activator depending on the stage of development (Dréan et al., 1998b). Although, genes involved in *Drosophila* segmentation interact combinatorially (Gergen and Wieschaus, 1985), less is known about *Drosophila* paralogues that could regulate *Osr1* expression in vertebrates. Studies in *Xenopus laevis* revealed that FGF and retinoic acid (RA) signaling pathways act upstream of *Osr1* and regulate lung specification (Rankin et al., 2012). However, during mice limb morphogenesis the regionalized expression in the distal part of RA and FGF signaling pathways do not suggest a similar interaction regulating *Osr1* expression.

8.1.2 Contribution of Osr1+ connective tissue cells to fetal tissues

Contribution of cells expressing Osr1 at E11.5 or E15.5 to different cell types at E18.5 was addressed using the reporter line R26-mTmG (Muzumdar et al., 2007) in combination with the tamoxifen inducible *Osr1*$^{GCE/+}$ line (Mugford et al., 2008). This allowed the tracking of Osr1+ cells that have been genetically labeled at selected embryonic stages. Immunohistochemistry analyses revealed that mesenchymal cells expressing *Osr1* at E11.5 and 15.5 gave rise to a wide number of embryonic tissues highlighting the potential of this embryonic population. Osr1+ descendant cells were found preferentially in a variety of connective tissues with typical structural functions such as MCT, connective tissue of peripheral nerves, lung fibroblasts, in fibroblasts associated to blood vessels and joints, and in the dermis, among others. Osr1+ descendant cells co-expressed specific markers for cells known to secrete the scaffold of proteins necessary to support tissue structure or giving physical properties to the tissue (see section 7.1.2). This indicates that *Osr1* may be part of a common (transcriptional) machinery of irregular connective tissues at diverse anatomical locations.

In addition, Osr1+ descendant cells were found in low amounts forming parts of tendon and skeletal structures (see section 7.1.2). Tendon and cartilage specification in proximal skeletal elements occurs before the earliest stage of Tamoxifen induction performed, E11.5 (Schweitzer et al., 2001; Akiyama et al., 2005). Expression data indicate that in mouse and chick embryos, *Osr1* is expressed in lateral plate mesoderm at E8.5 (So and Danielian, 1999; Mugford et al., 2008). Thus, one possibility is that *Osr1* expression is down-regulated in lateral plate mesoderm progenitors committed either to cartilage or tendon lineages, during tendon and cartilage specification. This could be tested in the future via Tamoxifen induction of *Osr1*^{GCE} mTmG mice at E8.5.

Strikingly, *Osr1*-derived cells were also found giving rise to fetal adipocytes. White adipose tissue has a described multilineage mesenchymal origin (Chau et al., 2014; Sanchez-Gurmaches and Guertin, 2014). Osr1+ descendant cells were found in adipocytes of presumptive white adipose tissue at E18.5. Additionally, Osr1+ descendant cells contributed to embryonic interscapular and dorsal brown adipose tissue, described to derive from a myogenic progenitor after lineage tracing analyses (Lepper and Fan, 2010; Seale et al., 2008). It remains unclear if myogenic cells giving rise to brown adipose tissue expressed *Osr1* at some point during development before undergoing adipogenic differentiation, or if Osr1+ descendants represent a complementary population of lateral plate derived cells contributing to brown fat in addition to the myogenic population.

Osr1+ descendants genetically labeled at E15.5 showed reduced contribution to different connective tissue lineage, such as lung reticular fibroblasts or connective tissue of

peripheral nerves as compared to labeling at E11.5. Based on *Osr1* lineage analysis in the intermediate mesoderm, it was previously described that *Osr1* expressing cells undergo progressive restriction to nephron progenitors (Mugford et al., 2008). This, combined with my results in the limb suggests a developmental lineage restriction of Osr1+ cells to specific supportive connective tissues derived from the lateral plate mesoderm. Whether *Osr1* is only active during embryonic stages and its downregulation can become re-activated at later stages remains to be elucidated.

Thus, my expression and lineage tracing analyses identify Osr1+ cells as a mesenchymal progenitor population derived from the lateral plate mesoderm, displaying a specific expression pattern for embryonic irregular connective tissue (ICT) and muscle connective tissue (MCT). Furthermore, Osr1+ descendants have manifold potentials during development, however in vivo they predominantly contribute to structural connective tissue components of diverse organs.

8.2 *Osr1* involvement in skeletal muscle formation

8.2.1 Muscle patterning impairments in *Osr1* knockout mice

Despite its poor functional characterization, it has been reported that connective tissue is involved in muscle and tendon formation during development (Kardon et al., 2003; Hasson et al., 2010; Mathew et al., 2011). The expression analysis in mice shown here as well as previous chick expression data (Stricker et al., 2006, 2012) suggested a potential functional relevance of Osr1+ cells during limb muscle formation. To evaluate this, I used an *Osr1* knockout mouse model (Mugford et al., 2008). Phenotypic characterization of muscle patterning was performed by a comprehensive immunostaining approach and 3-dimensional (3D) reconstructions of whole limb muscles. These analyses reported that E14.5 *Osr1*$^{GCE/GCE}$ embryos exhibited no lack of single muscles or groups of muscles in limbs and limb girdle. However, limbs presented a severe impairment in individual muscle patterning and muscle fiber organization. Muscle fibers displayed shortening and mislocation that ultimately lead to impaired muscle shape in *Osr1* mutant embryos. This confirms the importance of muscle connective tissue in muscle patterning and identifies the transcription factor OSR1 as a new molecular player of muscle connective tissue involved in muscle formation.

Interestingly, the appearance of the muscle phenotype is correlated with *Osr1* expression in the surrounding connective tissue. Thus, highly affected muscles exhibited more Osr1+ connective tissue cells or cells with a higher *Osr1* expression level surrounding them. Furthermore, I also demonstrated that limb *Osr1* expression was initiated independently of muscle formation, as limbs devoid of muscles in *Pax3*$^{GFP/GFP}$ mutant mice at E11.5

exhibited normal *Osr1* expression in dorsal and ventral regions. As development proceeds, muscleless limbs showed a muscle-like pattern of *Osr1* expression prefiguring the pattern of muscle segregation, as previously reported for *Tcf4* (Kardon et al., 2003).

Additionally, limb muscles showed defects in myofiber organization in *Osr1* mutant mice. In wild type embryos, multinuclear myofibers formed highly arranged stripes of MyHC-expressing fibers, in contrast *Osr1* knockout embryos exhibited general disorganized, frayed and thinner fibers that very often appeared to be wrongly oriented. Similar defects have been already observed in chick limbs infected with retrovirus containing a dominant-negative form of TCF4 (Kardon et al., 2003) and in mice with conditional inactivation of *Tbx4* or *Tbx5* in the limb mesenchyme (Hasson et al., 2010).

8.2.2 Muscle patterning defects are preceded by limited and mislocated myogenic cells

8.2.2.1 Limited myogenic pool in *Osr1*$^{GCE/GCE}$ mutants

BrdU assays showed that Pax7+ muscle progenitors and MyoD+ myoblasts exhibited reduced proliferation in proximal muscle masses of E11.5 *Osr1*-deficient forelimbs.

Reduced proliferation of Pax7+ and MyoD+ cells in proximal muscle masses in E11.5 *Osr1*$^{GCE/GCE}$ embryos was also accompanied by apoptosis of myogenic cells in these muscle masses. Pax7+ and MyoD+ cells producing the activated form of the apoptosis mediator caspase 3 were more abundant in E11.5 in *Osr1*$^{GCE/GCE}$ embryos in this region. Consistent with the low proliferative rate and high apoptosis of myogenic cells, E11.5 *Osr1*$^{GCE/GCE}$ mutant embryos exhibited a smaller pool of myogenic cells in forelimb muscle masses compared to E11.5 *Osr1*$^{+/+}$ embryos. Pax7+ progenitors were reduced at approximately 20% in proximal parts of forelimbs, in *Osr1* knockout embryos. In line with this, the number of MyoD+ myoblasts was decreased in the different muscle masses of the E11.5 forelimbs of *Osr1* knockout mutant embryos. The reduction of the myogenic cell pool was maintained at later stages, as reduced Pax7+ and MyoD+ cells were found in several muscles of hindlimbs in *Osr1*$^{GCE/GCE}$ embryos at E13.5. These results suggest that the environment created by muscle connective tissue cells influences myogenic capacities and is required to maintain the pool of myogenic cells.

Furthermore, reduction of Pax7+ cells was more pronounced in severe affected muscles at E13.5, such as gastrocnemius and biceps femoris muscles. These results suggest a more restricted pool of muscle progenitors for further fetal myogenesis correlating with stronger muscle impairments at late stages of development.

This leads to the hypothesis that the limited pool of myogenic cells at early stages is causative for the subsequently occurring muscle defects in *Osr1* knock out embryos (see

section 7.10 and 7.2). Final myogenic differentiation and myotube formation appeared disturbed or retarded in E13.5 *Osr1*$^{GCE/GCE}$ embryos. Whether these defects in late myogenesis would recover at later stages or would be prolonged remains unknown due to the lethality of *Osr1* KO embryos (at E14.5).

8.2.2.2 Osr1+ connective tissue cells drive muscle patterning

In *Osr1*$^{GCE/GCE}$ mutant embryos, muscle progenitors migrated from the VLL, formed the dorsal and ventral muscle masses and segregated into the different muscles in the limb. However, the localization of muscle progenitors and consequently of myoblasts was disturbed in *Osr1*$^{GCE/GCE}$ embryos from E11.5 until E14.5. As soon as E11.5, I observed a mispatterning of premuscle masses in forelimbs of E11.5 *Osr1*$^{GCE/GCE}$ embryos. Muscle masses were not established at the correct locations in the limb bud, and showed specific alterations. First, the borders of muscle masses were disturbed in *Osr1* mutant mice (see section 7.13) compared to wild type embryos, where muscle masses were clearly defined. Furthermore, closer appreciation of muscle progenitor organization highlighted a less compact organization of Pax7+ and MyoD+ cells in proximal muscle masses of limbs E11.5 *Osr1*$^{GCE/GCE}$ embryos compared to wild-type embryos. The number of myogenic cells (Pax7+, MyoD+) was reduced in Osr1 mutants compared to wild type embryos. These defects in myogenic cell positioning are likely the result of deficient instructive signals from the associated muscle connective tissue cells.

As development proceeds, masses of myogenic cells are precisely located in limb regions, where they will form nascent muscles. I observed that ectopic muscle fibers and improper growth of muscle fibers was preceded by a mislocation of myogenic cells, indicating that myogenic cells did not reach their allocated positions, or they were misdistributed to ectopic positions. This disturbed organization of myogenic cells may in addition locate them under inappropriate signals in areas of other developing tissues resulting in localized loss of myogenic cells, as we observed in several muscles of hindlimbs and forelimbs in *Osr1* mutant mice (see section 7.2.1).

In summary, *Osr1* knockout embryos exhibited a noticeable reduction in the pool of myogenic cells that together with their impaired distribution resulted in a diverse grade of muscle patterning defects.

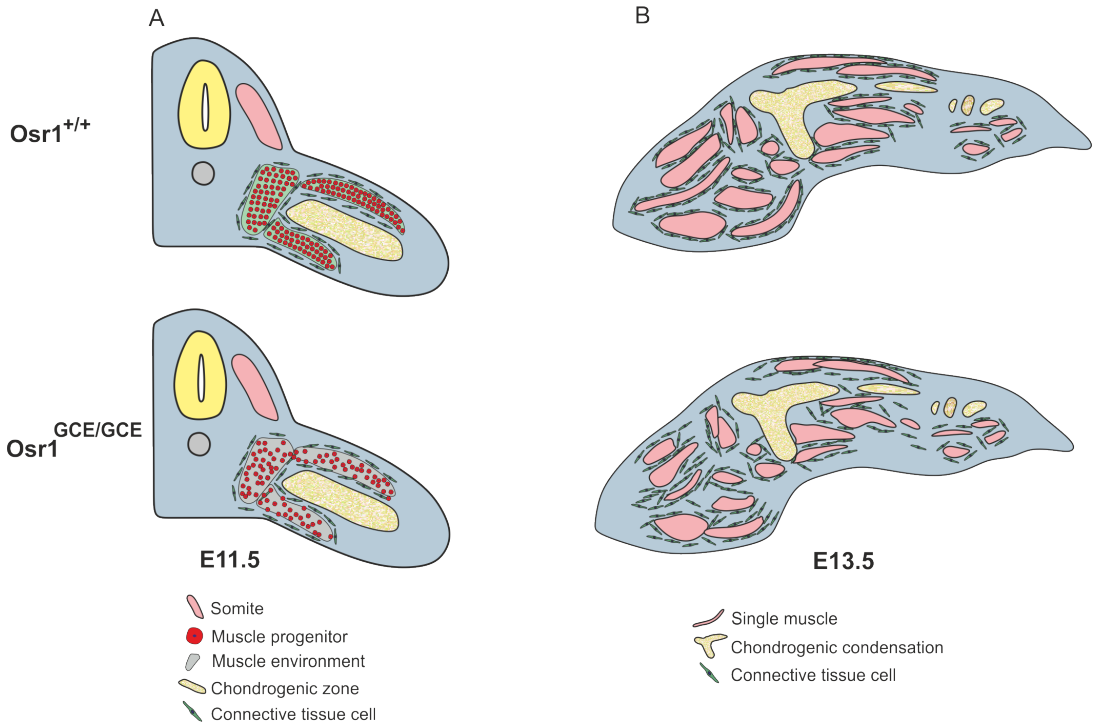

Figure 38: **Schematic representation of skeletal muscle impairments observed in *Osr1*$^{GCE/GCE}$ mutants**. Osr1+ connective tissue cells (green cells) are in close association with muscles during development and create the appropiate environment that instruct muscle patterning. At E11.5 reduced muscle progenitors (red cells) with limited proliferative capacities presented a disorganized aspect within the forelimb muscle masses of *Osr1*$^{GCE/GCE}$ mutants (A). During further development myogenic cells encounter a distorted environment formed by *Osr1*-deficient MCT cells lacking cues that ensure their correct positioning and differentiation. Thus, as a result limb muscles of E13.5 *Osr1*$^{GCE/GCE}$ mutants showed an impaired muscle patterning (B).

8.3 Defects in tendon formation

In the limb, correct tendon formation is achieved after precise cross-regulatory signals between the components of the musculoskeletal system. The importance of muscle development in axial and appendicular tendon formation has been already addressed (Schweitzer et al., 2001; Brent et al., 2003, 2005b; Edom-Vovard et al., 2002).

Connective tissue disorganization together with muscle patterning defects observed in *Osr1* knockout embryos identify Osr1 mutant mice as an interesting model to study the influence of muscle connective tissue on limb tendon development. Moreover, *Osr1* was not expressed in tendon structures and only very few Osr1+ descendant cells were found in tendon structures after lineage tracing experiments. In contrast, expression of the connective tissue marker *Tcf4* was found in tendon structures and, at low level, in myogenic cells (Kardon et al., 2003), suggesting that *Osr1* is a more suitable candidate to study the influence of connective tissue on tendon and muscle development. In limbs, similar to the as syndetome of the somites, FGF signaling was proposed to induce *Scx*

expression. In limb muscles, FGF4 is located at muscle tips close to tendons in somites and limbs and is capable to induce *SCX* and *TNC* expression, when applied ectopically in chick embryos (Edom-Vovard et al., 2002; Edom-Vovard and Duprez, 2004; Eloy-Trinquet et al., 2009). Muscle patterning defects observed in *Osr1*$^{GCE/GCE}$ knock out embryos included a range of muscle shape impairments that hindered the engagement of shortened muscle fibers with the abutting tendon cells. One hypothesis is that this spatial separation in *Osr1* mutant mice lead to impaired tendon development by affecting FGF signaling normally provided by muscle tips. The expression of components of the FGF signaling pathway has not been assessed yet in limbs of *Osr1*$^{GCE/GCE}$ embryos. Therefore, it is still possible that thinner and frayed muscle fibers are not able to produce the necessary FGF signals for further tendon development. Also, the tendon progenitor induction and early tendon patterning should be analyzed by e.g whole-mount ISH for *Scx*. In *Osr1*$^{GCE/GCE}$ embryos, affected muscles clearly exhibited a disrupted physical interaction between muscle fibers and tendons. In these regions, tendons degenerated and *Scx* expression was not detectable or abolished at presumptive muscle-tendon attachment zones. In hindlimbs of *Osr1*$^{GCE/GCE}$ embryos, the semimembranosus muscle was not severely shortened, but peripheral muscle fibers at the attachment zone with the fibula were located distantly from the tendon cells. Despite *Scx* expression at the attachment site, the further differentiation process appears to be compromised, since not all myofibers were attached to the network of type XII collagen that only formed a faint cord-like structure in E13.5 *Osr1*$^{GCE/GCE}$ embryos. These differential tendon impairments seemed to be correlated with the grade of muscle defects in *Osr1* knockout embryos suggesting that tendon defects might be secondary to muscle defects.

Recently, mutations in collagen XII (Col12a1) have been found in human patients with collagen VI-related myopathies. Severe reduction of type XII collagen led to a drastic restriction of mobility, where in the most severe case patients cannot stand or walk (Zou et al., 2014). Reduction of collagen type XII was observed in several tendons of *Osr1*$^{GCE/GCE}$ embryos and other essential connective tissue proteins such as collagen type VI as well as fibronectin were reduced in addition, suggesting that postnatal mice deficient for *Osr1* (i.e. a conditional mutant) might have a more severe phenotypic impairment in mobility compared to inactivation of *Col12a1* (Zou et al., 2014).

Furthermore, connective tissue organization has been described to play an important role in limb tendon patterning (Hasson et al., 2010). Immunohistochemistry analysis of type VI collagen and fibronectin revealed a decrease of these proteins as well as a general disorganized assembly of the connective tissue ECM also surrounding tendon structures in E13.5 *Osr1*$^{GCE/GCE}$ embryos . To which extent and by which mechanism connective tissue ECM impairments influence tendon formation and maintenance in *Osr1* knock out

embryos remains to be characterized.

8.4 Transcriptome analyses of *Osr1*$^{GCE/+}$ and *Osr1*$^{GCE/GCE}$ sorted cells

Osr1+ cells were present around affected muscles in *Osr1*$^{GCE/GCE}$ embryos, indicating that the lack of Osr1 does not affect cell viability. Hence, the muscle defects were not caused by a lack of muscle connective tissue cells, but rather by functional impairment of muscle connective tissue cells as a consequence of *Osr1* deletion. To gain insight into the transcriptional consequences caused by the lack of OSR1, RNA-sequencing analysis was performed on FACS-isolated Osr1+ cells from *Osr1*$^{GCE/+}$ and *Osr1*$^{GCE/GCE}$ embryos. At this point it is worth mentioning that *Osr1*$^{GCE/+}$ animals did not show any apparent defects or behavioral differences from their *Osr1*$^{+/+}$ littermates. Nevertheless, with this approach, gene transcription is compared between *Osr1* heterozygous versus mutant homozygous cells. Consequently, I am aware that the transcriptional differences between *Osr1*$^{GCE/+}$ and *Osr1*$^{GCE/GCE}$ cells are expected to be attenuated compared with those expected between *Osr1*$^{+/+}$ and *Osr1*$^{GCE/GCE}$ cells. However, this approach provides us with gene expression profiles specifically in Osr1+ cells, avoiding the interference of background noise from gene expression in cells that not do not expressed *Osr1*.

To achieve enrichment in muscle connective tissue cells, only cells from the shoulder, stylopod and zeugopod regions were used for FACS-sorting. The autopod, where *Osr1* is expressed in interdigital mesenchyme (Stricker et al., 2006) was discarded. After next-generation sequencing, further analyses revealed 511 de-regulated genes between *Osr1*$^{GCE/+}$ and *Osr1*$^{GCE/GCE}$ cells.

Analyses of de-regulated genes using gene ontology highlighted three major points for these connective tissue cells depleted in the transcription factor *Osr1*:

I .Lack of OSR1 leads to a switch of the transcriptional signature towards cartilage and tendon-like identity in Osr1+ cells.

II .Osr1+ cells are main producers of ECM proteins and OSR1 actively regulates the expression of genes related to the ECM of irregular connective tissue.

III .OSR1 positively regulates the expression of many signaling molecules related to cell-cell communication.

8.4.1 Maintenance of connective tissue identity

A wide range of tissues in the limb such as skeleton, cartilage/tendon, smooth muscle cells of the vasculature and connective tissues are derived from the lateral plate mesoderm (Chevallier et al., 1977; Christ et al., 1977; Kieny and Chevallier, 1979). Before they become specified into different cell types, progenitors of these diverse tissues shared a common identity or origin.

In vitro experiments in chick embryos have reported that OSR1 represses cartilage and tendon differentiation in addition to increasing the pool of connective tissue cells (Stricker et al., 2012). Transcriptome analyses of E13.5 *Osr1*$^{GCE/+}$ and *Osr1*$^{GCE/GCE}$ cells corroborated the previous *in vitro* results, since genes involved in cartilage and tendon formation were upregulated in *Osr1*-deficient cells. Consistently, a similar function has been described for *Osr1* in the neural crest lineage, where *Osr1* was required to suppress chondrogenesis in tongue mesenchyme (Liu et al., 2013). Thus this study expands the range of tissues where *Osr1* is required to maintain a connective tissue fate to limbs and limbs girdle connective tissue. The transcriptional switch was already observed in Osr1+ cells at E11.5, as cartilage and tendon related genes were up-regulated in *Osr1*$^{GCE/GCE}$ sorted cells. These results suggest that *Osr1* repressive activity on cartilage/tendon genes appeared already at or before E11.5 in mice, in accordance with the timing of cartilage and tendon specification during development (Schweitzer et al., 2001; Akiyama et al., 2005). It still remains unclear whether the lineage commitment of connective tissue cells, which are derived from a common lateral plate mesoderm progenitor, is fixed before tendon and cartilage lineages are committed or whether it is gradually restricted to a connective tissue lineage in early limb buds. The partial overlapping expression of *Osr1* and *Scx* and *Osr1* and *Sox9* mRNAs in chick limb buds (Stricker et al., 2012) together with the detectable contribution of Osr1+ cells to cartilage and tendon tissues shown in this study point to a gradual restriction model with a time window of cellular flexibility.

Despite the transcriptional switch to a cartilage/tendon-like signature and the loss of connective tissue identity in *Osr1*$^{GCE/GCE}$ cells, we did not observe any obvious ectopic formation of cartilage or tendon structures in *Osr1*$^{GCE/GCE}$ mutant embryos. However we detected very local occurrence of ectopic Scx+ cells in limbs of *Osr1*$^{GCE/GCE}$ mutant embryos (see section 7.4). While our results established a role for the transcription factor *Osr1* in the maintenance of a connective tissue fate, the loss of *Osr1* alone is not sufficient for cell fate conversion. Consequently, other factors must be involved in the maintenance of the connective tissue fate. One putative factor could be *Osr2*, which has been shown to act in partial redundancy with *Osr1* to maintain joint interzone cells and prevent their conversion to chondrocytes (Gao et al., 2011).

It appears that the effect of *Osr1* in maintaining a connective tissue cell identity is mainly based on a negative regulation of genes responsible for tendon and cartilage commitment. The dual role of OSR1 acting as a repressor as well as an activator of transcription has been described previously in other species (Goldstein et al., 2005; Rankin et al., 2012; Dréan et al., 1998b). It remains to be determined whether these tendon and cartilage genes represent direct or indirect OSR1 targets. In parallel, *Osr1* positively regulates a pool of genes characteristic for connective tissue belonging to the scaffold of extracellular matrix proteins or extracellular matrix-associated and modifying proteins.

8.4.2 Importance of Osr1+ connective tissue cells in extracellular matrix formation

Muscle connective tissue cells are the main cell type secreting the scaffold of extracellular matrix (ECM) that supports muscle fibers (Bönnemann, 2011). However, lack of specific markers for connective tissue and the complexity of the intricate matrix of proteins that form the ECM have hindered a precise assignment of the ECM-components produced by a certain type of cells.

Transcriptome analysis of Osr1+ FACS-isolated cells provided us with a transcriptional readout of ECM components produced by Osr1+ connective tissue cells during development. Many collagens as well as other ECM components were found highly expressed in Osr1+ cells. Furthermore, comparison of de-regulated genes between E13.5 *Osr1*$^{GCE/+}$ and *Osr1*$^{GCE/GCE}$ cells revealed that *Osr1* apparently is a positive regulator of ECM genes in embryonic irregular connective tissue. Among the ECM components that were down-regulated in *Osr1*$^{GCE/GCE}$ cells, we identified the structural collagen types III, V, and VI, genes encoding factors important for correct assembly of the ECM-structure such as proteinases and the small leucine-rich proteoglycans (SLRPs) *Lum*, *Dcn* and *Ktn*.

These results suggest that Osr1+ cells secrete several components necessary for correct assembly of connective tissue ECM during development. This intricate and highly organized network of proteins requires a dynamic assembly of many components to achieve proper consistency. Connective tissue in *Osr1*$^{GCE/GCE}$ embryos not only exhibited a deficient scaffold of ECM proteins and impaired ECM-organization but also displayed a down-regulation of genes responsible for correct ECM remodeling and assembly. Cellular contacts that muscle progenitors establish with both the ECM and mesenchymal cells during their way from the VLL into the limb are crucial for their correct pathfinding and concomitant differentiation (Brand-Saberi et al., 1996). Immunohistochemistry analysis indicate that ECM assembly defects appeared early in the limbs of *Osr1*$^{GCE/GCE}$ embryos, beginning at least at E11.5. Fibronectin is an important component of early ECMs ex-

press in early limb mesenchyme (Thorsteinsdottir et al., 2011) and is important for muscle progenitor migration in chick limbs (Brand-Saberi and Christ, 1993). Immunolabeling for fibronectin and type VI collagen at E11.5 revealed a slight reduction of these proteins surrounding limb muscle masses in *Osr1*$^{GCE/GCE}$ mutants. Thus, it can be speculated that the impaired-ECM in *Osr1*$^{GCE/GCE}$ embryos probably interferes with correct muscle progenitor-mesenchyme engagement hindering the path of muscle progenitors into the limb.

Dynamic changes in the ECM have been reported to occur in limb mesenchyme during myogenesis (Calve et al., 2010). Muscle connective tissue has been highlighted to play a crucial role in the process of muscle mass segregation and splitting (Kardon et al., 2003; Mathew et al., 2011; Brent et al., 2003; Hurle et al., 1990). During this process, the ECM matures, which is associated with new types of ECM proteins produced by the muscle connective tissue that will sustain and separate single muscles. In this thesis, I showed that *Osr1*-deficiency led to a specific impairment in muscle connective tissue ECM-components and matrix assembly. Reduction in fibronectin and COLVI protein abundance were observed in *Osr1* mutant mice. Fibronectin was described to play a role in myogenic cell migration (see above) but also in myofiber organization, which facilitates myoblast alignment and preparation for fusion (Snow et al., 2008). Furthermore, immunohistochemistry analyses of type VI collagen and fibronectin revealed a disorganized muscle connective tissue in *Osr1* knock out embryos, which was previously linked to defects in muscle patterning (Hasson et al., 2010). Nascent myofibers attach to the ECM via two main transmembrane complexes, integrin and dystroglycan complexes (Thorsteinsdottir et al., 2011). Myoblasts dynamically change their battery of integrins anchored in the membrane depending on the steps of myogenesis (Cachaço et al., 2005; Gullberg et al., 1995b). In parallel, primary myofibers change their repertoire of transmembrane proteins and produce $\alpha 6\beta 1$ and $\alpha 7\beta 1$ integrin complexes as well as dystroglycan, which both bind to proteins of the newly formed basal lamina, mainly laminin and type IV collagen. The basal lamina directly interconnects anchor protein complexes of the sarcolemma with the scaffold of ECM-proteins produced by muscle connective tissue cells (Nedergaard et al., 2013). *Osr1*$^{GCE/GCE}$ mutant embryos exhibited a defective muscle connective tissue ECM and additionally showed impaired basal lamina formation.

In summary, I demonstrated that Osr1+ cells are muscle connective tissue cells producing high amounts of ECM and ECM-modifying proteins and that *Osr1* is required for the correct formation and assembly of muscle connective tissue ECM. Failure of correct ECM assembly affects basal lamina establishment and henceforth impairs myofiber anchoring and stability.

8.4.3 Osr1+ connective tissue cells and secreted molecules

In addition to ECM proteins, RNA-seq analysis also indicated that Osr1+ connective tissue cells secrete diverse signaling molecules involved in cell migration and tissue organization, mainly chemokines. Chemokines and other growth factors are secreted to the extracellular media where they interact with ECM proteins that modulate their availability (Raz and Mahabaleshwar, 2009; Rozario and DeSimone, 2010). Therefore, impairments in ECM composition or assembly may also interfere with chemokine signaling. This prevents the clear attribution of defects observed in *Osr1* knockout embryos to either ECM or chemokine signaling. This functional interrelation however indicates that both mechanisms most likely act in combination to shape the environment where muscles develop.

The RNA-seq analyses showed transcriptional down-regulation of chemokines such as CCL2, CCL3, CCL4 and also CXCL12 at E13.5. RT-qPCR confirmed a lower but significant downregulation of *Cxcl12* already at E11.5 in *Osr1*$^{GCE/GCE}$ embryos. Additionally, the connective tissue ECM exhibited defects in both assembly/structure as well as protein abundancy at E11.5, indicating that a combined matrix/chemokine defect occurred already at this stage. In accordance fibronectin promotes myoblast proliferation (Gullberg et al., 1995a) rather than differentiation (García et al., 1999) in cell culture. Similarly, CXCL12/CXCR4 triggers the pERK/MAPK pathway in myoblast cultures promoting their proliferation (Hunger et al., 2012). Apart from CXCL12 other chemokines such as CCL2, CCL3 or CCL4 have been described to activate proliferation in myoblast cultures via the pERK/MAPK signaling pathway (Yahiaoui et al., 2008). In accordance, I detected a severe decrease in pERK protein in a subpopulation of muscle progenitor cells. Besides being downstream of the CXCL12/CXCR4 cascade, activation of the ERK pathway was also demonstrated downstream of Fibronectin-Integrin engagement (Thorsteinsdottir et al., 2011), enforcing the notion of a combined ECM/chemokine defect. In addition, chemokine signaling has a positive influence on integrin activation in leukocytes and in zebrafish gastrulation required for integrin-mediated cell attachment to the ECM (Mizoguchi et al., 2008; Nair and Schilling, 2008). This indicates an intricate cross-talk of both mechanisms.

Given the known proliferation-promoting role of ERK signaling in myoblasts, a decrease in proliferation of myogenic cells of E11.5 *Osr1*$^{GCE/GCE}$ embryos was expected. Indeed, the defective ECM (in connective tissue) as well as the reduced expression of chemokines in *Osr1*$^{GCE/GCE}$ embryos appear to negatively influence proliferation of myogenic progenitors and lead to a decreased pool of myogenic cells as soon as E11.5 in the different muscle masses of the limb. Muscle progenitors did not appear to recover their normal proliferative capacities at later stages. At E13.5, the number of Pax7+ cells in Osr1 mutants was still

reduced as was their proliferation rate. However, the role of the chemokines CCL2, CCL3, CCL4 in myoblast proliferation has only been addressed *in vitro* (Yahiaoui et al., 2008), consequently, their role in mouse myogenic proliferation *in vivo* is still unknown. The role of CXCL12 in muscle progenitor proliferation remains still poorly characterized and is only suggested in this work.

The chemokine CXCL12 has been described to play a crucial role in tissue organization in several animal models (Raz and Mahabaleshwar, 2009). *Cxcl12* is expressed in mouse limb mesenchyme at early stages and in muscle connective tissue as development proceeds (Vasyutina et al., 2005). The effect of CXCL12/CXCR4 signaling in muscle migration has been analyzed during the process of early proximodistal migration of muscle progenitors (Vasyutina et al., 2005). CXCL12/CXCR4 signaling was also involved in the retrograde migration of myoblast, the so-called "In-out" mechanism, forming perineal and limb girdle muscles (Evans et al., 2006; Rehimi et al., 2010; Masyuk et al., 2014). Interestingly several muscles of the shoulder and upper limb region were stronger affected in *Osr1*$^{GCE/GCE}$ embryos, possibly reflecting a defect in this mechanism. Thus, CXCL12 was of special interest due its possible pivotal role in cellular communication between muscle connective tissue fibroblasts and myogenic cells.

However, the mechanistic explanation of how CXCL12 guides migration of muscle progenitors or myoblast remains elusive. Chemokines that play a role in immune cell trafficking were proposed to form a signaling gradient that attracts and guides cells (Raz and Mahabaleshwar, 2009). Nevertheless, such gradients have not been described yet for CXCL12 in mouse limb mesenchyme (Vasyutina et al., 2005). The study by Vasyutina and colleagues describes a reduced number of Lbx1+ cells in the distal limb muscle masses in *Cxcr4*-deficient embryos from which they conclude a migratory impairment. A proliferation defect was not seen, at least in the limb premuscle masses at E10.75. At the same time increased apoptosis was observed in proximal dorsal Lbx1+ cells in *Cxcr4*$^{-/-}$ embryos , which is in accordance with literature reporting a role for CXCL12 in cell survival in different contexts (Bagri et al., 2002; Molyneaux et al., 2003; Zou et al., 1998). In line with this an increased apoptosis rate of myogenic cells in *Osr1* mutants was observed. It remains unclear whether the proliferation defect observed in *Osr1* mutants is independent of the CXCL12/CXCR4 axis or whether this discrepancy can be explained by the different developmental stages analyzed. Assessing proliferation rates of LBX1+ cells in *Cxcr4* mutants at E11.5 will help resolving this issue.

In addition the role of CXCL12/CXCR4 in cell migration has seen an unexpected twist, since it was demonstrated that under certain circumstances this signaling cascade does not induce migration of cells but is rather required for instructing cells to maintain their position (Raz and Mahabaleshwar, 2009). This was shown for different cell types in

the mouse brain, where CXCL12 signaling for example prevented Cajal-Retzius cells of the marginal zone from displacing to deeper layers (Paredes et al., 2006; Tiveron and Cremer, 2008), and also for primordial germ cells in the zebrafish gonad (Reichman-Fried et al., 2004). CXCL12 is preferentially expressed in the more central mesenchyme of the mouse and chick limb bud (Vasyutina et al., 2005), contra intuitive of a role in proximo-distal migration. An alternative role for CXCL12 controlling local position of myogenic precursors rather than influencing collective cell migration might be taken into account. Such effects could well explain the local misdistribution of myogenic cells seen in *Osr1* mutants. Clearly, this issue needs further clarification.

Finally it has to be noted that matrix-bound or soluble CXCL12 have different effects on myoblast migration in culture (Dalonneau et al., 2014). Thus it can be suggested that the modulatory activities of CXCL12 and other chemokines, which were down-regulated in E13.5 *Osr1*$^{GCE/GCE}$ cells, might also depend on their forms, matrix bound or soluble. Thus, once more, the ECM defects and downregulation of chemokines in connective tissue cells in *Osr1*$^{GCE/GCE}$ embryos can act in combination to influence myogenic cell migration and proliferation.

9 Future work

Despite the well characterized transcriptional expression pattern of *Osr1* in chick and mice, the expression pattern of OSR1 protein has not been characterized yet. Thus, in the future it will be of great importance to develop an antibody against OSR1 protein that might allow a wide range of approaches inaccessible so far. Lack of a functioning anti-OSR1 antibody has hindered OSR1 visualization remaining as a future work to confirm described transcriptional analyses and validate *Osr1*$^{GCE/+}$ as reliable reporter model of OSR1 during development. Additionally, it could provide important information about the cellular distribution of OSR1 protein.

How OSR1 controls expression of its target genes remains elusive and only its repressive mechanism has been described in *Drosophila* (Goldstein et al., 2005). In the future it would be important to further investigate first, the direct influence of this transcription factor on chromatin remodeling using *Osr1*$^{GCE/+}$ and *Osr1*$^{GCE/GCE}$ cells in a similar approach as already described in section to assess changes in methylation and acetylation-based chromatin profiling of *Osr1* knock out cells. Second, changes observed in expression levels of deregulated genes in *Osr1*$^{GCE/GCE}$ cells after RNA-seq have not been correlated yet with direct binding of OSR1 to regulatory elements of those genes. Immunoprecipitation of chromatin bound to OSR1 protein using chromatin immunoprecipitation (ChIP) approaches and further next-generation sequencing might be used to assess direct targets of OSR1. However, no anti OSR1-antibody has been described in such experiments so far, what might lead to reconsider the use of tagged OSR1 proteins in cell cultures experiments to accomplish such experiments.

Lineage tracing experiments within this work have tried to address general contribution of Osr1+ cells at E11.5 and E15.5 to different embryonic tissues. Similarly as for cartilage and tendon lineages, tracking of Osr1+ cells using Tamoxifen at earlier stages than E11.5 can be used in the future to reveal the precise contribution of Osr1+ descendant to brown adipose tissue, cartilage and tendon elements.

Osr1 inactivation in *Osr1*$^{GCE/GCE}$ mutant embryos has served as valuable model to study OSR1 function. However, embryonic lethality has restricted functional analysis to early embryonic stages. Conditional inactivation of Osr1 can be used in the future to bypass *Osr1*$^{GCE/GCE}$ embryo lethality and to address *Osr1* role at fetal stages of muscle development. This mouse model could provide a better understanding about the possible transitory defects observed during early limb development. Similarly, this model can be used to further investigate *Osr1* influence in tendon formation and maintenance at late developmental stages and during the adulthood.

In this study I could demonstrate impaired formation of several tendon structures in

muscles of hindlimbs and forelimbs in *Osr1* knockout embryos. Nevertheless, a more comprehensive analysis of muscle and tendon defects can be develop taking advantage of the *Scx*^{GFP} mouse model (Pryce et al., 2007). 3D reconstructions of limbs carrying homozygous mutations for *Osr1*$^{GCE/GCE}$ and heterozygous for *Scx*^{GFP} will provide a valuable readout of tendon and muscle defects after the lack of *Osr1*.

Further experiments should follow to underpin the proposed idea that reduced expression of *Cxcl12* in *Osr1*$^{GCE/GCE}$ cells could be responsible for a decreased pERK protein abundance in Lbx1+ cells. Downstream of CXCR4, reduced pERK might lead to a subsequent impaired proliferation of myogenic cells in *Osr1* knockout embryos. pERK protein abundance in muscle progenitors and proliferation of myogenic pools can be assess in mice devoid of CXCR4 taking advantage of the developed loss-of-function model for CXCR4 (*Cxcr4*$^{-/-}$) (Vasyutina et al., 2005; Odemis et al., 2005). Thus, a key element will be set pointing to the influence of the chemokine CXCL12 in myogenic proliferation via CXCR4 receptor. Lastly, *Osr1* positively regulates secreted factors and structural proteins responsible for correct formation of connective tissue ECM. Mouse models carrying mutations in ECM structural proteins such as collagen type VI or fibronectin have been developed and can be used to further investigate myogenic behavior in the absence of these structural proteins.

This work indicates a role for *Osr1* driving a transcriptional program in muscle connective tissue cells that supports myogenesis in the limb. It will be interesting to test in the future if *Osr1* positive cells can also be seen during muscle regeneration, and if *Osr1* plays an overlapping role in this context.

10 References

Adams, J. C. and Watt, F. M. (1993). Regulation of development and differentiation by the extracellular matrix. *Development*, 117(4):1183–1198.

Aguzzi, A., Kranich, J., and Krautler, N. J. (2014). Follicular dendritic cells: origin, phenotype, and function in health and disease. *Trends Immunol*, 35(3):105–113.

Akiyama, H., Kamitani, T., Yang, X., Kandyil, R., Bridgewater, L. C., Fellous, M., Mori-Akiyama, Y., and de Crombrugghe, B. (2005). The transcription factor sox9 is degraded by the ubiquitin-proteasome system and stabilized by a mutation in a ubiquitin-target site. *Matrix Biol*, 23(8):499–505.

Ameye, L. and Young, M. F. (2002). Mice deficient in small leucine-rich proteoglycans: novel in vivo models for osteoporosis, osteoarthritis, ehlers-danlos syndrome, muscular dystrophy, and corneal diseases. *Glycobiology*, 12(9):107R–116R.

Amthor, H., Christ, B., Weil, M., and Patel, K. (1998). The importance of timing differentiation during limb muscle development. *Curr Biol*, 8(11):642–652.

Aulehla, A. and Pourquié, O. (2010). Signaling gradients during paraxial mesoderm development. *Cold Spring Harb Perspect Biol*, 2(2):a000869.

Bagri, A., Gurney, T., He, X., Zou, Y.-R., Littman, D. R., Tessier-Lavigne, M., and Pleasure, S. J. (2002). The chemokine sdf1 regulates migration of dentate granule cells. *Development*, 129(18):4249–4260.

Bates, D., Taylor, G. I., and Newgreen, D. F. (2002). The pattern of neurovascular development in the forelimb of the quail embryo. *Dev Biol*, 249(2):300–320.

Bentzinger, C. F., Wang, Y. X., and Rudnicki, M. A. (2012). Building muscle: molecular regulation of myogenesis. *Cold Spring Harb Perspect Biol*, 4(2).

Bentzinger, C. F., Wang, Y. X., von Maltzahn, J., Soleimani, V. D., Yin, H., and Rudnicki, M. A. (2013). Fibronectin regulates wnt7a signaling and satellite cell expansion. *Cell Stem Cell*, 12(1):75–87.

Birchmeier, C. and Brohmann, H. (2000). Genes that control the development of migrating muscle precursor cells. *Curr Opin Cell Biol*, 12(6):725–730.

Biressi, S., Tagliafico, E., Lamorte, G., Monteverde, S., Tenedini, E., Roncaglia, E., Ferrari, S., Ferrari, S., Angelis, M. G. C.-D., Tajbakhsh, S., and Cossu, G. (2007). Intrinsic phenotypic diversity of embryonic and fetal myoblasts is revealed by genome-wide gene expression analysis on purified cells. *Dev Biol*, 304(2):633–651.

Bismuth, K. and Relaix, F. (2010). Genetic regulation of skeletal muscle development. *Exp Cell Res*, 316(18):3081–3086.

Bönnemann, C. G. (2011). The collagen vi-related myopathies ullrich congenital muscular dystrophy and bethlem myopathy. *Handb Clin Neurol*, 101:81–96.

Bobadilla, M., Sainz, N., Abizanda, G., Orbe, J., Rodriguez, J. A., Páramo, J. A., Prósper, F., and Pérez-Ruiz, A. (2014). The cxcr4/sdf1 axis improves muscle regeneration through mmp-10 activity. *Stem Cells Dev*, 23(12):1417–1427.

Bonafede, A., Köhler, T., Rodriguez-Niedenführ, M., and Brand-Saberi, B. (2006). Bmps restrict the position of premuscle masses in the limb buds by influencing tcf4 expression. *Dev Biol*, 299(2):330–344.

Bonnin, M.-A., Laclef, C., Blaise, R., Eloy-Trinquet, S., Relaix, F., Maire, P., and Duprez, D. (2005). Six1 is not involved in limb tendon development, but is expressed in limb connective tissue under shh regulation. *Mech Dev*, 122(4):573–585.

Braid, L. R., Lee, W., Uetrecht, A. C., Swarup, S., Papaianni, G., Heiler, A., and Verheyen, E. M. (2010). Nemo phosphorylates even-skipped and promotes eve-mediated repression of odd-skipped in even parasegments during drosophila embryogenesis. *Dev Biol*, 343(1-2):178–189.

Brand-Saberi, B., editor (2015). *Vertebrate Myogenesis*. Springer-Verlag Berlin Heidelberg.

Brand-Saberi, B. and Christ, B. (1993). Inhibition of myogenic cell migration by the application of antibodies raised against limb bud mesenchyme. *Prog Clin Biol Res*, 383B:541–552.

Brand-Saberi, B., Gamel, A. J., Krenn, V., Müller, T. S., Wilting, J., and Christ, B. (1996). N-cadherin is involved in myoblast migration and muscle differentiation in the avian limb bud. *Dev Biol*, 178(1):160–173.

Brandan, E., Cabello-Verrugio, C., and Vial, C. (2008). Novel regulatory mechanisms for the proteoglycans decorin and biglycan during muscle formation and muscular dystrophy. *Matrix Biol*, 27(8):700–708.

Braun, T. and Gautel, M. (2011). Transcriptional mechanisms regulating skeletal muscle differentiation, growth and homeostasis. *Nat Rev Mol Cell Biol*, 12(6):349–361.

Bren-Mattison, Y., Hausburg, M., and Olwin, B. B. (2011). Growth of limb muscle is dependent on skeletal-derived indian hedgehog. *Dev Biol*, 356(2):486–495.

Brent, A. E., Braun, T., and Tabin, C. J. (2005a). Genetic analysis of interactions between the somitic muscle, cartilage and tendon cell lineages during mouse development. *Development*, 132(3):515–528.

Brent, A. E., Braun, T., and Tabin, C. J. (2005b). Genetic analysis of interactions between the somitic muscle, cartilage and tendon cell lineages during mouse development. *Development*, 132(3):515–528.

Brent, A. E., Schweitzer, R., and Tabin, C. J. (2003). A somitic compartment of tendon progenitors. *Cell*, 113(2):235–248.

Bröhl, D., Vasyutina, E., Czajkowski, M. T., Griger, J., Rassek, C., Rahn, H.-P., Purfürst, B., Wende, H., and Birchmeier, C. (2012). Colonization of the satellite cell niche by skeletal muscle progenitor cells depends on notch signals. *Dev Cell*, 23(3):469–481.

Brohmann, H., Jagla, K., and Birchmeier, C. (2000). The role of lbx1 in migration of muscle precursor cells. *Development*, 127(2):437–445.

Buckingham, M. (1992). Making muscle in mammals. *Trends Genet*, 8(4):144–148.

Buckingham, M. (2003). How the community effect orchestrates muscle differentiation. *Bioessays*, 25(1):13–16.

Cachaço, A. S., Pereira, C. S., Pardal, R. G., Bajanca, F., and Thorsteinsdóttir, S. (2005). Integrin repertoire on myogenic cells changes during the course of primary myogenesis in the mouse. *Dev Dyn*, 232(4):1069–1078.

Calve, S., Odelberg, S. J., and Simon, H.-G. (2010). A transitional extracellular matrix instructs cell behavior during muscle regeneration. *Dev Biol*, 344(1):259–271.

Capetanaki, Y. and Milner, D. J. (1998). Desmin cytoskeleton in muscle integrity and function. *Subcell Biochem*, 31:463–495.

Chau, Y.-Y., Bandiera, R., Serrels, A., Martínez-Estrada, O. M., Qing, W., Lee, M., Slight, J., Thornburn, A., Berry, R., McHaffie, S., Stimson, R. H., Walker, B. R., Chapuli, R. M., Schedl, A., and Hastie, N. (2014). Visceral and subcutaneous fat have different origins and evidence supports a mesothelial source. *Nat Cell Biol*, 16(4):367–375.

Chevallier, A., Kieny, M., and Mauger, A. (1977). Limb-somite relationship: origin of the limb musculature. *J Embryol Exp Morphol*, 41:245–258.

Christ, B., Jacob, H. J., and Jacob, M. (1977). Experimental analysis of the origin of the wing musculature in avian embryos. *Anat Embryol (Berl)*, 150(2):171–186.

Christ, B. and Ordahl, C. P. (1995). Early stages of chick somite development. *Anat Embryol (Berl)*, 191(5):381–396.

Cinnamon, Y., Ben-Yair, R., and Kalcheim, C. (2006). Differential effects of n-cadherin-mediated adhesion on the development of myotomal waves. *Development*, 133(6):1101–1112.

Corish, P. and Tyler-Smith, C. (1999). Attenuation of green fluorescent protein half-life in mammalian cells. *Protein Eng*, 12(12):1035–1040.

Dalonneau, F., Liu, X. Q., Sadir, R., Almodovar, J., Mertani, H. C., Bruckert, F., Albiges-Rizo, C., Weidenhaupt, M., Lortat-Jacob, H., and Picart, C. (2014). The effect of delivering the chemokine sdf-1? in a matrix-bound manner on myogenesis. *Biomaterials*, 35(15):4525–4535.

Desiderio, M. A. (2007). Hepatocyte growth factor in invasive growth of carcinomas. *Cell Mol Life Sci*, 64(11):1341–1354.

Dietrich, S., Abou-Rebyeh, F., Brohmann, H., Bladt, F., Sonnenberg-Riethmacher, E., Yamaai, T., Lumsden, A., Brand-Saberi, B., and Birchmeier, C. (1999). The role of sf/hgf and c-met in the development of skeletal muscle. *Development*, 126(8):1621–1629.

Dréan, B. S.-L., Nasiadka, A., Dong, J., and Krause, H. M. (1998a). Dynamic changes in the functions of odd-skipped during early drosophila embryogenesis. *Development*, 125(23):4851–4861.

Dréan, B. S.-L., Nasiadka, A., Dong, J., and Krause, H. M. (1998b). Dynamic changes in the functions of odd-skipped during early drosophila embryogenesis. *Development*, 125(23):4851–4861.

Dubrulle, J. and Pourquié, O. (2004). Coupling segmentation to axis formation. *Development*, 131(23):5783–5793.

Duprez, D., Lapointe, F., Edom-Vovard, F., Kostakopoulou, K., and Robson, L. (1999). Sonic hedgehog (shh) specifies muscle pattern at tissue and cellular chick level, in the chick limb bud. *Mech Dev*, 82(1-2):151–163.

Edom-Vovard, F. and Duprez, D. (2004). Signals regulating tendon formation during chick embryonic development. *Developmental Dynamics*, 229(3):449–457.

Edom-Vovard, F., Schuler, B., Bonnin, M.-A., Teillet, M.-A., and Duprez, D. (2002). Fgf4 positively regulates scleraxis and tenascin expression in chick limb tendons. *Dev Biol*, 247(2):351–366.

Eloy-Trinquet, S., Wang, H., Edom-Vovard, F., and Duprez, D. (2009). Fgf signaling components are associated with muscles and tendons during limb development. *Dev Dyn*, 238(5):1195–1206.

Evans, D. J. R., Valasek, P., Schmidt, C., and Patel, K. (2006). Skeletal muscle translocation in vertebrates. *Anat Embryol (Berl)*, 211 Suppl 1:43–50.

Gao, Y., Lan, Y., Liu, H., and Jiang, R. (2011). The zinc finger transcription factors osr1 and osr2 control synovial joint formation. *Dev Biol*, 352(1):83–91.

García, A. J., Vega, M. D., and Boettiger, D. (1999). Modulation of cell proliferation and differentiation through substrate-dependent changes in fibronectin conformation. *Mol Biol Cell*, 10(3):785–798.

Gergen, J. P. and Wieschaus, E. F. (1985). The localized requirements for a gene affecting segmentation in drosophila: analysis of larvae mosaic for runt. *Dev Biol*, 109(2):321–335.

Goetsch, S. C., Hawke, T. J., Gallardo, T. D., Richardson, J. A., and Garry, D. J. (2003). Transcriptional profiling and regulation of the extracellular matrix during muscle regeneration. *Physiol Genomics*, 14(3):261–271.

Goldstein, R. E., Cook, O., Dinur, T., Pisanté, A., Karandikar, U. C., Bidwai, A., and Paroush, Z. (2005). An eh1-like motif in odd-skipped mediates recruitment of groucho and repression in vivo. *Mol Cell Biol*, 25(24):10711–10720.

Griffin, C. A., Apponi, L. H., Long, K. K., and Pavlath, G. K. (2010). Chemokine expression and control of muscle cell migration during myogenesis. *J Cell Sci*, 123(Pt 18):3052–3060.

Grifone, R., Demignon, J., Houbron, C., Souil, E., Niro, C., Seller, M. J., Hamard, G., and Maire, P. (2005). Six1 and six4 homeoproteins are required for pax3 and mrf expression during myogenesis in the mouse embryo. *Development*, 132(9):2235–2249.

Gros, J. and Tabin, C. J. (2014). Vertebrate limb bud formation is initiated by localized epithelial-to-mesenchymal transition. *Science*, 343(6176):1253–1256.

Gullberg, D., Sjöberg, G., Velling, T., and Sejersen, T. (1995a). Analysis of fibronectin and vitronectin receptors on human fetal skeletal muscle cells upon differentiation. *Exp Cell Res*, 220(1):112–123.

Gullberg, D., Velling, T., Sjöberg, G., and Sejersen, T. (1995b). Up-regulation of a novel integrin alpha-chain (alpha mt) on human fetal myotubes. *Dev Dyn*, 204(1):57–65.

Haas, P. and Gilmour, D. (2006). Chemokine signaling mediates self-organizing tissue migration in the zebrafish lateral line. *Dev Cell*, 10(5):673–680.

Hall, B. K. and Miyake, T. (2000). All for one and one for all: condensations and the initiation of skeletal development. *Bioessays*, 22(2):138–147.

Haninec, P. (1988). Study of the origin of connective tissue sheaths of peripheral nerves in the limb of avian embryos. *Anat Embryol (Berl)*, 178(6):553–557.

Harrison, M. R. M., Bussmann, J., Huang, Y., Zhao, L., Osorio, A., Burns, C. G., Burns, C. E., Sucov, H. M., Siekmann, A. F., and Lien, C.-L. (2015). Chemokine-guided angiogenesis directs coronary vasculature formation in zebrafish. *Dev Cell*, 33(4):442–454.

Hasson, P., Buono, J. D., and Logan, M. P. O. (2007). Tbx5 is dispensable for forelimb outgrowth. *Development*, 134(1):85–92.

Hasson, P., DeLaurier, A., Bennett, M., Grigorieva, E., Naiche, L. A., Papaioannou, V. E., Mohun, T. J., and Logan, M. P. O. (2010). Tbx4 and tbx5 acting in connective tissue are required for limb muscle and tendon patterning. *Dev Cell*, 18(1):148–156.

Havis, E., Bonnin, M.-A., Olivera-Martinez, I., Nazaret, N., Ruggiu, M., Weibel, J., Durand, C., Guerquin, M.-J., Bonod-Bidaud, C., Ruggiero, F., Schweitzer, R., and Duprez, D. (2014). Transcriptomic analysis of mouse limb tendon cells during development. *Development*, 141(19):3683–3696.

Huang, A. H., Riordan, T. J., Wang, L., Eyal, S., Zelzer, E., Brigande, J. V., and Schweitzer, R. (2013). Repositioning forelimb superficialis muscles: tendon attachment and muscle activity enable active relocation of functional myofibers. *Dev Cell*, 26(5):544–551.

Hunger, C., Odemis, V., and Engele, J. (2012). Expression and function of the sdf-1 chemokine receptors {CXCR4} and {CXCR7} during mouse limb muscle development and regeneration. *Experimental Cell Research*, 318(17):2178 – 2190.

Hurle, J. M., Ros, M. A., Gañan, Y., Macias, D., Critchlow, M., and Hinchliffe, J. R. (1990). Experimental analysis of the role of ecm in the patterning of the distal tendons of the developing limb bud. *Cell Differ Dev*, 30(2):97–108.

Hutcheson, D. A., Zhao, J., Merrell, A., Haldar, M., and Kardon, G. (2009). Embryonic and fetal limb myogenic cells are derived from developmentally distinct progenitors and have different requirements for beta-catenin. *Genes Dev*, 23(8):997–1013.

Jacob, M., Christ, B., and Jacob, H. J. (1979). The migration of myogenic cells from the somites into the leg region of avian embryos. an ultrastructural study. *Anat Embryol (Berl)*, 157(3):291–309.

Jagla, K., Dollé, P., Mattei, M. G., Jagla, T., Schuhbaur, B., Dretzen, G., Bellard, F., and Bellard, M. (1995). Mouse lbx1 and human lbx1 define a novel mammalian homeobox gene family related to the drosophila lady bird genes. *Mech Dev*, 53(3):345–356.

James, R. G., Kamei, C. N., Wang, Q., Jiang, R., and Schultheiss, T. M. (2006). Odd-skipped related 1 is required for development of the metanephric kidney and regulates formation and differentiation of kidney precursor cells. *Development*, 133(15):2995–3004.

Kardon, G. (1998). Muscle and tendon morphogenesis in the avian hind limb. *Development*, 125(20):4019–4032.

Kardon, G., Campbell, J. K., and Tabin, C. J. (2002). Local extrinsic signals determine muscle and endothelial cell fate and patterning in the vertebrate limb. *Dev Cell*, 3(4):533–545.

Kardon, G., Harfe, B. D., and Tabin, C. J. (2003). A tcf4-positive mesodermal population provides a prepattern for vertebrate limb muscle patterning. *Dev Cell*, 5(6):937–944.

Kassar-Duchossoy, L., Gayraud-Morel, B., Gomès, D., Rocancourt, D., Buckingham, M., Shinin, V., and Tajbakhsh, S. (2004). Mrf4 determines skeletal muscle identity in myf5:myod double-mutant mice. *Nature*, 431(7007):466–471.

Kieny, M. and Chevallier, A. (1979). Autonomy of tendon development in the embryonic chick wing. *J Embryol Exp Morphol*, 49:153–165.

Klein, R. S. and Rubin, J. B. (2004). Immune and nervous system cxcl12 and cxcr4: parallel roles in patterning and plasticity. *Trends Immunol*, 25(6):306–314.

Lalor, S. J. and Segal, B. M. (2010). Lymphoid chemokines in the cns. *J Neuroimmunol*, 224(1-2):56–61.

Lepper, C. and Fan, C.-M. (2010). Inducible lineage tracing of pax7-descendant cells reveals embryonic origin of adult satellite cells. *Genesis*, 48(7):424–436.

Li, G., Adesnik, H., Li, J., Long, J., Nicoll, R. A., Rubenstein, J. L. R., and Pleasure, S. J. (2008). Regional distribution of cortical interneurons and development of inhibitory tone are regulated by cxcl12/cxcr4 signaling. *J Neurosci*, 28(5):1085–1098.

Li, Y., Qiu, Q., Watson, S. S., Schweitzer, R., and Johnson, R. L. (2010). Uncoupling skeletal and connective tissue patterning: conditional deletion in cartilage progenitors reveals cell-autonomous requirements for lmx1b in dorsal-ventral limb patterning. *Development*, 137(7):1181–1188.

Lieberam, I., Agalliu, D., Nagasawa, T., Ericson, J., and Jessell, T. M. (2005). A cxcl12-cxcr4 chemokine signaling pathway defines the initial trajectory of mammalian motor axons. *Neuron*, 47(5):667–679.

Liu, H., Lan, Y., Xu, J., Chang, C.-F., Brugmann, S. A., and Jiang, R. (2013). Odd-skipped related-1 controls neural crest chondrogenesis during tongue development. *Proc Natl Acad Sci U S A*, 110(46):18555–18560.

Luster, A. D., Cardiff, R. D., MacLean, J. A., Crowe, K., and Granstein, R. D. (1998). Delayed wound healing and disorganized neovascularization in transgenic mice expressing the ip-10 chemokine. *Proc Assoc Am Physicians*, 110(3):183–196.

Mankoo, B. S., Collins, N. S., Ashby, P., Grigorieva, E., Pevny, L. H., Candia, A., Wright, C. V., Rigby, P. W., and Pachnis, V. (1999). Mox2 is a component of the genetic hierarchy controlling limb muscle development. *Nature*, 400(6739):69–73.

Martins, G. G., Rifes, P., Amandio, R., Rodrigues, G., Palmeirim, I., and Thorsteinsdottir, S. (2009). Dynamic 3d cell rearrangements guided by a fibronectin matrix underlie somitogenesis. *PLoS ONE*, 4(10):e7429.

Masyuk, M., Abduelmula, A., Morosan-Puopolo, G., Ödemis, V., Rehimi, R., Khalida, N., Yusuf, F., Engele, J., Tamamura, H., Theiss, C., and Brand-Saberi, B. (2014). Retrograde migration of pectoral girdle muscle precursors depends on cxcr4/sdf-1 signaling. *Histochem Cell Biol*, 142(5):473–488.

Mathew, S. J., Hansen, J. M., Merrell, A. J., Murphy, M. M., Lawson, J. A., Hutcheson, D. A., Hansen, M. S., Angus-Hill, M., and Kardon, G. (2011). Connective tissue fibroblasts and tcf4 regulate myogenesis. *Development*, 138(2):371–384.

MAURO, A. (1961). Satellite cell of skeletal muscle fibers. *J Biophys Biochem Cytol*, 9:493–495.

Merrell, A. J., Ellis, B. J., Fox, Z. D., Lawson, J. A., Weiss, J. A., and Kardon, G. (2015). Muscle connective tissue controls development of the diaphragm and is a source of congenital diaphragmatic hernias. *Nat Genet*, 47(5):496–504.

Messina, G., Biressi, S., Monteverde, S., Magli, A., Cassano, M., Perani, L., Roncaglia, E., Tagliafico, E., Starnes, L., Campbell, C. E., Grossi, M., Goldhamer, D. J., Gronostajski, R. M., and Cossu, G. (2010). Nfix regulates fetal-specific transcription in developing skeletal muscle. *Cell*, 140(4):554–566.

Meucci, O., Fatatis, A., Simen, A. A., and Miller, R. J. (2000). Expression of cx3cr1 chemokine receptors on neurons and their role in neuronal survival. *Proc Natl Acad Sci U S A*, 97(14):8075–8080.

Mizoguchi, T., Verkade, H., Heath, J. K., Kuroiwa, A., and Kikuchi, Y. (2008). Sdf1/cxcr4 signaling controls the dorsal migration of endodermal cells during zebrafish gastrulation. *Development*, 135(15):2521–2529.

Molyneaux, K. A., Zinszner, H., Kunwar, P. S., Schaible, K., Stebler, J., Sunshine, M. J., O'Brien, W., Raz, E., Littman, D., Wylie, C., and Lehmann, R. (2003). The chemokine sdf1/cxcl12 and its receptor cxcr4 regulate mouse germ cell migration and survival. *Development*, 130(18):4279–4286.

Montero, J. A. and Hurlé, J. M. (2010). Sculpturing digit shape by cell death. *Apoptosis*, 15(3):365–375.

Mugford, J. W., Sipilä, P., McMahon, J. A., and McMahon, A. P. (2008). Osr1 expression demarcates a multi-potent population of intermediate mesoderm that undergoes progressive restriction to an osr1-dependent nephron progenitor compartment within the mammalian kidney. *Dev Biol*, 324(1):88–98.

Murphy, M. M., Lawson, J. A., Mathew, S. J., Hutcheson, D. A., and Kardon, G. (2011). Satellite cells, connective tissue fibroblasts and their interactions are crucial for muscle regeneration. *Development*, 138(17):3625–3637.

Muzumdar, M. D., Tasic, B., Miyamichi, K., Li, L., and Luo, L. (2007). A global double-fluorescent cre reporter mouse. *Genesis*, 45(9):593–605.

Naiche, L. A. and Papaioannou, V. E. (2007). Tbx4 is not required for hindlimb identity or post-bud hindlimb outgrowth. *Development*, 134(1):93–103.

Nair, S. and Schilling, T. F. (2008). Chemokine signaling controls endodermal migration during zebrafish gastrulation. *Science*, 322(5898):89–92.

Nedergaard, A., Karsdal, M. A., Sun, S., and Henriksen, K. (2013). Serological muscle loss biomarkers: an overview of current concepts and future possibilities. *Journal of Cachexia, Sarcopenia and Muscle*, 4(1):1–17.

Odemis, V., Lamp, E., Pezeshki, G., Moepps, B., Schilling, K., Gierschik, P., Littman, D. R., and Engele, J. (2005). Mice deficient in the chemokine receptor cxcr4 exhibit impaired limb innervation and myogenesis. *Mol Cell Neurosci*, 30(4):494–505.

Ohl, L., Henning, G., Krautwald, S., Lipp, M., Hardtke, S., Bernhardt, G., Pabst, O., and Förster, R. (2003). Cooperating mechanisms of cxcr5 and ccr7 in development and organization of secondary lymphoid organs. *J Exp Med*, 197(9):1199–1204.

Okada, T., Ngo, V. N., Ekland, E. H., Förster, R., Lipp, M., Littman, D. R., and Cyster, J. G. (2002). Chemokine requirements for b cell entry to lymph nodes and peyer's patches. *J Exp Med*, 196(1):65–75.

Ordahl, C. P. and Douarin, N. M. L. (1992). Two myogenic lineages within the developing somite. *Development*, 114(2):339–353.

Palmeirim, I., Dubrulle, J., Henrique, D., Ish-Horowicz, D., and Pourquié, O. (1998). Uncoupling segmentation and somitogenesis in the chick presomitic mesoderm. *Dev Genet*, 23(1):77–85.

Paredes, M. F., Li, G., Berger, O., Baraban, S. C., and Pleasure, S. J. (2006). Stromal-derived factor-1 (cxcl12) regulates laminar position of cajal-retzius cells in normal and dysplastic brains. *J Neurosci*, 26(37):9404–9412.

Parker, M. H., Perry, R. L. S., Fauteux, M. C., Berkes, C. A., and Rudnicki, M. A. (2006). Myod synergizes with the e-protein heb beta to induce myogenic differentiation. *Mol Cell Biol*, 26(15):5771–5783.

Pryce, B. A., Brent, A. E., Murchison, N. D., Tabin, C. J., and Schweitzer, R. (2007). Generation of transgenic tendon reporters, scxgfp and scxap, using regulatory elements of the scleraxis gene. *Dev Dyn*, 236(6):1677–1682.

Pryce, B. A., Watson, S. S., Murchison, N. D., Staverosky, J. A., Dünker, N., and Schweitzer, R. (2009). Recruitment and maintenance of tendon progenitors by tgfbeta signaling are essential for tendon formation. *Development*, 136(8):1351–1361.

Ragozzino, D., Barabino, B., Fucile, S., and Eusebi, F. (1998). Ca2+ permeability of mouse and chick nicotinic acetylcholine receptors expressed in transiently transfected human cells. *J Physiol*, 507 (Pt 3):749–757.

Rankin, S. A., Gallas, A. L., Neto, A., Gómez-Skarmeta, J. L., and Zorn, A. M. (2012). Suppression of bmp4 signaling by the zinc-finger repressors osr1 and osr2 is required for wnt/b-catenin-mediated lung specification in xenopus. *Development*, 139(16):3010–3020.

Raz, E. and Mahabaleshwar, H. (2009). Chemokine signaling in embryonic cell migration: a fisheye view. *Development*, 136(8):1223–1229.

Rehimi, R., Khalida, N., Yusuf, F., Morosan-Puopolo, G., and Brand-Saberi, B. (2010). A novel role of cxcr4 and sdf-1 during migration of cloacal muscle precursors. *Dev Dyn*, 239(6):1622–1631.

Reichman-Fried, M., Minina, S., and Raz, E. (2004). Autonomous modes of behavior in primordial germ cell migration. *Dev Cell*, 6(4):589–596.

Relaix, F. (2006). Skeletal muscle progenitor cells: from embryo to adult. *Cell Mol Life Sci*, 63(11):1221–1225.

Riddle, R. D., Johnson, R. L., Laufer, E., and Tabin, C. (1993). Sonic hedgehog mediates the polarizing activity of the zpa. *Cell*, 75(7):1401–1416.

Rios, A. C., Serralbo, O., Salgado, D., and Marcelle, C. (2011). Neural crest regulates myogenesis through the transient activation of notch. *Nature*, 473(7348):532–535.

Rong, P. M., Teillet, M. A., Ziller, C., and Douarin, N. M. L. (1992). The neural tube/notochord complex is necessary for vertebral but not limb and body wall striated muscle differentiation. *Development*, 115(3):657–672.

Rozario, T. and DeSimone, D. W. (2010). The extracellular matrix in development and morphogenesis: a dynamic view. *Dev Biol*, 341(1):126–140.

Rueda, P., Richart, A., Récalde, A., Gasse, P., Vilar, J., Guérin, C., Lortat-Jacob, H., Vieira, P., Baleux, F., Chretien, F., Arenzana-Seisdedos, F., and Silvestre, J.-S. (2012). Homeostatic and tissue reparation defaults in mice carrying selective genetic invalidation of cxcl12/proteoglycan interactions. *Circulation*, 126(15):1882–1895.

Salcedo, R. and Oppenheim, J. J. (2003). Role of chemokines in angiogenesis: Cxcl12/sdf-1 and cxcr4 interaction, a key regulator of endothelial cell responses. *Microcirculation*, 10(3-4):359–370.

Sambasivan, R., Kuratani, S., and Tajbakhsh, S. (2011). An eye on the head: the development and evolution of craniofacial muscles. *Development*, 138(12):2401–2415.

Sanchez-Gurmaches, J. and Guertin, D. A. (2014). Adipocytes arise from multiple lineages that are heterogeneously and dynamically distributed. *Nat Commun*, 5:4099.

Schwanhäusser, B., Busse, D., Li, N., Dittmar, G., Schuchhardt, J., Wolf, J., Chen, W., and Selbach, M. (2011). Global quantification of mammalian gene expression control. *Nature*, 473(7347):337–342.

Schweitzer, R., Chyung, J. H., Murtaugh, L. C., Brent, A. E., Rosen, V., Olson, E. N., Lassar, A., and Tabin, C. J. (2001). Analysis of the tendon cell fate using scleraxis, a specific marker for tendons and ligaments. *Development*, 128(19):3855–3866.

Schweitzer, R., Zelzer, E., and Volk, T. (2010). Connecting muscles to tendons: tendons and musculoskeletal development in flies and vertebrates. *Development*, 137(17):2807–2817.

Schweizer, H., Johnson, R. L., and Brand-Saberi, B. (2004). Characterization of migration behavior of myogenic precursor cells in the limb bud with respect to lmx1b expression. *Anat Embryol (Berl)*, 208(1):7–18.

Seale, P., Bjork, B., Yang, W., Kajimura, S., Chin, S., Kuang, S., Scimè, A., Devarakonda, S., Conroe, H. M., Erdjument-Bromage, H., Tempst, P., Rudnicki, M. A., Beier, D. R., and Spiegelman, B. M. (2008). Prdm16 controls a brown fat/skeletal muscle switch. *Nature*, 454(7207):961–967.

Snow, C. J., Peterson, M. T., Khalil, A., and Henry, C. A. (2008). Muscle development is disrupted in zebrafish embryos deficient for fibronectin. *Dev Dyn*, 237(9):2542–2553.

So, P. L. and Danielian, P. S. (1999). Cloning and expression analysis of a mouse gene related to drosophila odd-skipped. *Mech Dev*, 84(1-2):157–160.

Stricker, S., Brieske, N., Haupt, J., and Mundlos, S. (2006). Comparative expression pattern of odd-skipped related genes osr1 and osr2 in chick embryonic development. *Gene Expr Patterns*, 6(8):826–834.

Stricker, S., Mathia, S., Haupt, J., Seemann, P., Meier, J., and Mundlos, S. (2012). Odd-skipped related genes regulate differentiation of embryonic limb mesenchyme and bone marrow mesenchymal stromal cells. *Stem Cells Dev*, 21(4):623–633.

Swartz, M. E., Eberhart, J., Pasquale, E. B., and Krull, C. E. (2001). Epha4/ephrin-a5 interactions in muscle precursor cell migration in the avian forelimb. *Development*, 128(23):4669–4680.

Thorsteinsdottir, S., Deries, M., Cachaco, A. S., and Bajanca, F. (2011). The extracellular matrix dimension of skeletal muscle development. *Developmental Biology*, 354(2):191 – 207.

Tiveron, M.-C. and Cremer, H. (2008). Cxcl12/cxcr4 signalling in neuronal cell migration. *Curr Opin Neurobiol*, 18(3):237–244.

Tozer, S., Bonnin, M.-A., Relaix, F., Di Savino, S., García-Villalba, P., Coumailleau, P., and Duprez, D. (2007). Involvement of vessels and pdgfb in muscle splitting during chick limb development. *Development*, 134(14):2579–2591.

Valasek, P., Evans, D. J. R., Maina, F., Grim, M., and Patel, K. (2005). A dual fate of the hindlimb muscle mass: cloacal/perineal musculature develops from leg muscle cells. *Development*, 132(3):447–458.

van de Pavert, S. A., Olivier, B. J., Goverse, G., Vondenhoff, M. F., Greuter, M., Beke, P., Kusser, K., Höpken, U. E., Lipp, M., Niederreither, K., Blomhoff, R., Sitnik, K., Agace, W. W., Randall, T. D., de Jonge, W. J., and Mebius, R. E. (2009). Chemokine cxcl13 is essential for lymph node initiation and is induced by retinoic acid and neuronal stimulation. *Nat Immunol*, 10(11):1193–1199.

Vasyutina, E., Stebler, J., Brand-Saberi, B., Schulz, S., Raz, E., and Birchmeier, C. (2005). Cxcr4 and gab1 cooperate to control the development of migrating muscle progenitor cells. *Genes Dev*, 19(18):2187–2198.

von Maltzahn, J., Bentzinger, C. F., and Rudnicki, M. A. (2012). Wnt7a-fzd7 signalling directly activates the akt/mtor anabolic growth pathway in skeletal muscle. *Nat Cell Biol*, 14(2):186–191.

Wan, Y., Lewis, A. K., Colasanto, M., van Langeveld, M., Kardon, G., and Hansen, C. (2012). A practical workflow for making anatomical atlases for biological research. *IEEE Comput Graph Appl*, 32(5):70–80.

Wang, Q., Lan, Y., Cho, E.-S., Maltby, K. M., and Jiang, R. (2005). Odd-skipped related 1 (odd 1) is an essential regulator of heart and urogenital development. *Dev Biol*, 288(2):582–594.

Weinstein, B. M. (2005). Vessels and nerves: marching to the same tune. *Cell*, 120(3):299–302.

Xu, J., Liu, H., Park, J.-S., Lan, Y., and Jiang, R. (2014). Osr1 acts downstream of and interacts synergistically with six2 to maintain nephron progenitor cells during kidney organogenesis. *Development*, 141(7):1442–1452.

Yahiaoui, L., Gvozdic, D., Danialou, G., Mack, M., and Petrof, B. J. (2008). Cc family chemokines directly regulate myoblast responses to skeletal muscle injury. *J Physiol*, 586(16):3991–4004.

Zou, Y., Zhang, R.-Z., Sabatelli, P., Chu, M.-L., and Bönnemann, C. G. (2008). Muscle interstitial fibroblasts are the main source of collagen vi synthesis in skeletal muscle: implications for congenital muscular dystrophy types ullrich and bethlem. *J Neuropathol Exp Neurol*, 67(2):144–154.

Zou, Y., Zwolanek, D., Izu, Y., Gandhy, S., Schreiber, G., Brockmann, K., Devoto, M., Tian, Z., Hu, Y., Veit, G., Meier, M., Stetefeld, J., Hicks, D., Straub, V., Voermans, N. C., Birk, D. E., Barton, E. R., Koch, M., and Bönnemann, C. G. (2014). Recessive and dominant mutations in col12a1 cause a novel eds/myopathy overlap syndrome in humans and mice. *Hum Mol Genet*, 23(9):2339–2352.

Zou, Y. R., Kottmann, A. H., Kuroda, M., Taniuchi, I., and Littman, D. R. (1998). Function of the chemokine receptor cxcr4 in haematopoiesis and in cerebellar development. *Nature*, 393(6685):595–599.

Appendix

Supplementary Material

The following data complement the presented work.

Gene	TPM Rank
Col3a1	4
Col1a2	6
Col1a1	10
Col5a2	36
Col5a1	38
Col6a3	62
Col6a1	69
Col6a2	86
Col12a1	130
Col2a1	148
Col4a1	312
Col11a1	334
Col4a2	619
Col14a1	813
Col16a1	885
Fn1	14
Fbn2	71
Fbn1	281
Tnc	321
Lum	338
Dcn	390
Nid2	440
Lama4	477
Mfap2	497
Lamc1	616
Ogn	646
Fbln1	657
Eln	687
Bgn	728
Emilin1	876

Figure 39: **ECM-structural genes are highly expressed in *Osr1*$^{GCE/+}$ sorted cells**. Relative abundancies in gene expression from RNA-Seq data were measured using transcript per million (TPM). It was taken into account all genes with a TPM value higher than 2 (more than 17.000 genes). Selected ECM-structural genes were within the 5% of genes with highest TPM values (more than 900 genes).

Gene	Relative gene expression
Tgfb3	1,311
Tgfbi	1,360
Tgfb1	0,678
Wnt11	0,666
Wnt2	0,617
Bmp4	0,772
Fst	0,738
Ccl9	0,410
Ccl2	0,549
Ccl4	0,498
Ccl3	0,536
Ccl24	0,443
Ccl7	0,586
Ccl11	0,632
Cxcl2	0,567
Cxcl13	0,369
Cxcl1	0,570
Cxcl12	0,734
Cxcl10	0,718
Il7	2,177
Il1rn	0,612
Il1a	0,613
Il1b	0,668
Serpinb7	0,332
Serpinb1a	0,420
Serpinb8	0,555
Dkk3	1,462

Up-regulated

Down-regulated

Figure 40: **Secreted factors de-regulated in E13.5 *Osr1*$^{GCE/GCE}$ sorted cells**. Gene and relative expression level in E13.5 *Osr1*$^{GCE/GCE}$ sorted cells are listed after RNA-seq analyses.

List of Figures

List of Tables

Scientific Publications **Conference contributions**

2015 March 11-14. Joint Meeting of the German and French Societies of Developmental Biologists
Presentation: Osr1 controls muscle patterning via extracellular matrix and chemokine signaling

2014 May 14-18. Molecular Biology of Muscle Development and Regeneration
Poster: Connective tissue controls muscle patterning via extracellular matrix

2013 June 16-26. Myograd Sommer School for Clinical Myology, Paris

June 2011-2014. Myograd Sommer School for Basic Muscle Science, Berlin

Publications

Kuss P, Kraft K, Stumm J, Ibrahim D, **Vallecillo-Garcia P**, Mundlos S, Stricker S: Regulation of cell polarity in the cartilage growth plate and perichondrium of metacarpal elements by HOXD13 and WNT5A . Developmental Biology. January 2014, Pages 83-93.